NORTHWESTERN UNIVERSITY

# Misregulation of Mitochondria-Lysosome Contact Sites in GBA-linked Parkinson's Disease

A DISSERTATION

SUBMITTED TO THE GRADUATE SCHOOL
IN PARTIAL FULLFILLMENT OF THE REQUIREMENTS

for the degree

DOCTOR OF PHILOSOPHY

Field of Neuroscience

By

Soojin Kim

EVANSTON, ILLINOIS

September 2021

# ABSTRACT

Mitochondria-lysosome contacts are recently identified sites for mediating crosstalk between both organelles, but their role in normal and diseased human neurons remains unknown. We used super-resolution and live-cell microscopy in human iPSC-derived neurons to demonstrate that mitochondria-lysosome contacts can dynamically form in the soma, axons, and dendrites of human neurons, allowing for their bidirectional crosstalk. To examine these contacts in diseased neurons, we have focused on Parkinson's disease that is characterized by preferential degeneration of midbrain dopaminergic neurons. Specifically, we examined Parkinson's disease patient neurons harboring mutations in *GBA1* gene that codes for lysosomal enzyme β-glucocerebrosidase (GCase). Interestingly, we found prolonged mitochondria-lysosome contacts in *GBA1*-PD neurons due to defective modulation of the protein TBC1D15, which mediates Rab7 GTP hydrolysis for contact untethering. Importantly, these defects in mitochondria-lysosome contacts resulted in disrupted mitochondrial distribution and function that was partially ameliorated by expression of TBC1D15 in PD patient neurons. Moreover, we found that dysregulation of TBC1D15 in patient neurons was partially rescued by correcting GCase activity with a small molecule activator of GCase. Together, our work demonstrates an important role of mitochondria-lysosome contacts as a regulator of mitochondrial function and dynamics in midbrain dopaminergic neurons, contributing to the pathogenesis of Parkinson's disease.

# ACKNOWLEDGEMENTS

"If I have seen further it is by standing on the shoulders of Giants." – Issac Newton

From adjusting to a new environment in a foreign country to managing classes, conducting research, and presenting my work, my time in graduate school has been one the most challenging adventures of my life. Looking back over the 5 years at Northwestern University, this journey would not have been possible without the people who have endlessly supported me along the way. They were “Giants” who have allowed me to see further.

First and foremost, I would like to express my deepest appreciation to my advisor, Dr. Dimitri Krainc, for his mentorship, encouragement, and inspiration throughout my studies in his laboratory. I truly value the opportunity to have learned from his insight and enthusiasm for science. I will forever be grateful for how much I have grown under his constructive guidance.

I would also like to extend my sincere thanks to all my thesis committee members - Dr. Robert Vassar, Dr. Kathleen Green and Dr. Robert Kalb, for their support in guiding my thesis research. This project could not have moved forward without their thoughtful inputs and comments. In addition, I am very thankful to Dr. Dongho Geum at Korea University who encouraged me to continue as a scientist, especially during the difficult times in research.

I have also had the great pleasure of working with past and present members of Dr. Krainc’s lab and gratefully acknowledge their technical advice and support during my PhD. I would especially like to thank Dr. Yvette Wong for providing her mentorship and for many enlightening discussions. Without her support, encouragement, and practical suggestions, my thesis research would hardly have been completed, and I am deeply grateful for her patience which cannot be underestimated.

Lastly, and most importantly, I wish to acknowledge the support and great love of my family. Whenever I experienced any self-doubt, it was their belief in me that helped keep me going, so that I could pursue my love for science and research.

# LIST OF ABBREVIATIONS

| | |
|---|---|
| ALS | Amyotrophic lateral sclerosis |
| ASAH1 | N-acylsphingosine amidohydrolase 1 |
| Atg5 | Autophagy related 5 |
| ATP | Adenosine triphosphate |
| BafA1 | Bafilomycin A1 |
| BDNF | Brain-derived neurotrophic factor |
| cAMP | Cyclic adenosine monophosphate |
| CBE | Conduritol-b-epoxide |
| Ccz1 | Caffeine, calcium, zinc sensitivity 1 |
| CLEM | Correlative light electron microscopy |
| c-myc | Cellular myelocytomatosis oncogene |
| CRISPR/Cas9 | Clustered regularly interspaced short palindromic repeats / CRISPR-associated protein 9 |
| CTSD | Cathepsin D |
| DA | Dopamine |
| DJ-1 (PARK7) | Parkinson disease protein 7 |
| ER | Endoplasmic reticulum |
| FBXO7 | F-box protein 7 |
| FIB-SEM | Focused ion beam scanning electron microscopy |
| Fis1 | Mitochondrial fission 1 protein |
| FoxA2 | Forkhead box protein A2 |
| FYCO | FYVE And Coiled-Coil Domain Autophagy Adaptor 1 |
| GAP | GTPase-activating proteins |
| GBA1 | Glucosylceramidase beta |
| Gcase | Glucocerebrosidase |
| GD | Gaucher disease |

| | |
|---|---|
| GDNF | Glial cell line-derived neurotrophic facto |
| GDP | Guanosine diphosphate |
| GEF | Guanine nucleotide exchange factors |
| GlcCer | Glucosylceramide |
| GTP | Guanosine-5'-triphosphate |
| GWAS | Genome-wide association study |
| HDAC4 | Histone deacetylase 4 |
| ICC | Immunocytochemistry |
| iPSC | Induced pluripotent stem cell |
| Klf4 | Kruppel-like factor 4 |
| Lamp1 | Lysosomal-associated membrane protein 1 |
| LC3 | Microtubule-associated protein 1A/1B-light chain 3 |
| LMX1A | LIM Homeobox Transcription Factor 1 Alpha |
| LRRK2 | Leucine-rich repeat kinase 2 |
| MAO | Monoamine oxidase |
| MAP2 | Microtubule associated protein 2 |
| MCCC1 | Methylcrotonoyl-CoA carboxylase 1 (alpha) |
| MCS | Membrane contact site |
| MCU | Mitochondrial calcium uniporter |
| MDV | Mitochondrial-derived vesicles |
| Mon1 | Monensin sensitivity 1 |
| MPTP | 1-methyl-4-phenyl-1,2,3,6-tetrahydropyridin |
| mtDNA | Mitochondrial DNA |
| NAD | Nicotinamide adenine dinucleotide |
| NBR1 | Next to BRCA1 gene 1 protein |
| NDP52 | Nuclear dot protein 52 kDa |
| NLS | Nuclear localization signal |
| NPC | Niemann-Pick disease type C |

| | |
|---|---|
| NPC1 | Niemann-Pick type C protein 1 |
| OCR | Oxygen consumption rate |
| Oct3/4 | Octamer binding transcription factor 3/4 |
| OPTN | Optineurin |
| ORF | Open reading frame |
| PD | Parkinson's disease |
| PDL | Poly-d-lysine |
| PFB-FDGlu | Di-β-D-glucopyranoside |
| PINK1 | PTEN-induced kinase 1 |
| PRKN | Parkin |
| Rab7 | Ras-Related small GTPases 7 |
| RILP | Rab interacting lysosomal protein |
| SCARB2 | Scavenger receptor class B member 2 |
| SCNA | Synuclein alpha |
| SE-FRET | Sensitized emission fluorescence resonance energy transfer |
| SIM | Structured illumination microscopy |
| SLC17A5 | Solute carrier family 17, member 5 |
| SMPD1 | Sphingomyelin Phosphodiesterase 1 |
| Sox2 | SRY-Box Transcription Factor 2 |
| ssODN | Single-strand oligodeoxynucleotide |
| TAX1BP1 | Tax1-binding protein 1 |
| TBC1D15 | TBC1 Domain Family Member 15 |
| TH | Tyrosine hydroxylase |
| TMEM | Transmembrane protein |
| TMRM | Tetramethylrhodamine, methyl ester |
| Tom20 | Translocase Of Outer Mitochondrial Membrane 20 |
| TUJ1 | β-III-tubulin |
| UCHL1 | Ubiquitin C-Terminal Hydrolase L1 |

| | |
|---|---|
| ULK1 | Unc-51 like autophagy activating kinase 1 |
| UPR | Unfolded protein response |
| VDAC1 | Voltage-dependent anion channel-1 |
| VPS35 | Vacuolar protein sorting ortholog 35 |
| WB | Western blot |
| WT | Wildtype |

# DEDICATION

To my mother, JeongLae Lee, my father, NamSeung Kim

and my sister, JiYun Kim, for their endless support.

# TABLE OF CONTENTS

# FIGURES & TABLES

# CHAPTER 1.

# INTRODUCTION

## 1.1 PARKINSON'S DISEASE

It is estimated that about 1 million people are currently afflicted with Parkinson's disease (PD) in US and about 60,000 Americans are newly diagnosed with PD each year (Marras et al. 2018). More than 10 million people worldwide are living with PD (Tysnes and Storstein 2017). PD is associated with the progressive loss of A9-dopaminergic neurons in the substantia nigra leading to the loss of dopamine and the dysregulation of fine motor control due to dysfunction of basal ganglia. Ultimately, the loss of dopaminergic neurons clinically manifests in bradykinesia, rigidity, and rest tremor (Kalia and Lang 2015) and pathologically involves the presence of Lewy Body aggregates comprised of α-synuclein (Spillantini et al. 1997). PD exists as a multifaceted disease that presents itself clinically with some degree of heterogeneity (Lewis et al. 2005; Vidailhet 2003). Approximately 10% of PD cases are familial with a genetically inherited mutations, while the rest are idiopathic and have an unclear etiology. At the cellular level, PD has been linked to defects in multiple pathways including abnormalities in mitochondrial and lysosomal function, protein accumulation, synaptic and axonal dysfunction, ER stress, and increased oxidative stress (Kalia and Lang 2015; Nguyen et al. 2019). Genetically, multiple genes have been linked to either dominant or recessive familial forms of PD including *SCNA, LRRK2, PINK1, PARK2* (parkin) and *GBA1*, as well as additional genes such as *DJ-1, PARK9 (ATP13A2), SJ-1* and *VPS35* (Klein and Westenberger 2012). However, how these genes and related pathways converge in PD

pathogenesis and cause of neuronal death is still not well understood, making it difficult to develop successful therapies.

### 1.1.1 Genetics

Most PD cases are sporadic or idiopathic PD, occurring in patients without a family history of PD. Since only ~10% of PD patients have a family history of PD, it was not originally considered a genetic disorder until the first mutation in α-synuclein (*SNCA*) was identified in 1996 (Polymeropoulos et al. 1996; Polymeropoulos et al. 1997). Since then, the identification of genetic forms of PD and accumulating evidence from recent studies have remarkably expanded our understanding of potential mechanisms involved in PD pathogenesis. To date, mutations in multiple genes including *SNCA, LRRK2, VPS35, TMEM230, PRKN, PINK1*, and *PARK7* (*DJ-1*) are known to cause familial PD (Klein and Westenberger 2012). In addition to mutations that directly cause PD, several risk genes (e.q. *GBA1* and *UCHL1*) may also increase the risk of PD (Gegg et al. 2012; Maraganore et al. 2004; Neumann et al. 2009; Sidransky et al. 2009). Thus, examining the biological pathways linked to known PD causative genes may help lead us to a deeper understanding of potential PD mechanisms involved in disease pathogenesis. In the case of idiopathic PD, the causes driving disease are likely to be multifactorial, potentially resulting from complex interactions between both environmental factors and possibly multiple genes. Importantly, idiopathic PD patients also demonstrate increased α-synuclein accumulation as well as decreased lysosomal GBA activity (Burbulla et al. 2017; Mazzulli et al. 2011), suggesting that insights into genetic forms of PD may further inform our understanding of idiopathic PD.

### 1.1.2 Mitochondrial dysfunction in Parkinson's disease

Most significantly, increasing evidence points to mitochondrial dysfunction as a central factor in PD pathogenesis. In addition to the accidental discovery in 1983 that 1-methyl-4-phenyl-1,2,3,6-tetrahydropyridine (MPTP) (Langston et al. 1983), an inhibitor of the mitochondrial respiratory chain complex I, could cause Parkinson-like symptoms, subsequently, multiple recessive genes related to mitochondrial function and turnover such as *parkin* (*PARK2*), *PINK1* (*PARK6*), *DJ-1* (*PARK7*), and *FBXO7* have been found to be associated with early-onset PD (Lucking et al. 2000; Valente et al. 2004; Bonifati et al. 2003; Burchell et al. 2013). Moreover, several genome-wide association studies (GWAS) have further provided evidence strengthening the link between mitochondrial function and PD. Recently, Chang et al. identified several risk factors linked to mitochondrial function including *COQ7* (coenzyme Q7, hydroxylase) and *ALAS1* (delta-aminolevulinate synthase 1) in addition to the previously identified gene *MCCC1* (methylcrotonoyl-CoA carboxylase 1 (alpha)) (Chang et al. 2017). Moreover, induced pluripotent stem cell (iPSC)-derived dopaminergic neurons from both familial and idiopathic Parkinson's patients demonstrate mitochondrial dysfunction including reduced mitochondrial respiration and increased mitochondrial oxidant stress (Burbulla et al. 2017).

### 1.1.3 Lysosomal dysfunction in Parkinson's disease

In addition to defective mitochondrial function, the lysosomal degradation pathway has also been found to be associated with PD. For example, PD-linked mutations in α-synuclein (SNCA), the first gene linked to familial PD (Polymeropoulos et al. 1997), induce lysosomal

dysfunction leading to its own aggregation caused by impaired degradation (Mazzulli et al. 2011; Mazzulli, Zunke, Isacson, et al. 2016). Furthermore, mutations in the lysosomal enzyme GBA (encoding glucocerebrosidase) were identified as the greatest risk factor for PD (Sidransky et al. 2009). In addition, mutations in *ATP13A2* (encoding a lysosomal ATPase) also cause familial PD in addition to lysosomal dysfunction and α-synuclein aggregation (Tsunemi, Hamada, and Krainc 2014; Park, Blair, and Sue 2015), while variants of *SMPD1* (encoding the lysosomal acid sphingomyelinase) have been associated with PD through several recent studies (Alcalay et al. 2019). Moreover, findings from recent GWAS have also supported the association between lysosomal dysfunction and PD. Nalls et al. identified risk loci associated with *GBA*, *SCARB2* (Scavenger receptor class B member 2) and *TMEM175* (Transmembrane protein 175) (Nalls et al. 2014). Additionally, Robak et al. replicated previous findings and also identified three more lysosomal PD genes: *CTSD* (cathepsin D), *SLC17A5* (solute carrier family 17, member 5) and *ASAH1* (N-acylsphingosine amidohydrolase 1) (Robak et al. 2017). Finally, iPSC-derived dopaminergic neurons from both familial and idiopathic Parkinson's patients also demonstrate lysosomal dysfunction including reduced lysosomal proteolysis and GBA enzymatic activity(Burbulla et al. 2017; Mazzulli et al. 2011).

## 1.2 *GBA1* MUTATIONS IN PARKINSON'S DISEASE

The *GBA1* gene encodes a lysosomal enzyme called glucocerebrosidase (also known as GCase or β-glucosidase) that catalyzes the hydrolysis of glucosylceramide (GlcCer) to glucose and ceramide, as well as the hydrolysis of D-glucosyl-N-acylsphingosine to D-glucose and N-

acylsphingosine. Homozygous or compound heterozygote *GBA1* mutations are known to cause Gaucher disease (GD), the most common lysosomal storage disorder. After the first report of GD patients with symptoms of Parkinsonism (Neumann et al. 2009), other studies confirmed the link between PD and *GBA1* mutation including insertion, deletion, frame shift and point mutations in *GBA1* (Gegg et al. 2012; Mazzulli et al. 2011; Murphy et al. 2014; Wong and Krainc 2016). Approximately 5-10% of PD patients carry *GBA1* mutations (Sidransky et al. 2009) and the two most common mutations in *GBA1* (N370S and L444P) account for ~3% of GBA-liked PD (Neumann et al. 2009; Sidransky et al. 2009). Clinically, *GBA1* mutation carriers tend to have an early onset (Gan-Or et al. 2010; Lesage et al. 2011) and more cognitive symptoms in addition to severe motor symptoms (Cilia et al. 2016; Oeda et al. 2015; Thaler et al. 2017).

Many studies have shown reduced protein levels and GCase activity in mutant *GBA1* patient iPSC-derived neurons across multiple *GBA1* mutations including N370S/N370S, N370S/c0.84dupG, N370S/WT, RecNcil/WT and L444P/WT (Aflaki et al. 2016; Kim, Yun, et al. 2018; Schondorf et al. 2014). In particular, abnormal GCase post-translation has also been observed in iPSC-derived neurons from N370S heterozygous patients (Fernandes et al. 2016). Moreover, in addition to α-synuclein accumulation in GD-linked *GBA1* iPSC-derived neurons (Mazzulli et al. 2011), increased α-synuclein levels (Aflaki et al. 2016; Fernandes et al. 2016; Schondorf et al. 2014; Woodard et al. 2014) and its aggregation (Kim, Yun, et al. 2018; Mazzulli, Zunke, Isacson, et al. 2016) have also been reported in PD-linked *GBA1* iPSC-derived neurons. Accumulation of lipids have also been identified as a major hallmark of mutant *GBA1* iPSC-derived DA neurons including GCase substrates, glycolipids glucosylceramide (GlcCer) and

glucosylsphingosine (GlcSph) which are increased in *GBA1* mutant neurons (Aflaki et al. 2016; Fernandes et al. 2016; Kim, Yun, et al. 2018; Schondorf et al. 2014).

Additionally, defective function of cellular organelles including lysosomes, mitochondria and the ER have been demonstrated in mutant *GBA1* iPSC-derived neurons. Increased size and number of lysosomes (Schondorf et al. 2014) which may result from the reported lysosomal degradation capacity impairment (Fernandes et al. 2016) have been clearly observed, along with evidence of autophagic defects (Fernandes et al. 2016; Schondorf et al. 2014), potentially rendering neurons more vulnerable to apoptosis. Moreover, mitochondrial dysfunction including decreased oxygen consumption rate (OCR), reduced complex I activity and altered NAD+ metabolism together with altered mitochondrial morphology have also been reported in mutant *GBA1* iPSC-DA neurons (Schondorf et al. 2018). Furthermore, upregulation of ER stress was also observed in multiple studies, leading to defective downstream cellular mechanisms such as calcium homeostasis and the unfolded protein response (UPR) (Fernandes et al. 2016; Schondorf et al. 2014; Schondorf et al. 2018). Lastly, the levels and uptake of dopamine were reduced in *GBA1* N370S iPSC-DA neurons (Aflaki et al. 2016; Woodard et al. 2014), along with upregulated mRNA and protein levels of MAO-B (Woodard et al. 2014), while 84GG/WT iPSC-DA neurons also showed elevated levels of oxidized dopamine (Burbulla et al. 2019). Of note, single-cell transcriptomic analysis of *GBA1* N370S iPSC-DA neurons have highlighted the transcriptional repressor *HDAC4* (histone deacetylase 4) as a potential upstream regulator of ER stress and disease pathogenesis (Lang et al. 2019). However, whether mitochondria-lysosome contact sites are disrupted in *GBA1* iPSC-DA neurons has not been previously studied. Thus, advancing our understanding of the role of *GBA1*

mutations in PD pathogenesis may further provide possible therapeutic strategies that target the mechanisms underlying both familial and idiopathic PD.

## 1.3 ORGANELLE MEMBRANE CONTACT SITES

### 1.3.1 Overview

Eukaryotic cells are characterized by membrane-bound organelles such as the endoplasmic reticulum (ER), Golgi apparatus, lysosomes, peroxisomes and mitochondria. As specialization and compartmentation is critical to each of these organelles, properly regulated interactions between different organelles, either indirectly or directly, may be important for modulating cellular homeostasis. Indeed, studies in the last 60 years have highlighted organelle interactions through membrane contact sites (MCSs). MCSs are regions of close apposition (10- 30nm in general (Elbaz and Schuldiner 2011)) between two membrane-bound organelles that enable functional crosstalk and cooperation. However, the function and molecular architecture of MCSs were not well understood until recently due to the limited resolution of previous microscopy techniques. Recent work using high-resolution microscopy and live cell imaging techniques now demonstrate the dynamic nature of organelle contacts and have started to further reveal the function and molecular tethers involved in MCSs.

The first MCS was identified between mitochondria and ER in 1959 using electron microscopy (EM) (Copeland and Dalton 1959). After this discovery, MCSs between ER, Golgi, mitochondria, vacuoles, lipid droplet, peroxisomes and plasma membrane were proposed in many

different types of cells, beginning with studies in yeast (Binns et al. 2006; Copeland and Dalton 1959; Dolman et al. 2005; Lopez-Crisosto et al. 2017; Shai et al. 2018; Shin et al. 2017; Valm et al. 2017) (**Figure 1.1**). Our lab (Wong, Ysselstein, and Krainc 2018) along with others (Aston et al. 2017; Chen et al. 2018; Fermie et al. 2018; Guo et al. 2018b; Han et al. 2017; Itoh et al. 2018; Khalil et al. 2017; Valm et al. 2017), recently identified dynamic MCSs forming between mitochondria and lysosomes in mammalian cells.

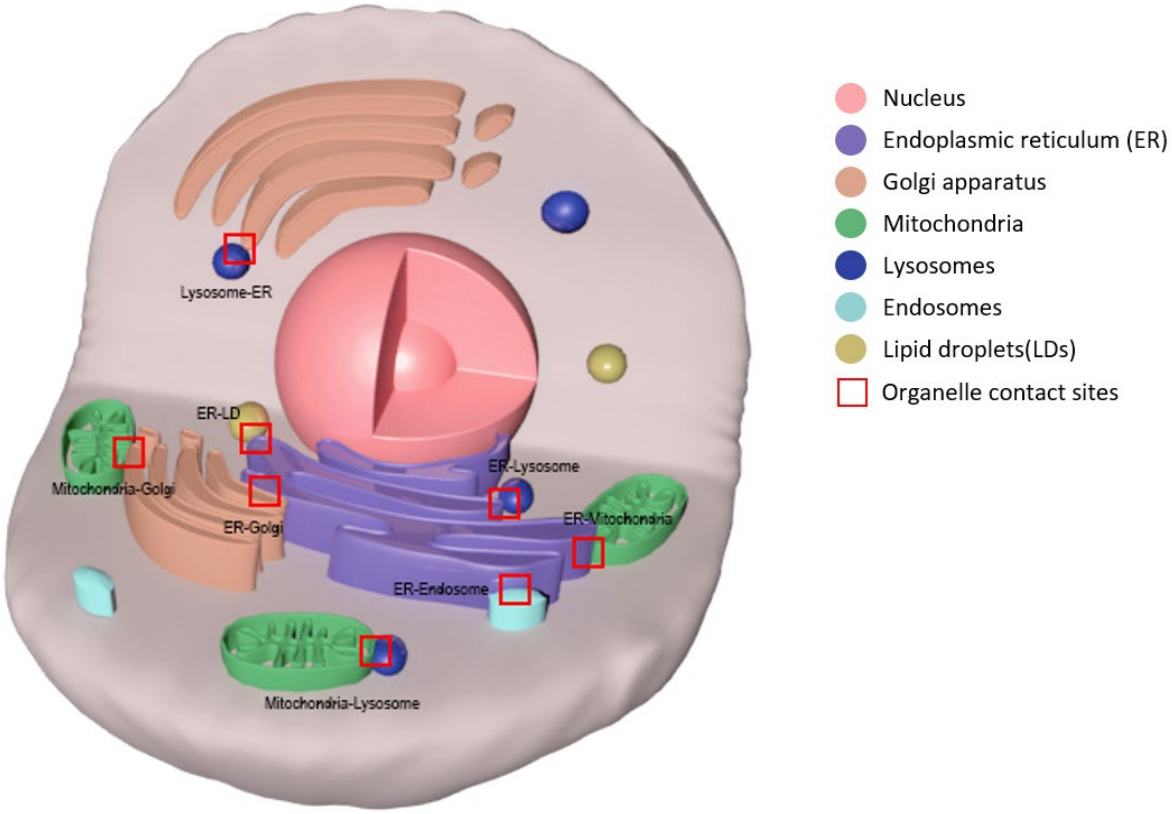


**Figure 1.1 Identified membrane contact sites (MCS) in mammalian cells.** Schematic diagram of a cell depicting contact sites between diverse organelles. The endoplasmic reticulum (ER) interacts with various organelles (mitochondria, Golgi, endosomes/lysosomes, lipid droplets) through multiple MCS. Mitochondria also participates in several different types of MCS with ER, Golgi and lysosomes. Many studies are ongoing to identify molecular tethers and functions of each MCS.

### 1.3.2 Mitochondria-lysosome contacts

Mitochondria and lysosomes as critical organelles in cellular homeostasis

Both mitochondria and lysosomes are critical for maintaining cellular homeostasis, which is further evinced by the fact that dysfunction of both organelles is functionally and genetically linked to multiple human diseases (Burte et al. 2015; Hutagalung and Novick 2011; Mc Donald and Krainc 2017; Plotegher and Duchen 2017b). Mitochondria are necessary for cellular respiration but also function as storage compartments for metabolites including calcium, iron, lipids, protons and ATP, and as gatekeepers for apoptosis and inflammation pathways (Friedman and Nunnari 2014; Sun, Youle, and Finkel 2016). Consequently, proper regulation of mitochondrial transport and dynamics is key to maintaining a functional mitochondrial network throughout the cell (Mishra and Chan 2016). Mitochondrial fission has multiple roles including mitochondrial biogenesis and mitochondrial DNA (mtDNA) synthesis (Lewis, Uchiyama, and Nunnari 2016; Mishra and Chan 2016) and is regulated by the GTPase *Drp1* (dynamin-related protein), endoplasmic reticulum (ER), dynamin-2 and actin (Friedman et al. 2011; Ji et al. 2015; Korobova, Ramabhadran, and Higgs 2013; Lee et al. 2016; Li et al. 2015; Manor et al. 2015; Moore et al. 2016; Smirnova et al. 2001). In contrast, mitochondrial membrane fusion allows for mixing of mitochondrial proteins, mtDNA and metabolites, and is mediated by the outer membrane GTPases *Mitofusin1* and *Mitofusin2* in consort with the inner membrane GTPase *Opa1* (Mishra and Chan 2016). Indeed, properly balanced mitochondrial fission and fusion is crucial as mutations in these proteins result in various diseases (Alexander et al. 2000; Burte et al. 2015; Delettre et al. 2000; Zuchner et al. 2004).

Similarly, lysosomes are highly dynamic organelles and responsible for the turnover of cellular contents including proteins and lipids via mature enzymes localized in the lysosomal lumen. However, lysosomes can also act as calcium and iron stores, and further mediate cell death pathways through the initiation of lysosomal membrane permeabilization (Aits and Jaattela 2013), highlighting a critical role for lysosomes in the maintenance of cellular homeostasis. Indeed, lysosomes must similarly undergo strict regulation of their maturation, positioning and network dynamics via the master regulator Rab7. Active, GTP-bound Rab7 is recruited to late endosomal/lysosomal membranes by GEFs (guanine nucleotide exchange factors) such as Mon1-Ccz1, but dissociates upon Rab GTP hydrolysis mediated by Rab GAPs (GTPase-activating proteins) resulting in an inactive, cytosolic GDP-bound form of Rab7 (Hutagalung and Novick 2011; Zhen and Stenmark 2015). Importantly, GTP-bound Rab7 promotes lysosomal tethering and fusion and can further bind Rab7 effectors to mediate lysosomal transport in the cell (Langemeyer, Frohlich, and Ungermann 2018). In addition, human mutations in Rab7 lead to peripheral neuropathy (Houlden et al. 2004; Meggouh et al. 2006; Verhoeven et al. 2003; Wang et al. 2014), further emphasizing the importance of properly regulated lysosomal dynamics in maintaining cell viability.

Identification of dynamic mitochondria-lysosome membrane contact sites

Contacts between mitochondria and lysosomal-related organelles including melanosomes, multi-vesicular bodies and yeast vacuoles have been previously described (Daniele et al. 2014; Elbaz-Alon et al. 2014; Honscher et al. 2014; Sugiura et al. 2014). Importantly, while contacts are

maintained by tethering proteins which allow for the dynamic formation and subsequent untethering of organelle membranes, additional proteins may also be present at contact sites which do not physically bridge membranes but help to regulate contact function such as mediating metabolite transfer, or regulatory proteins which help coordinate contacts and their response to the cellular environment (Eisenberg-Bord et al. 2016). Functionally, previous contact sites have been found to be important for mediating multiple cellular functions. These include the metabolite transfer of lipids, calcium and iron, the regulation of organelle dynamics such as mitochondrial division (Friedman et al. 2011) and endosomal division (Rowland et al. 2014) which are marked by ER tubules, and additional cellular pathways (Simmen and Herrera-Cruz 2018; Wu, Carvalho, and Voeltz 2018), demonstrating a critical role for inter-organelle contact sites in maintaining cellular homeostasis.

Recently, multiple studies using diverse imaging techniques have demonstrated that inter-organelle contact sites also form between mitochondria and lysosomes in multiple different cell types under healthy conditions (Aston et al. 2017; Chen et al. 2018; Fermie et al. 2018; Han et al. 2017; Valm et al. 2017; Wong, Ysselstein, and Krainc 2018). Mitochondria-lysosome contacts were observed using 2D and 3D electron microscopy (Aston et al. 2017; Wong, Ysselstein, and Krainc 2018) as well as correlative light electron microscopy (CLEM) of LysoTracker-positive vesicles in contact with mitochondria (Wong, Ysselstein, and Krainc 2018) or CLEM combined with focused ion beam scanning electron microscopy (FIB-SEM) which showed Lamp1 and dextran positive vesicles stably contacting mitochondria (Fermie et al. 2018). Contacts between mitochondria and lysosomes were also observed by lattice light sheet spectral imaging (Valm et al. 2017), and were found to be less frequent than contacts involving the ER (Valm et al. 2017). In

addition, mitochondria-lysosome contacts were observed by structured illumination microscopy (SIM) imaging of organelles labeled by mitochondrial (Chen et al. 2018) or lysosomal (Han et al. 2017) dyes or fluorescently-labeled proteins (Wong, Ysselstein, and Krainc 2018) which showed that mitochondria could first contact one lysosome and subsequently move on to contact another lysosome (Han et al. 2017). Moreover, contacts were also seen by immunofluorescent staining of endogenous mitochondrial (Tom20) and lysosomal (Lamp1) membrane proteins by confocal microscopy (Itoh et al. 2018) or 3D SIM imaging (Wong, Ysselstein, and Krainc 2018). Finally, mitochondria-lysosome contacts were also labeled by sensitized emission fluorescence resonance energy transfer (SE-FRET) between TOM20–Venus on the outer mitochondrial membrane and LAMP1–mTurquoise2 on the lysosomal membrane (Wong, Ysselstein, and Krainc 2018).

Mitochondria-lysosome contact sites have an average distance between mitochondrial and lysosomal membranes (Aston et al. 2017; Wong, Ysselstein, and Krainc 2018) consistent with previously observed membrane contact sites (10–30 nm) (Csordas et al. 2006; Phillips and Voeltz 2016). Approximately 15% of lysosomes are in contact with mitochondria at any point in time with mitochondria-lysosome contact sites remaining stably tethered for an average of 60 sec (Wong, Ysselstein, and Krainc 2018) although contacts demonstrate a varying range of tethering durations, lasting as long as 13 minutes (Han et al. 2017). Bulk transfer of either lysosomal luminal contents or mitochondrial matrix or inter-membrane space proteins across organelles are not observed at sites of contact (Wong, Ysselstein, and Krainc 2018), and contacts do not represent autophagosome biogenesis events or mitophagy as they are negative for multiple autophagosome markers including *ULK1*, *Atg5*, and *LC3* (Wong, Ysselstein, and Krainc 2018). Contact formation was further confirmed to be independent of mitophagy as knockout of five autophagy receptors

(NDP52, OPTN, NBR1, TAX1BP1 and p62) did not prevent mitochondria-lysosome contact formation (Chen et al. 2018). In addition, mitochondria that form contacts are distinct from mitochondrial-derived vesicles (MDVs) as they contain both outer mitochondrial membrane and matrix proteins (Wong, Ysselstein, and Krainc 2018) and are substantially larger than previously described MDVs (~100 nm (MDVs) versus ~500 nm (mitochondria)) (Sugiura et al. 2014), suggesting that mitochondria-lysosome contact sites do not represent sites of mitophagy or lysosomal engulfment of bulk mitochondria. (Wong et al. 2019)

Regulation of mitochondria-lysosome contact tethering/untethering

Mitochondria-lysosome contact site tethering is mechanistically regulated by multiple proteins on both the mitochondrial and lysosomal membranes (**Figure 1.2**). The small GTPase Rab7 which is a master regulator of lysosomal dynamics modulates mitochondria-lysosome contact site tethering and untethering dynamics through its ability to alternate between an active, lysosomal-localized GTP-binding state and an inactive, cytosolic GDP-binding state. Contact tethering is promoted by lysosomal GTP-bound Rab7 and may be tethered to mitochondria via Rab7 effector proteins which bind GTP-bound Rab7 on the lysosome. Importantly, expression of RAB7 Q67L, a constitutively active GTP-bound form which is unable to undergo GTP hydrolysis, is sufficient to increase the number of lysosomes contacting mitochondria and results in prolonged contacts (Wong, Ysselstein, and Krainc 2018).

Subsequent mitochondria-lysosome contact untethering is mediated by Rab7 GTP hydrolysis which first involves the recruitment of cytosolic TBC1D15 (Rab7 GAP) to

mitochondria via the outer mitochondrial membrane protein Fis1 (Onoue et al. 2013; Peralta, Martin, and Edinger 2010; Zhang et al. 2005). Once recruited to mitochondria, TBC1D15 is able to interact with lysosomal GTP-bound Rab7 to drive its hydrolysis to a GDP-bound state. GDP-bound Rab7 can no longer bind Rab7 effectors and also loses its lysosomal membrane localization (Langemeyer, Frohlich, and Ungermann 2018), leading to mitochondria-lysosome contact untethering (Wong, Ysselstein, and Krainc 2018) potentially via the loss of Rab7 effector tethering. Importantly, inhibition of Rab7 GTP hydrolysis with either TBC1D15 (D397A or R400K) mutants, which lack GAP activity (Onoue et al. 2013), prevents efficient mitochondria-lysosome contact untethering, resulting in prolonged contacts (Wong, Ysselstein, and Krainc 2018). Interestingly, TBC1D15 mutants have no effect on contact formation, suggesting that TBC1D15-dependent Rab7 GTP hydrolysis is limited to regulating contact untethering but not the formation of contacts. In addition, mutant Fis1 (LA), which is unable to recruit TBC1D15 to mitochondria (Onoue et al. 2013), as well as complete knockout of either TBC1D15 or Fis1, prevent efficient mitochondria-lysosome contact untethering, leading to prolonged contacts (Wong, Ysselstein, and Krainc 2018). Thus, Rab7 GTP hydrolysis, which requires interaction of both lysosomal (Rab7) and mitochondrial-localized (TBC1D15, Fis1) proteins at contact sites, provides a mechanism for the regulation of mitochondria-lysosome untethering. Recently, Rab7 was also found to regulate contacts between mitochondria and late endosomes associated with ribosomes undergoing local protein synthesis in axons of retinal ganglion cells, which were further disrupted by disease-associated mutations in *Rab7* (Cioni et al. 2019). Of note, as previous inter-organelle contact sites have been associated with multiple types of tethers (Eisenberg-Bord et al. 2016), other proteins

distinct from Rab7 or its effectors may also contribute to mitochondria-lysosome contact site tethering.

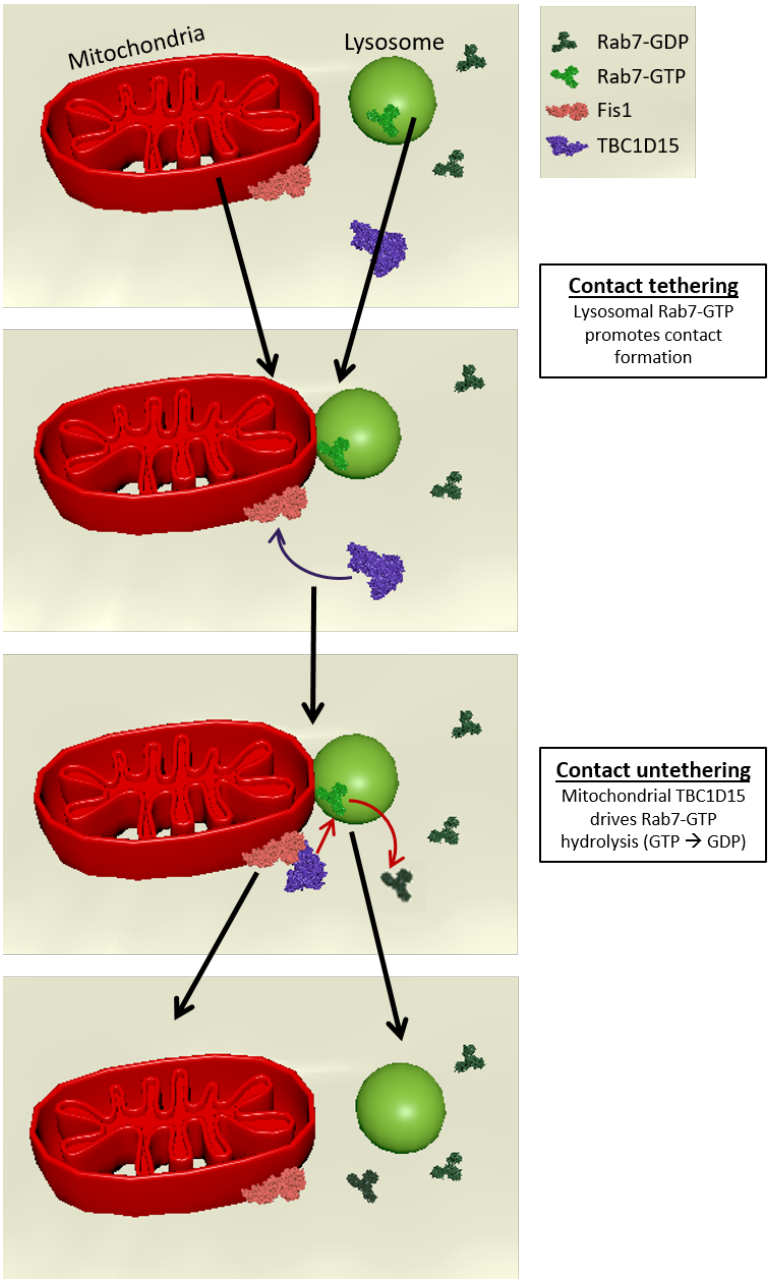


**Figure 1.2 Regulation of Mitochondria–Lysosome Contact Tethering/Untethering by Rab7 GTP Hydrolysis.** Mitochondria–lysosome contact dynamics involve: (1) contact tethering, which is promoted by lysosomal GTP-bound Rab7 and is potentially mediated by Rab7 effector proteins (which bind GTP-bound Rab7) to directly tether lysosomes to mitochondria (Wong, Ysselstein, and Krainc 2018); (2) contacts subsequently undergo untethering, which is mediated by recruitment of cytosolic TBC1D15 (Rab7 GAP) to mitochondria via the outer mitochondrial membrane protein Fis1. At mitochondria–lysosome contact sites, mitochondrial TBC1D15 is able to interact with lysosomal GTP-bound Rab7 to drive Rab7 GTP hydrolysis from a GTP-bound to GDP-bound state. GDP-bound Rab7 can no longer bind Rab7 effectors and also loses its lysosomal membrane localization, leading to the loss of tethers and mitochondria–lysosome contact untethering (Wong, Ysselstein, and Krainc 2018). Additional proteins apart from Rab7 may also be involved in regulating mitochondria–lysosome contact tethering.

Bidirectional regulation of organelle dynamics at mitochondria-lysosome contact sites

Lysosomal dynamics are acutely regulated by Rab7 effector proteins which preferentially bind GTP-bound Rab7 on the lysosomal membrane, such as RILP and FYCO which mediate lysosomal retrograde and anterograde microtubule transport respectively (Jordens et al. 2001; Pankiv et al. 2010), and the HOPS complex which mediates lysosomal tethering and fusion (Balderhaar and Ungermann 2013). Mitochondria-lysosome contact sites thus offer a platform for mitochondrial-localized proteins to regulate lysosomal dynamics via modulation of Rab7-GTP binding. As mitochondrial TBC1D15 promotes Rab7 GTP hydrolysis at contacts leading to the termination of GTP-bound Rab7 (Wong, Ysselstein, and Krainc 2018), this can simultaneously result in both contact site untethering and the release of Rab7 effector proteins from GTP-bound Rab7 and the lysosomal membrane (**Figure 1.2**), thus regulating lysosomal dynamics. Indeed, expression of mitochondrial-localized mutant TBC1D15 (D397A or R400K) lacking GAP activity leads to enlarged lysosomes (Wong, Ysselstein, and Krainc 2018), consistent with the lysosomal morphology observed upon inhibition of RAB7 GTP hydrolysis. Thus, mitochondria-lysosome contact sites may help promote Rab7 GTP hydrolysis and regulate the dynamics of a subset of lysosomes within the cell which are in contact with mitochondria.

Mitochondria-lysosome contact sites are also able to regulate mitochondrial dynamics, as the majority of mitochondrial fission events (>80%) are marked by LAMP1-positive vesicles but not early endosomes or peroxisomes (Wong, Ysselstein, and Krainc 2018). Disrupting mitochondria-lysosome contact untethering dynamics by inhibiting Rab7 GTP hydrolysis with mutants GTP-bound Rab7 Q67L, TBC1D15 (D397A or R400K) or Fis1 (LA) decreases rates of mitochondrial fission and disrupts the mitochondrial network (Wong, Ysselstein, and Krainc 2018).

All mitochondrial fission events marked by lysosomes were also positive for Drp1, a dynamin-related GTPase that facilitates the constriction of the outer mitochondrial membrane during mitochondrial fission (Friedman and Nunnari 2014). Interestingly, a novel, brain-enriched mouse isoform of *DRP1* containing four alterative exons, DRP1ABCD, was recently identified which associated with LAMP1-positive vesicles and localized to the interface between mitochondria and lysosomes (Itoh et al. 2018). Proper localization of DRP1ABCD depended on the acidification but not the proteolytic activity of late endosomes and lysosomes (Itoh et al. 2018) and may point to additional roles for *Drp1* isoforms at mitochondria-lysosome contact sites. Thus, mitochondria-lysosome contact sites additionally act to regulate the mitochondrial network by marking sites of mitochondrial fission and regulating the rate of fission events, but the mechanistic details of the interplay between Rab7 GTP hydrolysis and mitochondrial fission machinery remains to be further elucidated.

## 1.4 INDUCED PLURIPOTENT STEM CELLS (iPSC) - DERIVED NEURONS

### 1.4.1 Induced Pluripotent Stem Cells (iPSC)

The discovery in 2006 of four transcription factors (*Sox2*, *Oct3/4*, *c-myc*, and *Klf4*) marked the development of pluripotent stem cells from mouse fibroblasts (Takahashi and Yamanaka 2006), and was later replicated in human somatic cells (Nakagawa et al. 2008; Yu et al. 2007). Current research efforts have identified protocols for generating induced pluripotent stem cells (iPSCs) from dermal fibroblasts, hematopoietic stem cells, adipocytes, and peripheral blood mononuclear cells (Gu et al. 2018; Qu et al. 2012; Takenaka et al. 2010; Wiedemann et al. 2012). Together,

these findings have opened the field to new advances in patient-specific cell lines and circumvented the need for embryonic stem cells which require gene editing and are linked to ethical concerns (Barker and de Beaufort 2013; Robertson 2001; Urbach, Schuldiner, and Benvenisty 2004). Furthermore, pluripotency now allows researchers to selectively differentiate stem cells into any somatic cell type, resulting in the generation of disease relevant tissues for study. iPSCs additionally offer a strategy for disease modeling using patient-specific cell lines and disease-relevant genetic backgrounds, thus allowing for new opportunities in therapeutic development and drug screening applications (**Figure 1.3**).

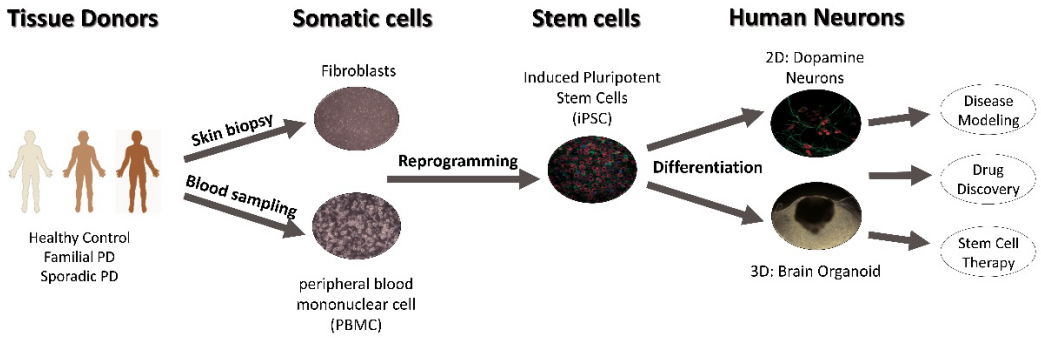


**Figure 1.3 Application of human induced pluripotent stem cell-derived neurons for disease modeling and drug discovery in Parkinson's disease.** Human somatic cells such as fibroblasts or peripheral blood mononuclear cell (PBMC) from healthy control, familial and sporadic PD patients are reprogrammed into human iPSCs. Human iPSCs are further differentiated into dopamine neurons or 3D brain organoid depending on the purpose. Differentiated tissues enable replication of Parkinson's disease in vitro and can be further used for disease modeling, drug discovery and dopamine replacement stem cell therapy.

### 1.4.2 iPSC-derived neurons

Due to the lack of access to human neuronal tissues (Arthur et al. 2016) and the intrinsic differences in animals models from human pathologies (Burbulla et al. 2017; Gitler, Dhillon, and Shorter 2017), iPSCs provide new methods for modeling disease pathology for multiple neurodegenerative diseases including Alzheimer's, Parkinson's, Amyotrophic Lateral Sclerosis (ALS), and Huntington's disease. Specifically, the identification of neural fate induction by TGFβ antagonists through dual SMAD inhibition (Chambers et al. 2009) has led researchers to further develop protocols for differentiating iPSCs into multiple different neuronal subtypes (cortical, cholinergic, dopaminergic, GABAergic, hippocampal, hypothalamic, motor, serotonergic and Purkinje neurons) as well as glial cells (astrocytes and oligodendrocytes) (Abud et al. 2017; Emdad et al. 2012; Hu et al. 2016; Kirkeby et al. 2012; Kirkeby et al. 2017; Kriks et al. 2011; Little et al. 2019; Lu et al. 2016; Maroof et al. 2013; Merkle et al. 2015; Nicholas et al. 2013; Nistor et al. 2005; Nizzardo et al. 2010; Shi, Kirwan, and Livesey 2012; Wang et al. 2015; Yang et al. 2017; Yu et al. 2014). Furthermore, iPSC differentiation protocols have also been optimized to produce mature electrophysiological neurons supporting basic synaptic functions (Bardy et al. 2015; Gunhanlar et al. 2018) and have also been transplanted into primates for potential therapeutic applications (Kikuchi et al. 2017). For Parkinson's disease (PD), the ability to generate patient-derived dopaminergic neurons has proved to be particularly insightful, with current differentiation protocols using dual-SMAD inhibition followed by Sonic Hedgehog and FGF8b signaling, and subsequent maintenance in BDNF, GDNF, ascorbic acid, and cAMP (Garcia-Leon, Vitorica, and Gutierrez 2019). Importantly, multiple studies have been able to recapitulate key PD pathological

features and shed light on new mechanistic pathways using patient-derived iPSC dopamine neurons.

### 1.4.3 Parkinson's disease patient iPSC-derived neurons

PD patient iPSC-derived DA neurons represent an important model for studying pathogenic phenotypes and mechanisms in PD (Burbulla et al. 2017). Importantly, Burbulla et al. emphasized the importance of human iPSC-DA neurons as a model for PD research by showing that time-dependent pathological cascade of PD pathogenesis is observed only in human neurons, and not reproduced in mouse neurons, due to the species-specific dopamine metabolism (Burbulla et al. 2017). Moreover, iPSC PD neurons have further been found to be relevant for investigations studying the GCase pathway as a potential therapeutic target for PD. GBA chaperones NCGC758 and NCGC607 were found to restore GCase activity and reduce substrate accumulation in the lysosome in multiple PD models of iPSC-DA neurons (Aflaki et al. 2016; Mazzulli, Zunke, Tsunemi, et al. 2016). In addition, studies on GCase have identified quinazoline inhibitors that can be derived into activators that stabilize GCase activity within iPSC-DA neurons and fibroblasts (Zheng et al. 2019). Moreover, inhibition of acid ceramidase using carmofur was shown to reduce α-synuclein accumulation in *GBA1* mutant iPSC-DA neurons (Kim, Jeon, et al. 2018), while reducing glycosphingolipids in *GBA1* mutant (N370S/c.84dupG) or α-synuclein triplication neurons diminished pathology and restored physiological α-synuclein conformers that associated with synapses (Zunke et al. 2018). Finally, recent work has identified a novel chemical series of GCase activators, including a new small-molecule modulator (S-181) that increased wild-type

GCase activity in iPSC-derived dopaminergic neurons from patients with 84GG-GBA1, as well as in LRRK2-, Parkin-, DJ-1-linked and sporadic PD (Burbulla et al. 2019). Thus, iPSC-derived patient neurons offer an important strategy for studying PD mechanisms, and for investigating GCase activity as a major target for PD therapeutic treatment that is associated with multiple forms of PD, including both genetic and idiopathic cases (Marotta, Kim, and Krainc 2020).

# CHAPTER 2.

# METHODS & MATERIALS

## 2.1 Human iPSC culture and characterization

Detailed procedures for iPSC culture and neuronal differentiation have been described previously (Burbulla et al. 2019). (**Figure 2.1**) Healthy control and PD patient skin fibroblasts16 (GBA1 heterozygous 84GG mutation (c.84dupG frameshift mutation) which prevents the expression of the mutant allele, resulting in reduced GCase levels arising from a single wild-type copy of GBA1; and GBA1 heterozygous p.N370S mutation) were reprogrammed into iPSCs through Northwestern University Stem Cell Core Facility, using Sendai virus (SeV) based delivery of four Yamanaka factors (Oct, Sox2, Klf4 and c-Myc). We also generated an isogenic control iPSC line by correcting the mutation using CRISPR/Cas9 protocols (Ran et al. 2013) as recently described (Burbulla et al. 2019). Guide RNAs targeting the mutation were cloned into vector PX461 (Addgene #48140) carrying the cDNA encoding for GFP-tagged Cas9 nuclease. The plasmid was electroporated into GBA1 84GG mutant iPSCs together with ssODN carrying the corrected sequence. After 48 hours, generation of an isogenic control line was confirmed by FACS-sorting and sequencing. All iPSCs were maintained either in mTeSR™1 or mTeSR™ Plus media (Stemcell technologies, #85850, #05825) and cells were passaged as small chunks every 6-8 days depending on confluence. All iPSC lines have been routinely characterized for expression of pluripotency markers. Cells were plated on PDL coated coverslips and subjected to immunofluorescence staining for NANOG, OCT4, SSEA4, and TRA1-81. Genomic integrity was

confirmed as described previously (Burbulla et al. 2019). Mycoplasma tests were performed on a monthly basis to maintain qualified iPSC lines.

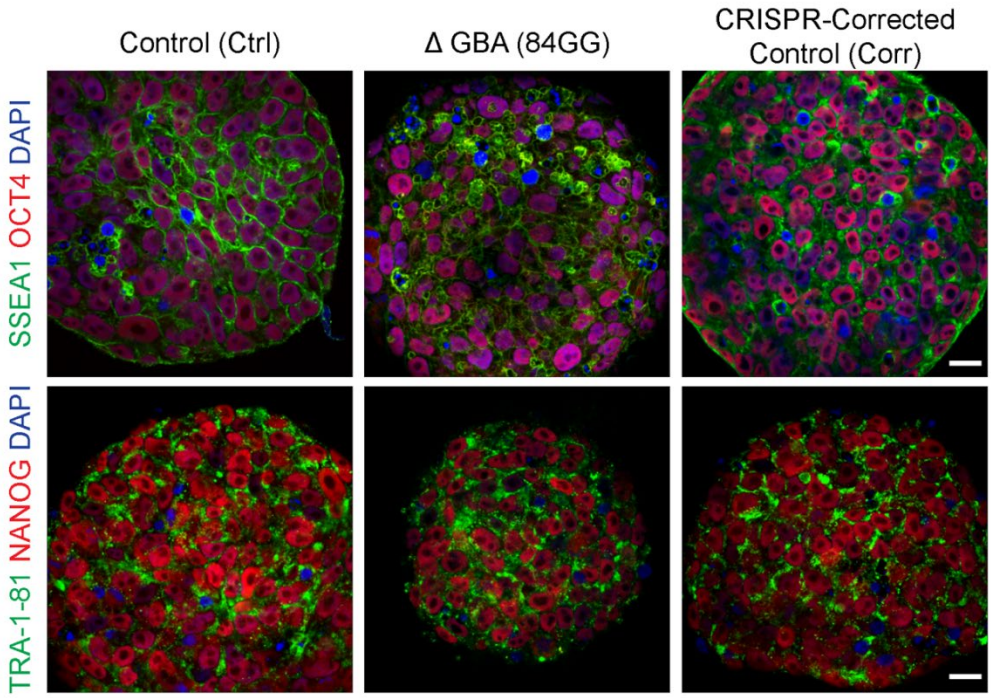


**Figure 2.1 Characterization of wild-type control, PD patient mutant GBA1 and CRISPR-corrected isogenic control human iPSCs.** Immunocytochemistry demonstrated that wild-type Control (Ctrl), Mutant GBA1 (ΔGBA; het 84GG) and CRISPR-corrected isogenic control (Corr) human induced Pluripotent Stem Cells (iPSCs) expressed pluripotency markers including Oct4, SSEA1, TRA-1-81 and Nanog. Top panel, merged images of Oct4 (red), SSEA1 (green), and DAPI (blue) nuclear staining from each line. Bottom panel, merged images of Tra 1-81 (green), Nanog (red), and DAPI (blue) nuclear staining. Scale bar, 10μm. (N = 3 independent experiments).

## 2.2 Generation and characterization of hiPSC - derived dopaminergic neurons

Human dopaminergic iPSC-derived neurons were differentiated using previously established protocol (Kriks et al. 2011) for analysis of mitochondria-lysosome contacts (**Figure 2.2**). Briefly, after plating single iPSCs, cells were treated with factors according to the original protocol. At day 13 of differentiation, cells were passaged en bloc (size of 1–2 mm) onto 10cm culture dishes pre-coated with poly-d-lysine (PDL) (Sigma, #P1149) / laminin (Invitrogen, #23017-015). At day 25, neurons were treated with accutase and passaged onto PDL / laminin coated culture dishes, and subjected to dopaminergic marker characterization through immunocytochemistry (ICC) using tyrosine hydroxylase (TH), forkhead box protein A2 (FOXA2), LIM Homeobox Transcription Factor 1 Alpha (LMX1A) together with neural specific marker β-III-tubulin (TUJ1) at day 30. After day 50, neurons were considered mature and maintained in Neurobasal media (Life Technologies, # 21103049) containing Neurocult SM1 (Stemcell technologies, #5711). Neurons at day 50-60 were used for immunostaining, electron microscopy, live cell time-lapse confocal imaging, live cell or fixed cell super-resolution structured illumination microscopy (SIM). Neurons from $N \geq 3$ independent experiments (biological replicates; batches of neuron differentiation) per condition were used for each experiment.

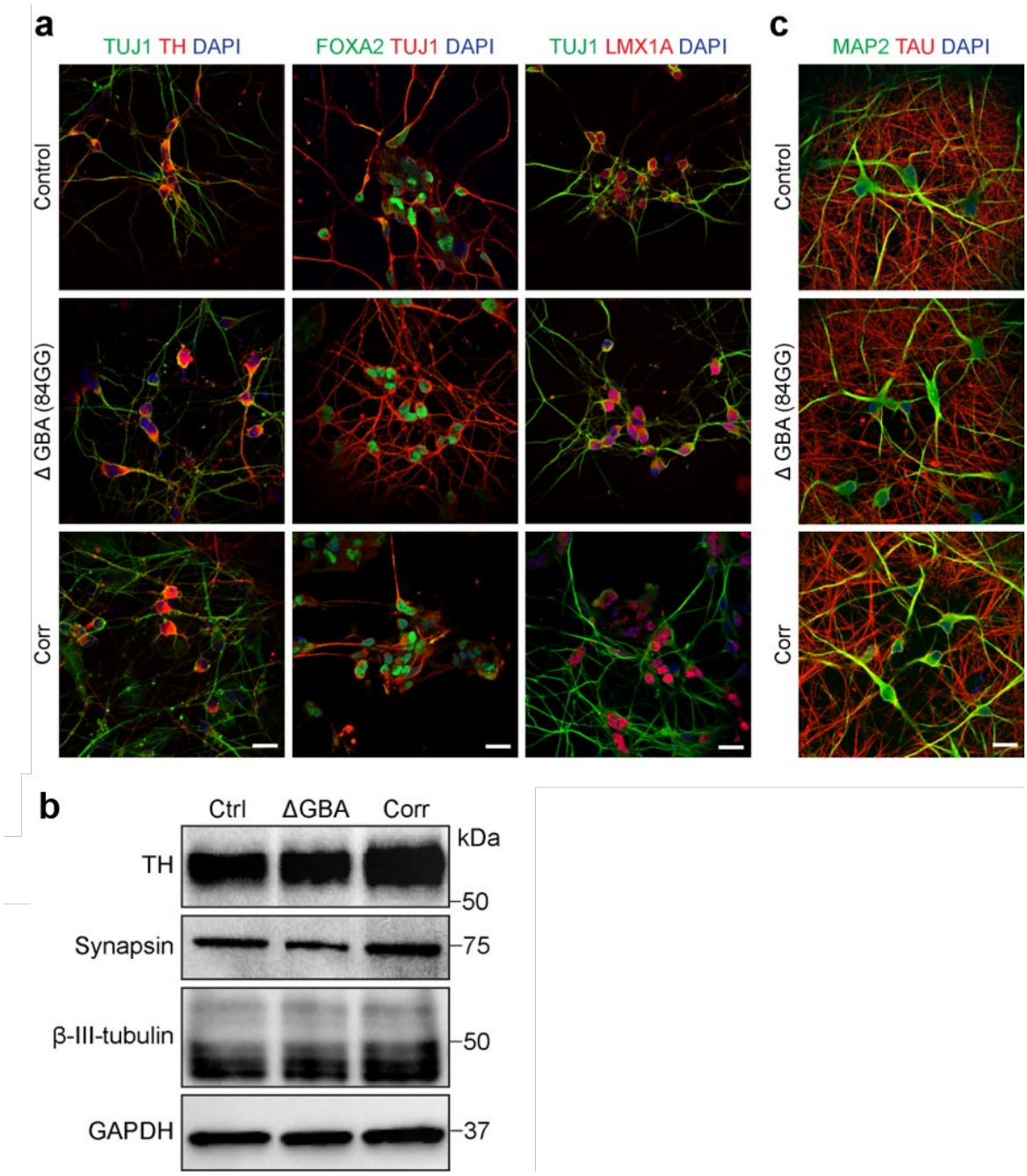
a
TUJ1 TH DAPI
FOXA2 TUJ1 DAPI
TUJ1 LMX1A DAPI
Control
Δ GBA (84GG)
Corr
c
MAP2 TAU DAPI
Control
Δ GBA (84GG)
Corr
b
Ctrl
ΔGBA
Corr
kDa
TH
50
Synapsin
75
β-III-tubulin
50
GAPDH
37

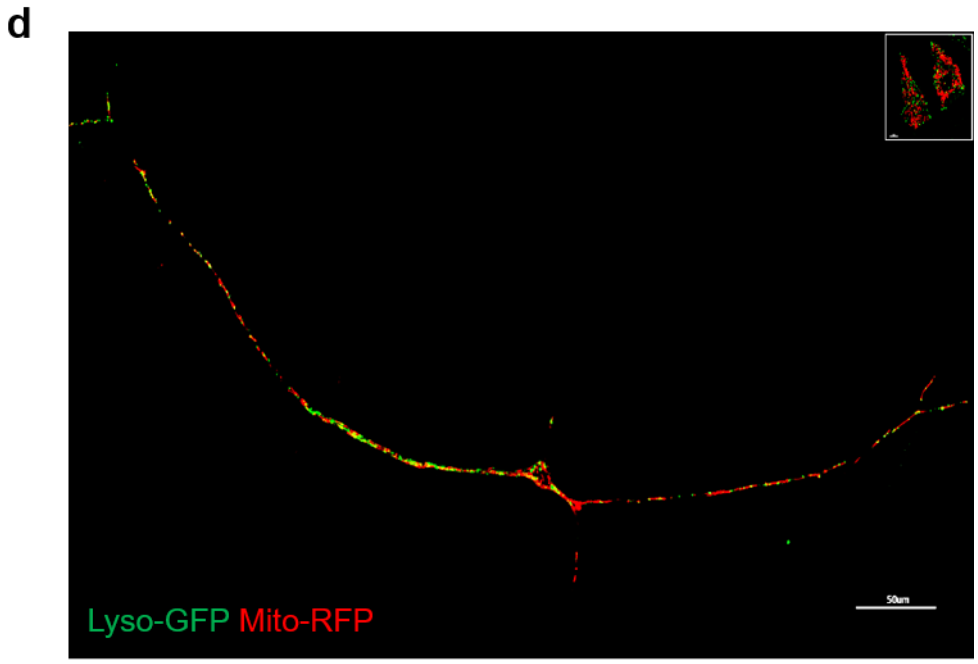


**Figure 2.2 Characterization of wild-type control, PD patient mutant GBA1 and CRISPR-corrected isogenic control human iPSC-derived dopaminergic neurons.** (a) Human iPSCs from wild-type control (Control), mutant GBA1 (ΔGBA) and CRISPR-corrected isogenic control (Corr) lines were differentiated into midbrain dopaminergic neurons. Neurons were analyzed by immunofluorescence for the expression of dopamine (TH; tyrosine hydroxylase), midbrain (FOXA2, LMX1A) and neuronal cytoskeletal (Tuj1) markers at day 30. Scale bar = 20µm. (b) Western blot analysis of human iPSC-derived dopaminergic neurons at day 50. The expression of dopaminergic neuronal markers (TH, Synapsin and β−iii Tubulin) were confirmed in Ctrl, ΔGBA and Corr neurons. GAPDH was used as a loading control. (N = 3 independent experiments). (c) Immunocytochemistry of dendritic marker Map2 (green) and axonal marker tau (red) in human iPSC-derived dopaminergic neurons at day 50. Scale bar = 20µm. (N = 3 independent experiments). (d) A tiled confocal image of an iPSC-derived human dopaminergic neuron and a single frame of Hela cells (white box) expressing baculoviral Lysosome-GFP and Mitochondria-RFP. Scale bar = 50µm.

### 2.3 Immunocytochemistry (ICC)

Cells were immunostained for multiple antibodies depending on the purpose of each experiment. Neurons were plated on PDL / laminin-coated coverslips and fixed in 4% paraformaldehyde in PBS for 20 min and permeabilized with 10% FBS and 0.1% saponin in PBS

at room temperature. For GlcCer staining, 10% FBS was substituted with 2% gelatin (Sigma, #G1393). Cells were then immuno-labeled with the following primary antibodies: Oct4 (Abcam, #19857, 1:100); SSEA1 (Millipore, MAB#4304, 1:100); Nanog (R&D systems, #AF1997, 1:50); Tra-1-81 (Millipore, #MAB4381, 1:100); TH (Calbiochem, #657012, 1:500); β-III-tubulin (Biolegend, #801202, #802001, 1:1000); Lmx1a (Milipore, MAB#10533, 1:500); FoxA2 (Santa Cruz, #sc-101060, 1:100); Tom20 (Abcam, #78547, 1:100); Lamp1 (Santa Cruz, #sc-20011, 1:100); Map2 (Novus Biological, #NB300213, 1:3000); Tau (DAKO, #A002401-2, 1:300); GlcCer (Glycobiotech, #RAS_0011, 1:100). After overnight incubation at 4°C, coverslips were washed three times with PBS for 5 min each, incubated in Alexa-conjugated secondary antibodies (Invitrogen, #A21206, #A21202, #A11029, #A11011, #A10042, #A10037, #A21449, 1:1000) for 1 h at room temperature, washed three times and mounted onto Superfrost Plus microscope slides (Fisherbrand, #12-550-15) with VECTASHIELD HardSet Antifade Mounting Medium (Vector Labs, #H-1400). Alternatively, ProLong™ Diamond Antifade Mountant (ThermoFisher Scientific, #P36959) was used for SIM sample preparation. Images were obtained on either a Leica DMI4000B confocal microscope using Leica Application Suite X (Leica) or a Nikon A1R laser scanning confocal microscope with GaAsp detectors using NIS-Elements (Nikon). Colocalization was measured using the EzColocalization plugin in ImageJ (National Institutes of Health (NIH)) (Stauffer, Sheng, and Lim 2018).

**2.4 Proximity Ligation Assay (PLA)**

Proximity between outer mitochondrial membrane protein Tom20 and lysosomal membrane protein Lamp1 was detected using Duolink™ proximity ligation assay kit (Sigma

Aldrich, #DUO92101) according to the manufacturer's protocol. Neurons were plated on PDL / laminin-coated coverslips and cells were immuno-labeled with Tom20 (Abcam, #78547, 1:100) and Lamp1 (Santa Cruz, #sc-20011, 1:100). Images of red PLA signals were collected using Nikon A1R laser scanning confocal microscope with GaAsp detectors.

**2.5 Electron Microscopy (EM)**

For electron microscopy (EM), neurons were grown on PDL / laminin-coated glass coverslips. Neurons were fixed with 2.5% glutaraldehyde and 2% paraformaldehyde in 0.1 M cacodylate buffer, pH 7.3 for 30 min at room temperature, and then submitted to the Northwestern EM core facility for subsequent processing. After post-fixation in 1% osmium tetroxide and 3% uranyl acetate in PBS, cells were dehydrated in an ethanol series, embedded in Epon resin and polymerized for 48 h at 60 °C. Ultrathin sections were made using a UCT ultramicrotome (Leica Microsystems) and contrasted with 4% uranyl acetate and Reynolds's lead citrate. Samples were imaged on a FEI Tecnai Spirit G2 transmission electron microscope (FEI) operated at 80 kV. Images were captured with an Eagle 4k HR 200kV CCD camera and analyzed using ImageJ (National Institutes of Health (NIH)).

**2.6 Live-cell time lapse confocal microscopy**

Live cell time-lapse confocal imaging was conducted of mitochondria and lysosomes labeled with the following reagents: Lentivirus expressing Tom20-RFP or Lamp1-GFP (MOI=3, 3 days); CellLight® BacMam 2.0 baculovirus (PPC (particles per cell) = 40, 2 days)

[ThermoFisher: Lysosomes-GFP (#C10596), Lysosomes-RFP (#C10597), Mitochondria-RFP (# C10601), ER-GFP (#C10590)]; LysoTracker™ Red DND-99 (2μM, 45min;ThermoFisher, #L7528); MitoTracker™ Green FM (0.125μM, 45min; ThermoFisher, #M7514); and TMRM (0.1μM, 45min; Fisher scientific, #T669), which is a cell-permeant dye that accumulates in active mitochondria with intact membrane potential (ΔΨm). For analysis of lysosomal-drug treated cultures, neurons were treated with GCase inhibitor conduritol-b-epoxide (CBE) (50μM, 7 days) (Cayman Chemicals, #15216), carmofur (7.5μM, 2 days) (Cayman Chemicals, #14243), E-64D (10μM, 24hrs) (Cayman Chemicals, #13533) or Pepstatin A (10μM, 24 hrs) (Milipore, #516481). For live imaging, neurons were grown on glass-bottomed culture dishes (MatTek, #P35G-1.5-14-C) in Neurobasal media (Life Technologies, # 21103049) containing Neurocult SM1 (Stemcell technologies, #5711). Samples were imaged on a Nikon A1R laser scanning confocal microscope with GaAsP detectors using a Plan Apo λ 100x 1.45 NA oil immersion objective (Nikon) using NIS-Elements (Nikon). During the imaging, culture dishes were kept in a temperature-controlled chamber (37 °C) at 5% CO2.

**2.7 Structured illumination microscopy (SIM)**

Mitochondria-lysosome contact sites in both fixed and live neurons were imaged using super-resolution structured illumination microscopy (SIM). For SIM analysis, neurons were cultured on nitric acid treated, PDL/laminin coated High Precision Glass Cover Slip (Bioscience Tools, #CSHP-No1.5-12). Samples were prepared using the same protocol for regular immunocytochemistry (ICC). Super-resolution images were taken on a Nikon N-SIM system with

a 100× oil immersion objective lens, 1.49 NA (Nikon). Images were captured and reconstructed using Nikon NIS-Elements.

### 2.8 Neuronal compartmentalization of mitochondria-lysosome contacts

Dendrites and axons were identified as positive for either MAP2 or Tau immunostaining respectively in fixed cells. In live cell imaging, axons and dendrites were distinguished using Map2-GFP lentiviral expression. Neuron cultures had dendrites that were thicker and shorter than axons, with many axons branching from dendrites, consistent with previous observations in dopaminergic neurons (Hausser et al. 1995). Using these characteristic morphologies, neurites were further characterized as dendrites in subsequent imaging experiments involving live or fixed neurons.

### 2.9 Image Analysis

To quantify contacts, live neurons were imaged at 2-sec intervals for 3-6 min. Contacts were defined as mitochondria and lysosomes in close proximity at the beginning of the video and which lasted for greater than 20 sec. The duration, number of contacts and the density of mitochondria were analyzed manually in NIS-Elements (Nikon) for further examination. The minimum duration of contacts was quantified as the time before contact termination and dissociation (mitochondria and lysosomes detaching from one another) over the course of 5-min videos. Any contacts that lasted beyond 5-min were categorized as 300 sec in bar graphs and as >300 sec in histograms for the minimum duration of mitochondria–lysosome contacts. The

percentage of lysosomes in contacts was quantified as the percentage of lysosomes in contact with mitochondria for greater than 20 sec divided by the total number of Lyso-GFP positive vesicles in the region of interest. The length of neurites and the area of cell bodies were measured using a built-in function of ImageJ (National Institutes of Health (NIH)).

### 2.10 Generation and transduction of lentiviral constructs

Human MAP2 Lentiviral cDNA ORF vector was purchased from Sino Biological Inc. (#HG13690-ACGLN). Lentiviral vectors were packaged and transfected into HEK 293FT cells using X-treme Gene HP DNA transfection (Roche, #06366236001) together with helper plasmids psPAX2 (Addgene, #12260) and pLP3 (Invitrogen). Quantitation of retroviral antigens was determined using ZeptoMetrix Corporation RETROtek HIV-1 p24 Antigen ELISA kits (Fisher Scientific, #22-156-700). Concentrated viruses were aliquoted and kept at -80°C for future use. For Map2 expression, neurons were transduced with Map2 Lentivirus and incubated 4 days before live cell confocal imaging or fixation.

### 2.11 Live cell Glucocerebrosidase (GCase) activity assay

The enzymatic activity of GCase in live human neurons was measured as previously described15 with minor modifications. The neuron culture media was changed to phenol red-free Neurobasal media (Thermo Fisher, # 12348017) containing Neurocult SM1 (Stemcell technologies, #5711) a day before the measurement. The next day, half of the neurons were treated with DMSO and 50μg/ml fluorescein di-ß-D-glucopyranoside (PFB-FDGluc) (Fisher Scientific, #

P11947) in phenol red-free Neurobasal media. Another half were treated with 400nM Bafilomycin A1 (BafA1) (Cayman chemicals, #11038) and 50µg/ml PFB-FDGluc in phenol red-free Neurobasal media. Neurons were incubated for 1 h at 37°C in the dark to allow for the accumulation of PFB-FDGluc, a substrate of GCase, in lysosomes. GCase activity was quantified for 4.5 h with 30 min intervals by measuring fluorescence upon the cleavage of PFB-FDGluc over time in a Spectramax i3 plate reader (Molecular Devices) (Ex=485nm, Em=525nm). Activity within the lysosomal compartment was determined by measuring the response to BafA1. Non-lysosomal GCase activity was interpreted as the activity that was not responsive to BafA1. After the last measurement, neurons were washed 3 times with PBS, and were lysed in RIPA lysis buffer. BCA protein assay was done according to the manufacturer's protocol (Thermo Fisher, #23225) to measure total protein amount required for normalization. Total GCase activity was quantified by calculating the area under the DMSO curve (AUC) using Prism7 (GraphPad) software. Lysosomal GCase activity was obtained by measuring the area between BafA1 and DMSO curves.

**2.12 SDS-PAGE and Western blotting (WB)**

Neurons were collected in ice-cold PBS and centrifuged at 400x g for 5 min at specific time points (e.g. day 30 for neuron characterization, day 40-70 for biochemical analysis of organelle contacts). Pellets were lysed in N-PER™ Neuronal Protein Extraction Reagent (Thermo Scientific, #87792) with cOmplete protease inhibitor cocktail (Sigma, #11836170001), and lysates were collected according to the manufacturer's protocol. After boiling for 20 min in 4X Laemmeli sample buffer, protein samples were separated on 4-20% Tris-glycine precasted gel (Invitrogen, #XP04202BOX) and transferred to PVDF or nitrocellulose membranes using Trans-blot TurboTM

transfer system (Biorad). Membranes were blocked with 5% milk in 1X Tris-buffered saline [50 mM Tris, pH 7.4, 150 mM NaCl] with 0.1% Tween (TBST) for 1 h at room temperature and incubated with a primary antibody, 4°C, overnight: Rab7 (Cell Signaling, #D95F2, 1:1000; Abcam, #ab137029, 1:1000); TBC1D15 (Sigma Aldrich, #SAB2701508, 1:500); Fis1 (Alexis, # ALX-210-1037-0100, 1:1000); GAPDH (Millipore, #MAB374, 1:2000); GBA (Abnova, #H00002629-M01, 1:500); TH (Calbiochem, #657012, 1:1000); Synapsin (Santa Cruz, #sc-398849, 1:1000); βIII tubulin (tuj1) (Biolegend, #801202, 1:5000); AMPKα (Cell Signaling, #2532, 1:1000); Phospho-AMPKα (Cell Signaling, #2535, 1:1000); Ccz1 (Santa Cruz, #sc-514290, 1:1000); Mon1 (Abcam, #ab103919, 1:500); Tom20 (Abcam, #ab56783, 1:1000); Lamp1 (Santa Cruz, #sc-20011, 1:500). The next day, after three times of washing with 1X TBST, membranes were incubated in secondary goat anti-mouse and goat anti-rabbit HRP antibody (Jackson Immuno Research lab, #115-035-146, #111-035-144, 1:10,000) diluted in 5% milk in 1X TBST for 1 h and washed three times with 1X TBST. HRP signal was developed using Clarity chemiluminescence substrate (Biorad, #170-5061) or Lumigen ECL Ultra (Lumigen, #TMA-100), and images were taken on the ChemiDoc XRS+ imaging station (Biorad). Protein levels were normalized against GAPDH. Quantification was done using ImageJ (National Institutes of Health (NIH)).

**2.13 Quantitative RT-PCR**

Total RNA was purified from neurons using RNeasy Micro Kit (Qiagen, #74004) and transcribed to cDNA using the High-Capacity cDNA Reverse Transcription Kit (ThermoFisher, # 4368814). Quantitative RT-PCR was performed using the 7500 Fast Real-Time PCR system (Applied Biosystems), with ssoAdvanced universal SYBR Green Supermix (BioRad, # 1725271).

The following pre-designed primer sets were used: TBC1D15 (PrimerBank ID # 226342866c3) and GAPDH (PrimerBank ID #378404907c2) (Table 1).

| | Primer Bank ID | Forward primer sequence | Reverse primer sequence |
|---|---|---|---|
| **TBC1D15** | 226342866c3 | AAAAGGACCCTTATACGGCAAC | CGCTGCCTCTCAAACTGTCAA |
| **GAPDH** | 378404907c2 | ACAACTTTGGTATCGTGGAAGG | GCCATCACGCCACAGTTTC |

**Table 2.1 Primer sequences for quantitative RT-PCR.**

## 2.14 Glutathione Transferase-Rab Interacting Lysosomal Protein (GST-RILP) Pull-Down Assay

To determine active GTP-bound Rab7 levels in neurons, GST-RILP pull-down assay was performed as previously described25 with minor modifications. Plasmids were gifts from Aimee Edinger (Addgene plasmid #79149). GST-control and GST-fused Rab7 binding domain of RILP protein (nucleotides 658-897) were expressed in BL21 bacteria. Bacteria were collected and lysed in B-PER™ Bacterial Protein Extraction Reagent (Thermo Scientific, #78248) with DTT 1,4-Dithiothreitol (1mM), EDTA (1mM) and cOmplete protease inhibitor cocktail (Sigma, #11836170001). Proteins were purified using pre-equilibrated 50% slurry of glutathione-Sepharose 4B beads (GE Healthcare) and quantified using the BCA assay. Neurons to be analyzed in the pull-down assay were pelleted and lysed in pull-down buffer (20 mM HEPES, 100 mM NaCl, 5 mM MgCl2, 1% TritonX-100, and protease inhibitors). GST-control beads and GST-RILP beads were added to the neuron lysates and the samples were rocked overnight at 4°C, followed

by washing with cold pull-down buffer. Bound proteins were eluted by boiling in 2X Laemmli sample buffer (Sigma Aldrich, # S3401) and used for western blot analysis.

### 2.15 Seahorse XF Cell Mito Stress Test

Oxygen consumption rate (OCR) of neurons was analyzed using an XF 24 Extracellular Flux Analyzer (Seahorse Biosciences) according to the manufacturer's protocol. 1.25 x 10^5 neurons were plated on one well of XF24 cell culture microplates. Four empty wells without neurons were used as background control for temperature-sensitive fluctuations in OCR analysis. Before the assay, culture medium was replaced with Seahorse XF medium (Seahorse Bioscience, #103575-100) supplemented with 1mM sodium pyruvate (Corning®, #25-000-CI), 10mM D-glucose (Sigma Aldrich, #G8769) and 2mM glutamine (gibco, #25030-081) and incubated for 1 hour in a CO2-free incubator. OCR was measured, after sequential injection of 1 μM oligomycin, carbonyl cyanide p-trifluoromethoxyphenylhydrazone (CCCP) and Antimycin A. After the assay, neurons were lysed and subjected to BCA protein assay (Thermo Fisher, #23225) for normalization.

### 2.16 Total Cellular ATP Assay

Total cellular ATP content was measured using the ATPlite kit (PerkinElmer, #6016943) according to the manufacturer's protocol. Neurons were plated on black 96-well plates (Thermo Fisher, #237108) at a density of 5 x104/well. Neurons were lysed in lysis solution provided in the

kit and luminescence was measured in a Spectramax i3 plate reader (Molecular Devices). Neuron lysates were subjected to BCA protein assay (Thermo Fisher, #23225) for normalization.

### 2.17 Mitochondrial Drug Treatment

HeLa cells were cultured in Dulbecco's modified Eagle's medium (DMEM) (Gibco, #11995-065) supplemented with 10% FBS, 100 U/mL Penicillin-Streptomycin (Gibco, #15140-122). A day after passaging, cells were treated for 0, 4 and 8 hrs with CCCP (10μM) (Sigma Aldrich, #C2759), Rotenone (100nM) (Sigma Aldrich, #R8875), Antimycin (1μM) (Sigma Aldrich, #A8674) or Oligomycin (1μM) (Sigma Aldrich, #O4876). Treated cells were lysed in RIPA buffer (Boston Bioproduct, #BP-115-5x) with cOmplete protease inhibitor cocktail (Sigma, #11836170001), and lysates were subjected to BCA protein assay (Thermo Fisher, #23225) and SDS-PAGE.

### 2.18 Statistical Analysis

For all statistical tests, cells from $N \geq 3$ independent experiments (biological replicates) per condition were used (see text and figure legends for details). Data were analyzed using unpaired two-tailed Student t-test (for two datasets) or one-way ANOVA with Tukey's post hoc test (for multiple datasets). Bar graph presented are in the form of means ± SEM. Statistics and graphing were performed using Prism 7 (GraphPad) software. Videos and images were processed using NIS-Elements (Nikon) and assembled using ImageJ. All figures were assembled in Adobe Illustrator.

# CHAPTER 3.

# DYNAMICS OF MITOCHONDRIA – LYSOSOME CONTACT IN HUMAN NEURONS

## 3.1 OVERVIEW

Inter-organelle contacts are dynamic sites of membrane tethering between two different organelles, allowing for cellular homeostatic regulation such as metabolite transfer, cellular signaling and regulation of organelle dynamics (Gatta and Levine 2017). However, as the majority of work on inter-organelle contacts has been conducted in non-neuronal cells, investigating the role of a new inter-organelle contact between mitochondria and lysosomes (Wong, Ysselstein, and Krainc 2018) in neurons will further elucidate the importance and homeostatic function of neuronal inter-organelle contacts.

Neurons are highly polarized cells comprised of 1) a long and thin axon that can be >1 meter in length, 2) a cell body where the majority of cellular organelles reside, and 3) dendrites with multiple branches (Sheng 2014) (**Figure 2.2 d**). Due to their complex and asymmetrical morphology, the dynamics of mitochondria-lysosome contacts may be differentially regulated across different neuronal compartments.

To investigate mitochondria-lysosome contact sites in human neurons, we utilized iPSC technology (**Figure 2.1**) to generate human midbrain dopaminergic neurons from healthy controls

(**Figure 2.2**). Using fluorescence proteins or antibodies to mark distinct neuronal compartments, we investigated the dynamics (rate of formation, distribution and contact duration) of mitochondria-lysosome contacts in axons, dendrites and cell bodies.

Here, we could visualize mitochondria-lysosome contacts across multiple neuronal compartments in human neurons and confirmed the dynamic formation of mitochondria-lysosome contacts that mediate crosstalk between two organelles. Notably, we found that contacts in axons were longer in duration than contacts in cell bodies, suggesting that mitochondria-lysosome contacts are differentially regulated in each neuronal compartment.

## 3.2 RESULTS

### 3.2.1 Mitochondria-lysosome contact sites dynamically form in human neurons

To investigate mitochondria-lysosome contact sites in human neurons, we utilized induced pluripotent stem cell (iPSC) technology (**Figure 2.1**) to generate human midbrain dopaminergic neurons from healthy controls using previously established protocols (Burbulla et al. 2019; Kriks et al. 2011). Differentiated neurons expressed the neural specific marker β-III-tubulin (TUJ1) and midbrain dopaminergic neuron specific markers: tyrosine hydroxylase (TH), forkhead box protein A2 (FOXA2) and LIM Homeobox Transcription Factor 1 Alpha (LMX1A) (**Figure 2.2 a, b**), and were subsequently imaged for mitochondrial and lysosomal dynamics in live neurons (**Figure 2.2 d; Figure 3.1**).

Using 3D super-resolution structured illumination microscopy (3D N-SIM), we found that mitochondria and lysosomes (Mito-RFP, Lyso-GFP) formed stable inter-organelle contacts in

human neurons (**Figure 3.2 a**). Neuronal mitochondria-lysosome contacts were further confirmed to be <10nm apart using electron microscopy (**Figure 3.2 b**), consistent with other contact sites (Csordas et al. 2006; Wong, Ysselstein, and Krainc 2018). Next, we conducted confocal time-lapse microscopy of live neurons, and found that mitochondria-lysosome contacts dynamically formed over time and remained tethered together (yellow arrows) before subsequently untethering from one another (white arrows) (**Figure 3.2 c**). Mitochondria in contact with lysosomes maintained their membrane potential, as visualized by TMRM imaging (**Figure 3.3**), and dynamic mitochondria-lysosome contact tethering could be further observed in human neurons by imaging outer mitochondrial membrane and lysosomal membrane proteins (TOM20-RFP, LAMP1-GFP) (**Figure 3.1c**), as well as by imaging mitochondrial and lysosomal-targeted dyes (MitoTracker, LysoTracker) (**Figure 3.1d**). In addition, we could also visualize mitochondria-lysosome contacts in human neurons by proximity ligation assay (PLA) imaging of TOM20 and LAMP1 on the outer mitochondrial and lysosomal membrane (**Figure 3.4**). Mitochondria-lysosome contacts in human neurons remained tethered for an average duration of 88.07 ± 5.05 seconds (**Figure 3.2 d, e**), with approximately 18% of lysosomes in contact with mitochondria at any point in time (**Figure 3.2 f**). Thus, mitochondria-lysosome contacts can dynamically form to mediate crosstalk between mitochondria and lysosomes in human neurons.

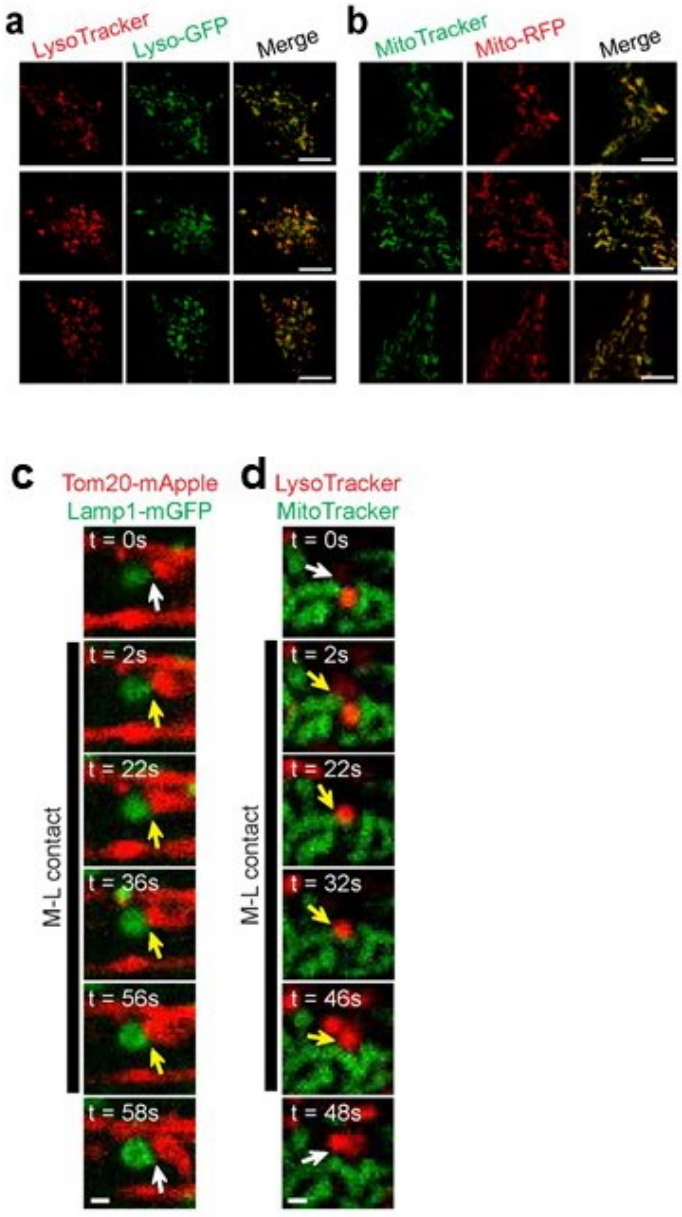


**Figure 3.1 Characterization of mitochondria-lysosome contact sites in human dopaminergic neurons.** (a) Representative fluorescence confocal live-cell images of lysosomal markers in wild-type human iPSC-derived dopaminergic neurons showing CellLight® Lysosome-GFP (Lyso-GFP, green) colocalized with LysoTracker™ Red DND-99. (b) Representative fluorescence confocal live-cell images of mitochondrial markers in wild-type neurons showing CellLight® Mitochondria-RFP (Mito-RFP, red) colocalized with MitoTracker Green FM. (c-d) Mitochondria-lysosome contacts were visualized by multiple methods for labeling mitochondria and lysosomes: Representative time-lapse confocal images of mitochondria-lysosome contacts between (c) outer mitochondrial membrane fluorescent marker (red, Tom20-mApple) and lysosomal membrane fluorescent marker (green, Lamp1-mGFP) or (d) LysoTracker (red) and MitoTracker (green) in control neurons. Yellow arrows mark stable mitochondria-lysosome contacts. White arrows mark the site of mitochondria-lysosome contacts before and after contacts. Black line shows duration of contacts. Scale bar = 500nm

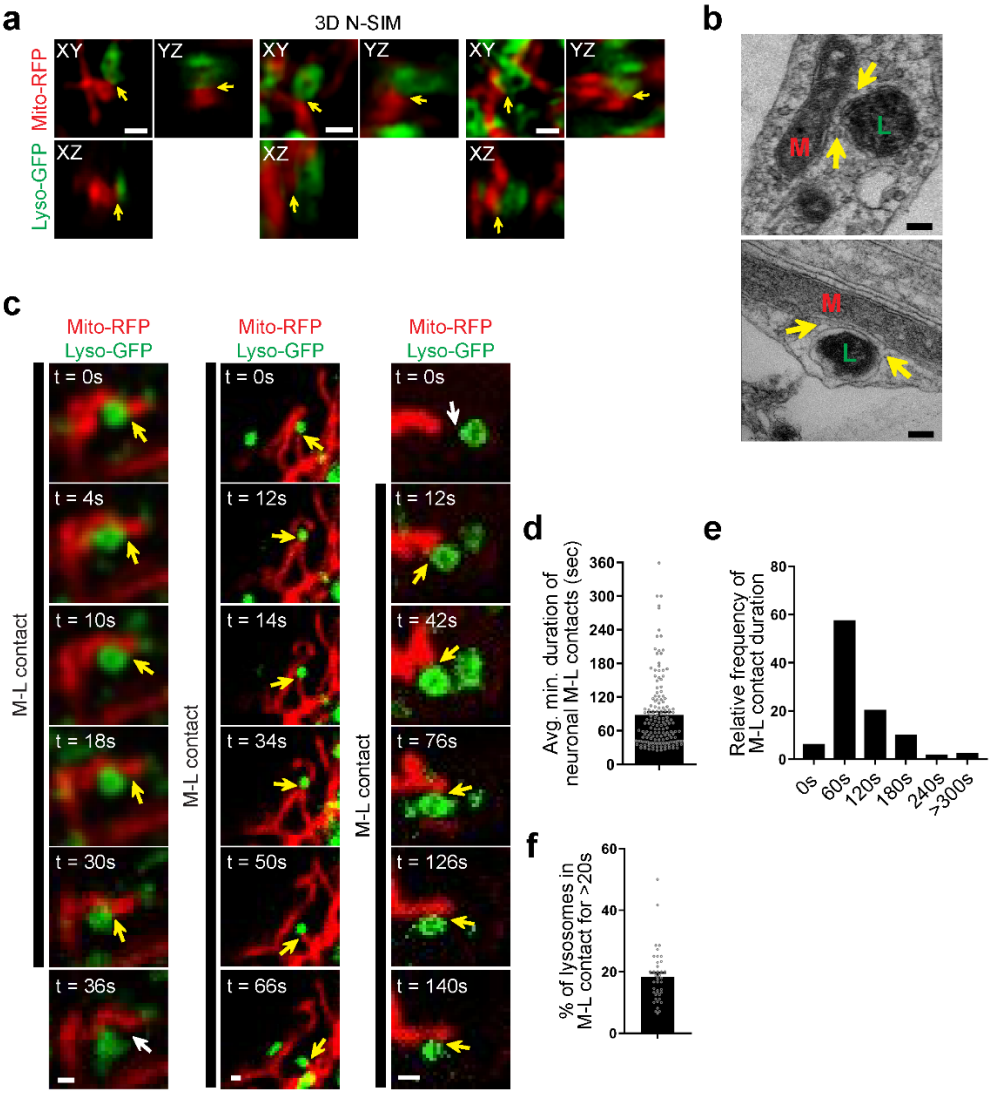


**Figure 3.2 Mitochondria-lysosome contacts dynamically form in human neurons.** (a) Representative 3D N-SIM images of M-L contacts (yellow arrows) in wild-type human neurons (mitochondria: red, Mito–RFP; lysosomes: green, Lyso-GFP) (b) Representative EM images of M-L contacts (yellow arrows) with distance between membranes <10nm (mitochondria, M; lysosomes, L). (c) Representative time-lapse confocal images of dynamic contacts between mitochondria (red, Mito-RFP) and lysosomes (green, Lyso-GFP). Yellow arrows mark stable M-L contacts. White arrows mark the site of M-L contacts before contact formation or after contact untethering. Black line shows duration of contacts. (d-e) Quantification of duration of stable M-L contacts from confocal images. (d) Average minimum duration of neuronal M-L contacts. (e) Relative frequency (percentages) distribution of M-L contacts. X-axis represents bin centers. Bin width = 60 sec. (f) Percentage of lysosomes contacting mitochondria (for >20 sec) For all quantifications, data are means ± S.E.M. Scale bars, 500nm (a, c); 100nm (b).

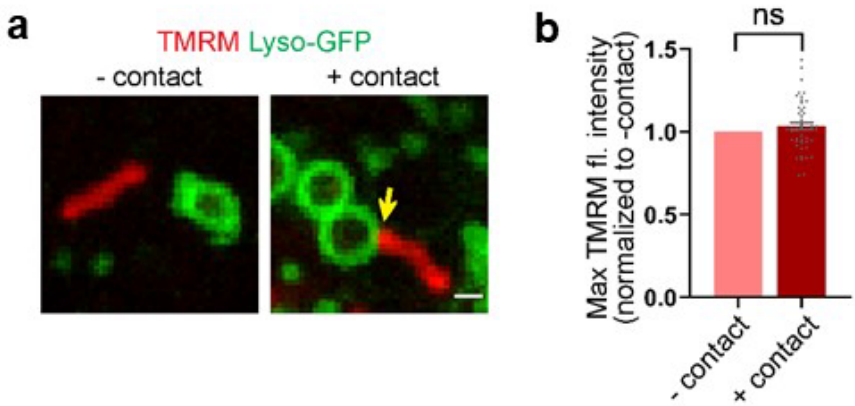


**Figure 3.3 Tetramethylrhodamine ethyl ester (TMRM) staining of Mitochondria in contact with lysosomes.** TMRM (red) accumulates in active mitochondria with intact membrane potentials (ΔΨm). (a) Representative live-cell images of TMRM signal in mitochondria that are not in contact (left; - contact) or in contact with a lysosome (right; + contact). Yellow arrow marks stable M-L contacts. Scale bar = 500nm. (b) Quantification of maximum TMRM fluorescence intensity in mitochondria showing that it is similar for mitochondria that are not in contact compared to mitochondria in contact with a lysosome. Paired two-sided Student's t-test. Data are the means ± S.E.M. ns: not significant.

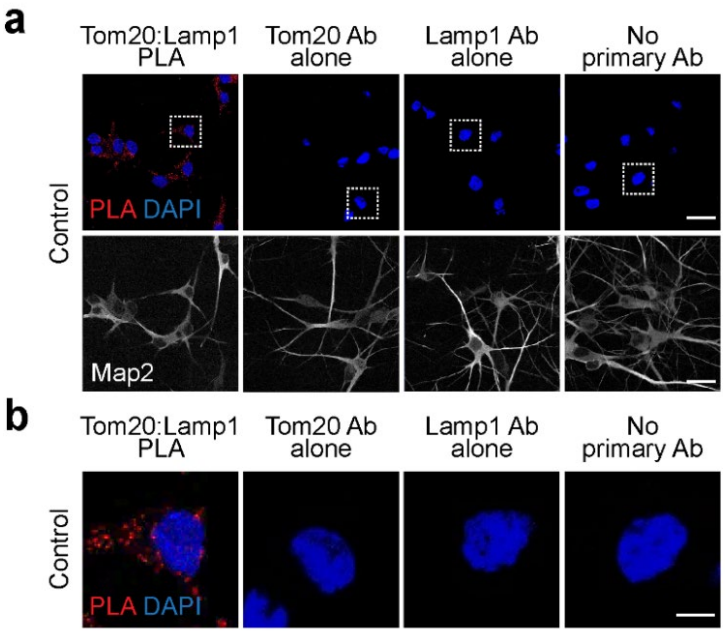


**Figure 3.4 Proximity ligation assay (PLA) of mitochondria-lysosome contact sites in human dopaminergic neurons.** Representative confocal images of mitochondria-lysosome contact sites in human iPSC-derived dopaminergic neurons using imaging of in situ proximity ligation assay (red) for endogenous Tom20 and Lamp1 in (a; inset in b) wild-type control.

### 3.2.2 Spatial compartmentalization of neuronal mitochondria-lysosome contact dynamics

Next, we investigated the spatial compartmentalization of neuronal mitochondria-lysosome contacts in the soma, dendrites, and axons of human neurons, as both organelles are localized throughout multiple neuronal compartments. Dendrites and axons were identified as being positive for MAP2 or Tau respectively (**Figure 2.2 c**). Importantly, we found that mitochondria and lysosomes tethered at contact sites (yellow arrows) within all three neuronal compartments in the soma (**Figure 3.5 a (left)**), dendrites (**Figure 3.5 a (middle)**), and axons (**Figure 3.5 a (right)**). Mitochondria-lysosome contacts in dendrites and axons exhibited decreased mitochondrial and lysosomal motility (yellow arrows) (**Figure 3.5 b**). To further examine whether the dynamics of contacts differed by spatial compartmentalization, we quantified the duration of mitochondria-lysosome contacts and percentage of lysosomes in contact with mitochondria across different neuronal compartments. Interestingly, live cell imaging analysis revealed that the average minimum duration of mitochondria-lysosome contacts was significantly increased in axons compared to those in the soma (soma: 80.6 ± 6.2 sec; dendrites: 82.4 ± 9.7 sec; axons: 112.5 ± 13.2 sec) (**Figure 3.5 c**). In contrast, the percentage of lysosomes contacting mitochondria in the soma, dendrites and axons did not differ (**Figure 3.5 d**). Together, these results demonstrate that mitochondria-lysosome contacts are able to form with varying dynamics across multiple neuronal compartments in human neurons.

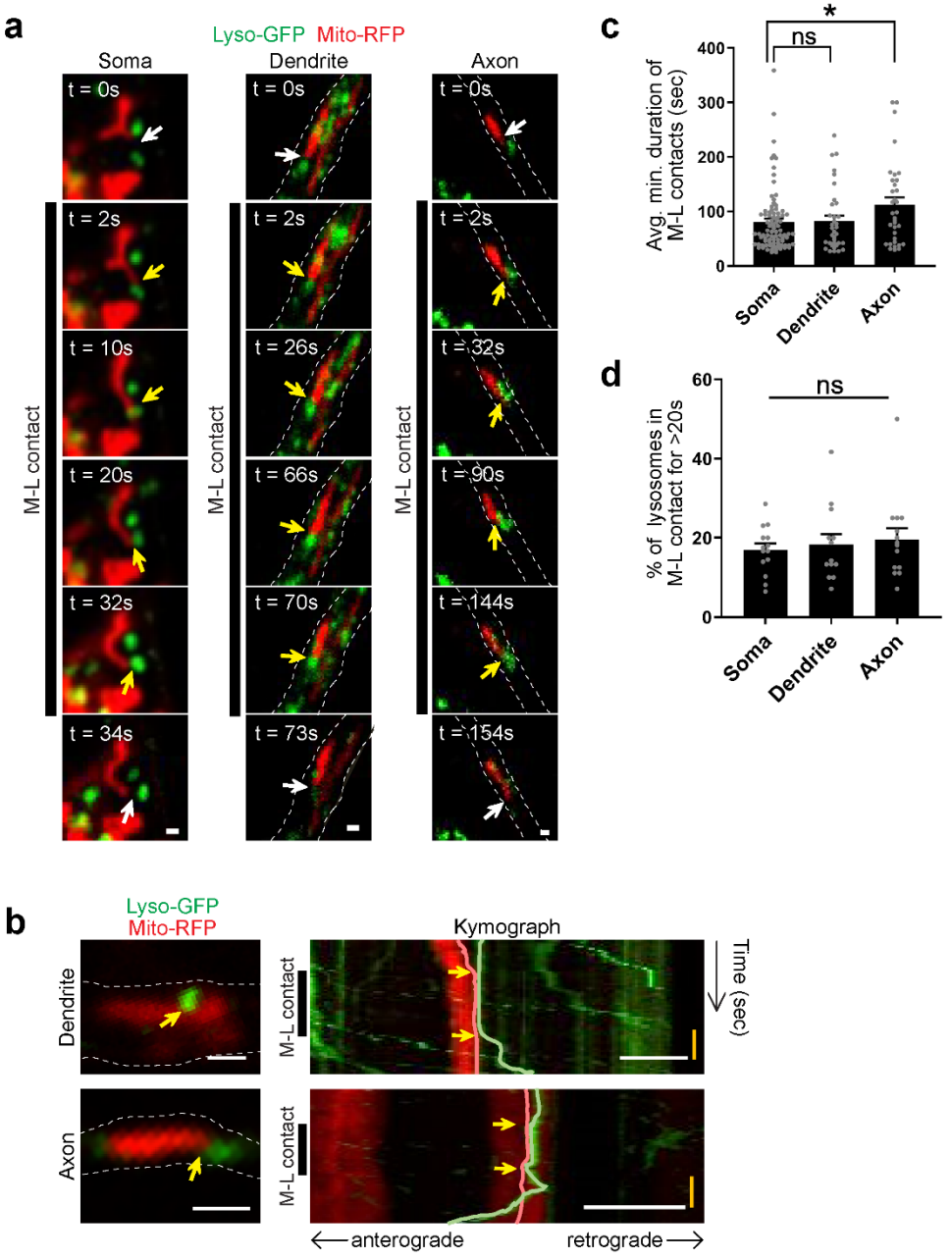


**Figure 3.5 Spatial compartmentalization of neuronal mitochondria–lysosome contact dynamics.** (a) Representative time-lapse confocal images of contacts between mitochondria (red, Mito-RFP) and lysosomes (green, Lyso-GFP) in soma, dendrites, and axons of wild-type human neurons. Time-lapse recordings were taken at 2 sec intervals for 5 min. Yellow arrows mark stable M-L contacts. White arrows mark the site of M-L contacts before contact formation or after contact untethering. Black line shows duration of contacts. Scale bar = 500nm. (b) Representative frames of live cell imaging (left) and dual color kymographs (right) of M-L contacts in dendrites and axons (mitochondria: red, Mito–RFP; lysosomes: green, Lyso-GFP). In confocal image frames

(left), contact sites are denoted by yellow arrows. In kymographs: white scale bar = 1 μm, yellow vertical bar = 30 seconds. Yellow arrows in kymograph point to start and end timepoints of M-L contact tethering. Left black line shows duration of contacts. (c-d) Quantification of M-L contacts across different neuronal compartments. One-way ANOVA followed by Tukey's multiple comparisons test. c Comparison of average minimum durations of M-L contacts in soma, dendrites, and axons *p=0.0335. (d) Percentage of lysosomes contacting mitochondria in soma, dendrites, and axons (for >20 sec). For all quantifications, data are means ± S.E.M. *p ≤0.05, ns: not significant.

## 3.3 DISCUSSION

Our live-cell imaging data demonstrate that mitochondria-lysosome contacts dynamically form in healthy iPSC-derived human neurons. Given the extremely polarized structure of neurons, dynamics and interaction of organelles may be diferentially regulated in neurons. Indeed, we found that average duration of mitochondria – lysosome contacts is longer in neurons (~90 sec) compared to non-neuronal cells (~60 sec, (Wong, Ysselstein, and Krainc 2018)). In addition, mitochondria-lysosome contacts show different dynamics across different neuronal compartments. Specifically, the average duration of contact tethering was significantly longer in axons compared to those in cell bodies, while the percentage of lysosomes contacting mitochondria in soma, dendrites and axons were not different. Importantly we also found that two organelles which were tethered with one another at a mitochondria-lysosome contact sites were less motile than free organelles, suggesting that mitochondria-lysosome contacts may regulate the motility and the distribution of both organelles in human neurons.

Wong et al. found that mitochondria-lysosomes contacts regulate mitochondrial fission events (Wong, Ysselstein, and Krainc 2018), suggesting that contacts may further modulate mitochondrial network dynamics and trafficking in neurons. Axonal trafficking of mitochondria is

critical for their positioning and supply of ATP to distal parts of the neuron. However, the relationship between mitochondrial trafficking and mitochondria-lysosome contact dynamics is not known, and offers a potential mechanism for mitochondrial trafficking to bidirectionally regulate lysosomal dynamics and function in neurons.

In addition, inter-organelle contacts often represent sites for transfer of metabolites such as calcium and lipids (Eisenberg-Bord et al. 2016; Gatta and Levine 2017; Hoglinger et al. 2019; Peng, Wong, and Krainc 2020; Phillips and Voeltz 2016), which are important metabolites for both mitochondria and lysosomal function (Muallem et al. 2017; Raffaello et al. 2016a). Indeed, recent studies on calcium (Peng, Wong, and Krainc 2020) and lipid (Hoglinger et al. 2019) exchange at mitochondria-lysosome contacts suggest that this pathway may also modulate the neuronal regulation of calcium and lipid dynamics by mitochondria and lysosomes. Thus, future studies investigating the neuronal roles of mitochondria-lysosome contacts in both mitochondrial trafficking and metabolite transport using advanced imaging of iPSC-derived human neurons will significantly extend our knowledge of the crosstalk between mitochondria and lysosomes in neurons, and their contribution to maintaining neuronal function and homeostasis over time.

# CHAPTER 4.

# MITOCHONDRIA – LYSOSOME CONTACT DYSFUNCTION IN *GBA1*-LINKED PARKINSON'S DISEASE

## 4.1 OVERVIEW

Both mitochondria and lysosomes are critical for regulating cellular metabolism, signaling, degradation, and metabolite storage, as reflected in the numerous diseases associated with dysfunction of either organelle (Kalia and Lang 2015; Mc Donald and Krainc 2017; Plotegher and Duchen 2017b, 2017a). However, the majority of previous work studying their direct interactions has been restricted to lysosomal degradation of mitochondria, either via mitophagy or mitochondrial-derived vesicles (McLelland et al. 2014; Pickrell and Youle 2015). Our lab's recent identification of mitochondria-lysosome contacts (Wong, Ysselstein, and Krainc 2018) allows for their bidirectional crosstalk independent of mitochondrial degradation, and suggests additional unexplored roles for this contact site in maintaining cellular homeostasis and driving pathogenesis of diseases such as PD linked to both organelles' dysfunction (Kalia and Lang 2015; Mc Donald and Krainc 2017; Plotegher and Duchen 2017b, 2017a).

*GBA1* encodes a lysosomal enzyme whose mutations cause lysosomal abnormality and represent the greatest risk factor for PD and are directly linked to familial forms of PD (Sidransky

et al. 2009). However, whether lysosomal contacts with mitochondria are disrupted in PD patient neurons harboring mutant *GBA1* was previously not studied.

Here, we show that patient neurons harboring mutant *GBA1* 84GG exhibit significantly increased mitochondria-lysosome contact site duration as compared to neurons from healthy controls (**Figure 5.2 a-b**). We also investigated the potential mechanisms driving mitochondria-lysosome contact site defects and the downstream consequences of prolonged contact duration in PD patient *GBA1*-linked neurons, which together highlight a novel role for this pathway in PD pathogenesis.

## 4.2 RESULTS

### 4.2.1 *GBA1* mutant reduces lysosomal GCase activity in PD patient-derived human neurons

We have shown that mitochondria-lysosome contact sites dynamically form in healthy control human dopaminergic neurons (Chapter 3; **Figure 3.2**). However, as mitochondria-lysosome contacts were only examined in wild type neurons, we additionally investigated whether mitochondria-lysosome contacts were disrupted in PD, by specifically looking at lysosomal *GBA1* mutations which are the highest risk factor for PD and have also been linked to mitochondrial dysfunction. First, we started with the heterozygous mutation 84GG (84GG Het) *GBA1* which leads to familial PD, and in which the mutant protein is not expressed due to a frame shift mutation (Burbulla et al. 2019). From previously reported studies using dried blood spots and tandem mass spectrometry (Zhang et al. 2008), GCase activity is ~40% decreased in blood samples of heterozygous 84GG mutation carrier (Alcalay et al. 2015).

Using PD patient fibroblasts harboring 84GG mutation, we generated human iPSCs and their isogenic controls by CRISPR-Cas9 (**Figure 2.1**) which were subsequently differentiated into midbrain dopaminergic neurons (mutant *GBA1* (ΔGBA); isogenic control (Corr)) (**Figure 2.2 a-c**). Both mutant *GBA1* and its isogenic control did not affect the efficiencies of fibroblast reprogramming to iPSCs or differentiation into midbrain dopaminergic neurons from iPSCs (Burbulla et al. 2019).

We first confirmed that PD patient-derived mutant *GBA1* dopaminergic neurons exhibited decreased GCase protein levels (**Figure 4.1 a, b**). To confirm the disrupted GCase activity in live ΔGBA neurons, we performed live-cell GCase activity assays (Mazzulli, Zunke, Isacson, et al. 2016), using 5-(pentafluorobenzoylamino) fluorescein Di-β-D-glucopyranoside (PFB-FDGlu) as the GCase enzyme substrate. Our data using iPSC-derived DA neurons from *GBA1* 84GG mutant at day 70 showed reduced total GCase enzymatic activity compared to its isogenic control (**Figure 4.1 c-e**). To compare lysosomal and non-lysosomal GCase activity separately, we used Bafilomycin A1 (BafA1), an inhibitor of organelle acidification which causes lysosomal enzyme malfunction, as an established protocol for examining lysosomal GCase activity. Activity within the lysosomal compartment was determined by measuring the response to BafA1 while non-lysosomal GCase activity was interpreted as the activity that was not affected by BafA1 treatment (Mazzulli, Zunke, Isacson, et al. 2016). Importantly, our data show a significant decrease in lysosomal GCase activity in patient-derived mutant *GBA1* neurons compared to isogenic control neurons (**Figure 4.1 c-d, f**), consistent with previous findings (Burbulla et al. 2019).

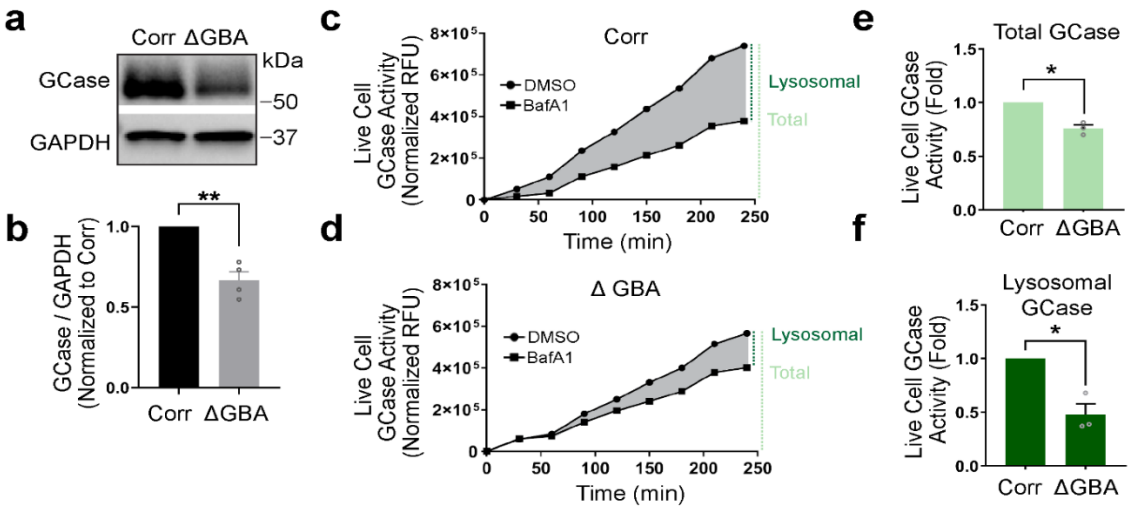


**Figure 4.1 *GBA1* mutant reduces lysosomal GCase activity in PD patient-derived human neurons.** (a-b) Western blot analysis of PD patient-derived mutant *GBA1* dopaminergic neurons (ΔGBA; het 84GG) and its CRISPR-corrected isogenic control (Corr) neurons. GCase level was significantly reduced in ΔGBA neurons. Paired two-sided Student's t-test; **p=0.0083. (c-f) ΔGBA and Corr neurons were treated with either DMSO or BafA1 and subjected to live cell GCase activity analysis. e Quantification of the area under each curve (AUC) demonstrates decreased total GCase activity in ΔGBA neurons. Paired two-sided Student's t-test; *p=0.0183. (f) Lysosomal GCase activity was calculated by subtracting BafA1 values from DMSO. Values are expressed as fold-change compared to isogenic controls. Paired two-sided Student's t-test; *p=0.0352.

### 4.2.2 Loss of GCase activity disrupt mitochondria-lysosome contact untethering in PD patient dopaminergic neurons.

PD has been genetically and functionally linked to both mitochondrial and lysosomal defects (Burbulla et al. 2017; Mazzulli et al. 2011; Nguyen et al. 2019), but whether mitochondria-lysosome contacts are disrupted in PD has not been previously investigated. As mutations in the lysosomal enzyme GCase (*GBA1*) represent the greatest genetic risk factor for PD (Sidransky and Lopez 2012), and GCase activity is decreased in both idiopathic and multiple types of familial PD patient neurons (Burbulla et al. 2019; Burbulla et al. 2017; Mazzulli et al. 2011; Nguyen et al.

2018; Ysselstein et al. 2019), we examined mitochondria-lysosome contact dynamics in *GBA1*-PD (Δhet 84GG) patient neurons.

We investigated whether lysosomal contacts with mitochondria were disrupted by loss of lysosomal GCase activity by conducting confocal live cell microscopy of mitochondria and lysosomes in mutant *GBA1* and CRISPR-corrected isogenic control neurons. Interestingly, while mitochondria-lysosome contacts dynamically formed in both conditions (yellow arrows) (**Figure 4.2 a**), the average duration of mitochondria-lysosome contact tethering was significantly increased in mutant *GBA1* neurons, indicative of inefficient untethering events (**Figure 4.2 b**). However, the percentage of lysosomes in contacts was similar between conditions (**Figure 4.2 c**), suggesting that the subsequent untethering but not initial formation of mitochondria-lysosome contact tethering was disrupted in mutant *GBA1* neurons.

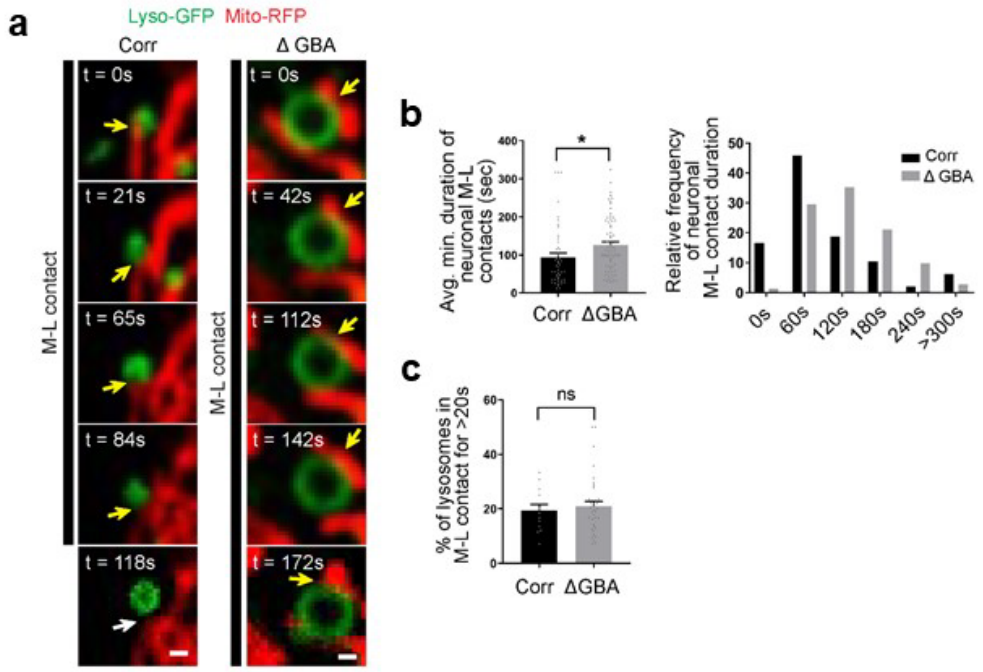


**Figure 4.2 Loss of GCase activity disrupts mitochondria-lysosome contact untethering in *GBA1*-PD patient dopaminergic neurons.** (a) Representative time-lapse confocal images of contacts between mitochondria (red, Mito-RFP) and lysosomes (green, Lyso-GFP) in Corr (left) and ΔGBA (right) human neurons. Yellow arrows mark stable M-L contacts. White arrows mark the site of M-L contacts after contact untethering. Black line shows duration of contacts. Scale bar = 500nm. (b) Quantification of average minimum duration (left) and relative frequency distribution of the duration of stable M-L contacts (right), showing increased duration of stable M-L contacts in ΔGBA neurons. X-axis of the histogram represents bin centers. Bin width = 60 sec. Unpaired two-sided Student's t-test; *p=0.0204. (c) Percentage of lysosomes contacting mitochondria (for >20 sec). Unpaired two-sided Student's t-test. For all quantifications, data are means ± S.E.M. *p ≤0.05, ns: not significant.

To further examine mitochondria-lysosome contacts, we conducted PLA imaging of mitochondria-lysosome contacts in mutant *GBA1* and CRISPR-corrected isogenic control neurons (**Figure 4.3 a**), and similarly found that mitochondria-lysosome contacts could still form in both conditions (**Figure 4.3 b**). In addition, we conducted electron microscopy imaging of mitochondria-lysosome contacts in mutant *GBA1* and CRISPR-corrected isogenic control neurons

(**Figure 4.3 c**), and also found that mitochondria-lysosome contacts tethered together in both conditions, with the length of membrane contact between mitochondria and lysosomes not altered in mutant *GBA1* neurons (**Figure 4.3 d**). Of note, ER-mitochondria contact, and ER-lysosome contact formation were also not disrupted in mutant *GBA1* neurons (**Figure 4.4**). Together, our results suggest that loss of GCase activity does not disrupt mitochondria-lysosome contact formation, but preferentially disrupts the untethering of mitochondria-lysosome contact sites, resulting in prolonged contact site tethering between mitochondria and lysosomes.

We further examined whether these changes in mitochondria-lysosome contact dynamics might be specific to loss of GCase activity rather than general lysosomal enzyme dysfunction. Mutant *GBA1* neurons had altered lysosomal morphology, including enlarged lysosomes (**Figure 4.2 a; Figure 4.5**). However, inhibition of other lysosomal enzymes in human neurons which also led to enlarged lysosomal morphology (**Figure 4.6 a**) including inhibition of lysosomal acid ceramidase (carmofur treatment), cysteine proteases (E64D treatment), or aspartyl proteases (pepstatin A treatment) did not disrupt mitochondria-lysosome contact dynamics (**Figure 4.6 b**). Thus, our results suggest that this pathway is selectively disrupted by loss of GCase activity rather than general lysosomal defects or enzyme dysfunction.

In addition, we assessed whether rescuing GCase activity in mutant *GBA1* neurons was sufficient to restore defective mitochondria-lysosome contact dynamics. The modulator S-181 was recently found to increase GCase activity in mutant *GBA1* neurons (Burbulla et al. 2019). Importantly, S-181 treatment (**Figure 4.6 c**) rescued the prolonged mitochondria-lysosome contact tethering in mutant *GBA1* neurons (**Figure 4.6 d**), further highlighting the role of GCase activity in regulating mitochondria-lysosome contact dynamics.

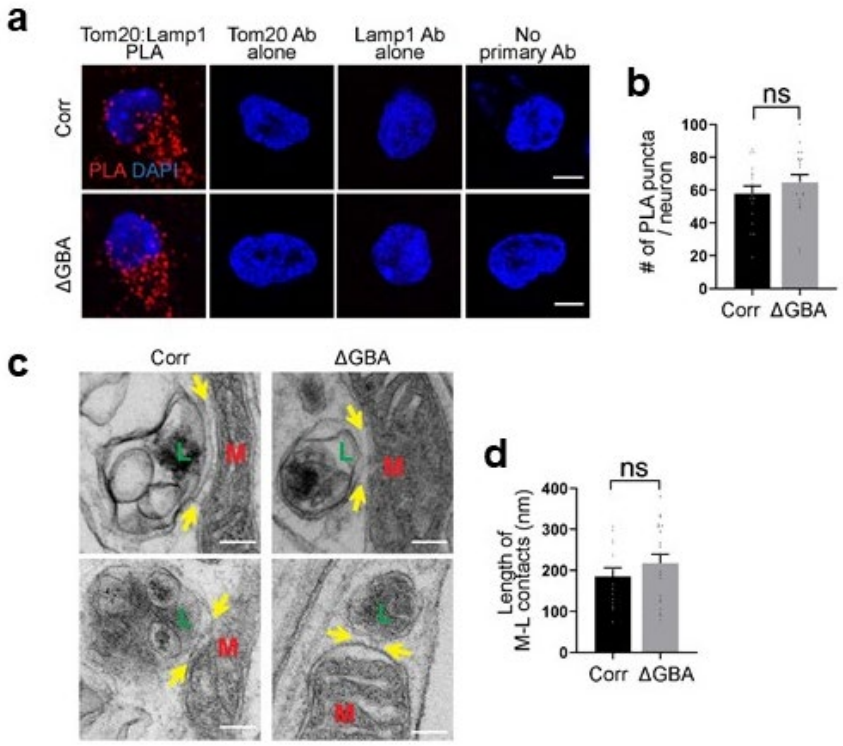


**Figure 4.3 Proximity ligation assay (PLA) and electron microscopy of mitochondria-lysosome contact sites in PD neurons.** (a) PD patient-derived mutant *GBA1* dopaminergic neurons (ΔGBA) and its CRISPR-corrected isogenic control (Corr) neurons. Neurons immunostained with only Tom20 or Lamp1, or without primary antibody were used as negative controls. The nucleus is stained with DAPI (blue). Scale bar = 5μm. (b) Quantification of the number of PLA puncta in Corr and ΔGBA neurons. (c-d) Representative electron microscopy (EM) images of M-L contacts (yellow arrows) with distance between membranes <10nm (mitochondria, M; lysosomes, L) in Corr and ΔGBA neurons. (c) Scale bar = 100nm. (d) Quantification of the length of contacts (membrane contact distance). Unpaired two-sided Student's t-test. For all quantifications, data are the means ± S.E.M., ns: not significant.

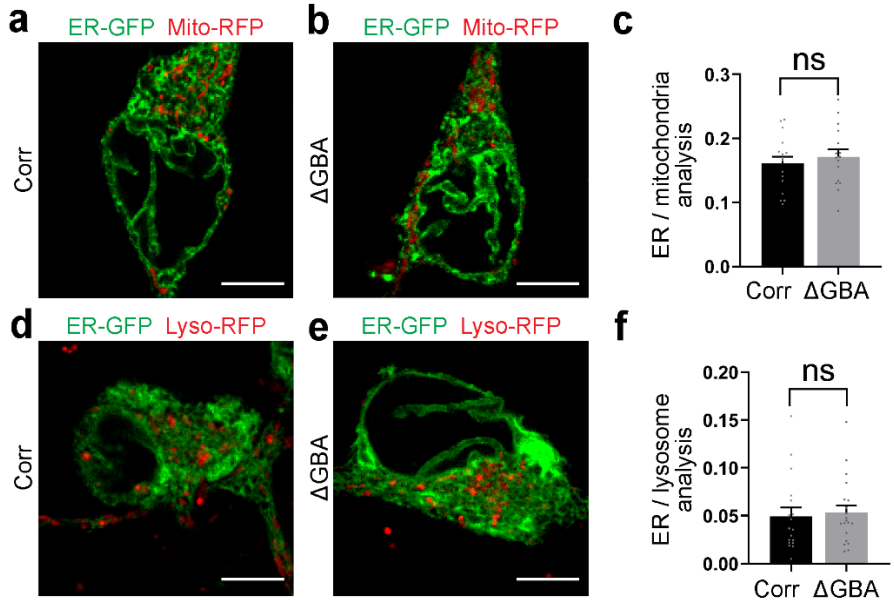


**Figure 4.4 ER-mitochondria and ER-lysosome contact site analysis in *GBA1*-PD patient dopaminergic neurons.** (a-b) Representative confocal images of ER-mitochondria contacts (ER: green, ER-GFP; mitochondria: red, Mito-RFP) in soma of PD patient-derived mutant *GBA1* dopaminergic neurons (ΔGBA) and its CRISPR-corrected isogenic control (Corr) neurons. (c) Mander's overlap coefficient (MOC) values measured from each frame of 150 sec time-lapse imaging movie were averaged to quantify the fraction of ER overlapped with mitochondria. (d-e) Representative confocal images of ER-lysosome contacts (ER: green, ER-GFP; lysosome: red, Lyso-RFP) in Corr and ΔGBA neurons. (f) MOC values measured from each frame of 150 sec time-lapse imaging movies were averaged to quantify the fraction of ER overlapped with lysosomes. (c), (f) Unpaired two-sided Student's t-test. For all quantifications, data are the means ± S.E.M. ns: not significant. Scale bar = 5μm.

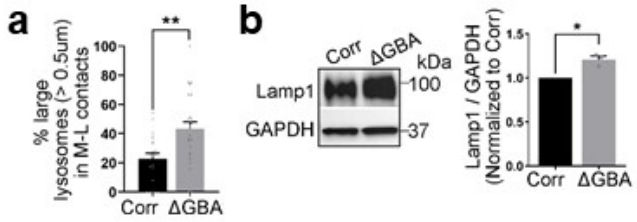


**Figure 4.5 Altered lysosomal morphology in mutant *GBA1* neurons** (a) Quantification of the percentage of large lysosomes (diameter >0.5um) in M-L contacts in Corr and ΔGBA neurons. Unpaired two-sided Student's t-test; **p=0.0016. (b) Western blot analysis of Lamp1 in Corr and ΔGBA neurons. For all quantifications, data are the means ± S.E.M. *p≤ 0.05, **p≤0.01.

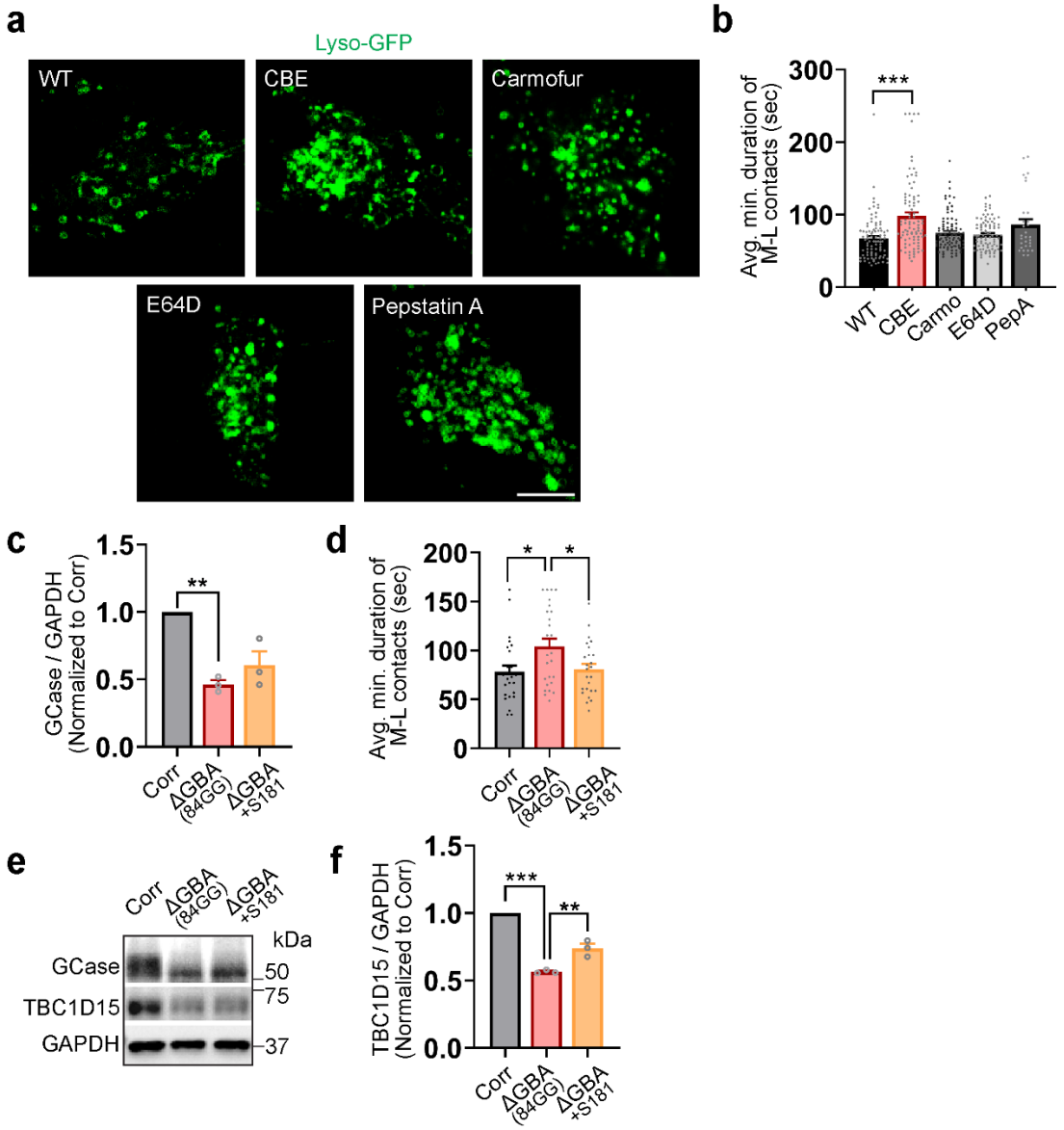


**Figure 4.6 Lysosomal dysfunction specifically from loss of GCase activity disrupts mitochondria-lysosome contact dynamics.** (a) Representative confocal images of lysosomes in wild-type human iPSC-derived dopaminergic neurons treated with lysosomal enzyme inhibitors: CBE (inhibitor of GCase); Carmofur (inhibitor of acid ceramidase); E64D (inhibitor of cysteine proteases); Pepstatin A (inhibitor of aspartyl proteases). Scale bar = 5µm. (b) CBE treatment in wild-type neurons increased the average minimum duration of stable M-L contacts compared to untreated neurons (WT). One-way ANOVA followed by Tukey's multiple comparisons test; ***p<0.0001. (c), (e), (f) Western blot analysis of (c) GCase (**p=0.0021) and (f) TBC1D15 (***p<0.0001; **p=0.0024) in *GBA1* dopaminergic neurons (ΔGBA) and its CRISPR-corrected isogenic control (Corr) neurons, and S181-treated ΔGBA neurons. GAPDH was used as a loading control. Values are expressed as fold-change compared to Corr. (d) Quantification of average minimum duration of M-L contacts in Corr, ΔGBA, and S181-treated ΔGBA neurons. (*p= 0.0178

(left); *p=0.0400 (right)). (c), (d), (f) One-way ANOVA followed by Tukey's multiple comparisons test. For all quantifications, data are the means ± S.E.M. *p≤ 0.05, **p≤0.01, ***p≤0.001, ns: not significant.

### 4.2.3 Tethering proteins mediating mitochondria-lysosome contact are disrupted in *GBA1*-PD patient dopaminergic neurons

We subsequently examined the potential mechanism through which mutant *GBA1* might disrupt mitochondria-lysosome contact dynamics. We recently showed that mitochondria-lysosome contact untethering is mechanistically regulated by lysosomal RAB7-GTP hydrolysis from GTP to GDP-bound Rab7 (Wong, Ysselstein, and Krainc 2018), and is driven by the GAP (GTPase-activating protein) activity of mitochondrial TBC1D15 (Rab7 GAP) (Peralta, Martin, and Edinger 2010; Zhang et al. 2005), which is recruited to the outer mitochondrial membrane by Fis1 (Onoue et al. 2013; Yamano et al. 2014). Thus, we investigated whether RAB7-GTP hydrolysis might be disrupted by mutant *GBA1* in patient neurons. We first measured the total protein levels of RAB7 together with Fis1 and TBC1D15 in PD patient-derived mutant *GBA1* dopaminergic neurons compared to isogenic controls (**Figure 4.7 a-d**). We observed no differences in total Rab7 levels (**Figure 4.7 c**) or Fis1 levels (**Figure 4.7 d**), and Fis1 levels were not altered even after normalizing for mitochondrial levels (Fis1/Tom20: Corr vs *GBA1*, p=0.23 (not significant)). Of note, TBC1D15 and Fis1 localization to mitochondria (**Figure 4.8 a,b**), and Rab7 localization to lysosomes (**Figure 4.8 c**), as well as the levels of the Rab7 GEF complex proteins Mon1 and CCZ1 (**Figure 4.8 d**) were also not altered in mutant *GBA1* neurons. However, we surprisingly found that TBC1C15 levels were significantly decreased in mutant *GBA1* patient-derived neurons (*P ≤ 0.05) (**Figure 4.7 b**).

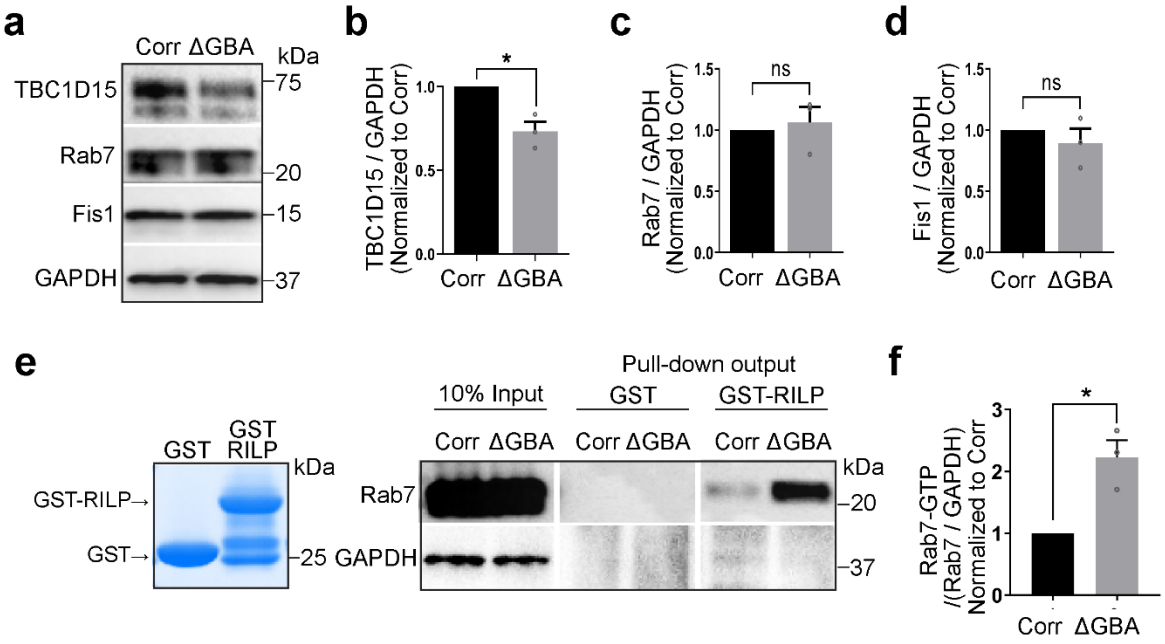


**Figure 4.7 Tethering proteins mediating mitochondria-lysosome contact are disrupted in *GBA1*-PD patient dopaminergic neurons.** (a-d) Western blot analysis of (b) TBC1D15, (c) Rab7 and (d) Fis1 levels in PD patient-derived mutant *GBA1* dopaminergic neurons (ΔGBA) and its CRISPR-corrected isogenic control (Corr) neurons. Protein levels were normalized to loading control GAPDH. Values are expressed as fold-change compared to Corr. Paired two-sided Student's t-test; *p=0.0442. (e-f) GST-RILP pull-down to measure GTP-bound Rab7 levels in ΔGBA and Corr neurons. (f) Rab7-GTP levels were normalized to total Rab7 normalized to GAPDH. Values are expressed as fold-change compared to Corr. Paired two-sided Student's t-test; *p=0.0478. For all quantifications, data are means ± S.E.M. *p ≤0.05.

Based on these findings, we hypothesized that disrupted mitochondria-lysosome contact untethering in mutant *GBA1* neurons might be due to defective Rab7-GTP hydrolysis as a consequence of reduced TBC1D15 levels (Rab7 GAP). To test this, we performed GST-RILP (Glutathione Transferase-Rab Interacting Lysosomal Protein) pull-down assays (Romero Rosales et al. 2009) to measure GTP-bound Rab7 levels, as RILP preferentially binds to GTP-bound Rab7

(Cantalupo et al. 2001; Jordens et al. 2001; Romero Rosales et al. 2009) (**Figure 4.7 e**). Importantly, we found that PD patient-derived mutant *GBA1* dopaminergic neurons demonstrated significantly increased levels of RAB7-GTP/total Rab7 compared to CRISPR-corrected isogenic control neurons (**P ≤ 0.01) (**Figure 4.7 e, f**). Together, these results suggest that decreased TBC1D15 levels in mutant *GBA1* neurons disrupt Rab7 GTP hydrolysis, resulting in increased GTP-bound Rab7 and prolonged mitochondria-lysosome contact tethering dynamics.

To further investigate the downregulation of TBC1D15 in mutant *GBA1* neurons, we analyzed TBC1D15 by qPCR and showed that decreased TBC1D15 protein levels in mutant *GBA1* neurons were not due to lower TBC1D15 transcripts levels (**Figure 4.9 a**). Rather, decreased TBC1D15 protein levels resulted from elevated proteasomal degradation of TBC1D15, which could be inhibited by lactacystin, leading to similar TBC1D15 protein levels between mutant *GBA1* and isogenic control neurons (**Figure 4.9 b**). We next examined whether mitochondrial dysfunction was sufficient to disrupt TBC1D15 expression levels. Treatment of either the mitochondrial uncoupler CCCP, Complex I inhibitor rotenone, Complex III inhibitor Antimycin or the ATP synthase inhibitor Oligomycin did not disrupt TBC1D15 expression levels in HeLa cells (**Figure 4.9 c-f**). In contrast, increasing GCase activity in mutant *GBA1* neurons using the modulator S-181 (Burbulla et al. 2019) was sufficient to rescue the decreased levels of TBC1D15 (**Figure 4.6 e-f**). Thus, these findings suggest that TBC1D15 levels are downregulated at the protein level by proteosomal degradation in mutant *GBA1* neurons, due to the loss of GCase activity rather than general mitochondrial dysfunction.

Finally, we examined if loss of TBC1D15 was able to disrupt mitochondria-lysosome contact dynamics in human neurons. Knockdown of TBC1D15 in wild-type iPSC-derived neurons

(**Figure 4.10 a**) increased mitochondria-lysosome contact tethering duration (**Figure 4.10 b**), consistent with findings in non-neuronal cells and further supporting our results that decreased TBC1D15 levels in PD *GBA1*-linked patient neurons disrupt mitochondria-lysosome contact dynamics.

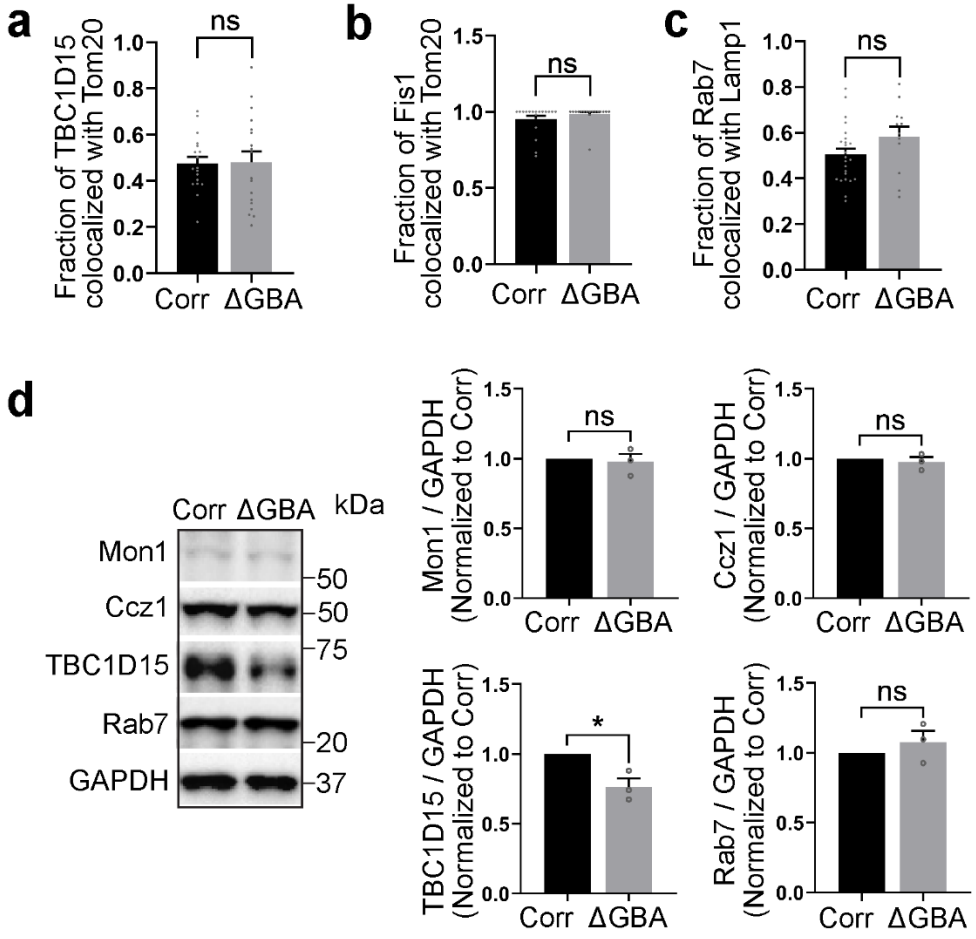


**Figure 4.8 Analysis of regulators of mitochondria-lysosome contact sites in *GBA1*-PD patient dopaminergic neurons**. (a-c) Mander's overlap coefficient (MOC) values were measured to quantify the fraction of (a) TBC1D15 colocalized with mitochondrial marker Tom20, (b) Fis1 colocalized with mitochondrial marker Tom20 and (c) Rab7 colocalized with lysosomal marker Lamp1 from immunostained confocal images in PD patient-derived mutant *GBA1* dopaminergic neurons (ΔGBA) and its CRISPR-corrected isogenic control (Corr) neurons. (a-c) Unpaired two-

sided Student's t-test. (d) Western blot analysis of Mon1 and Ccz1 (Rab7-GEF), TBC1D15 (Rab7-GAP) and Rab7 protein levels in ΔGBA and Corr neurons. Protein levels were normalized to loading control GAPDH. Values are expressed as fold-change compared to Corr. Paired two-sided Student's t-test; *p=0.0181. For all quantifications, data are the means ± S.E.M. *p≤ 0.05, ns: not significant.

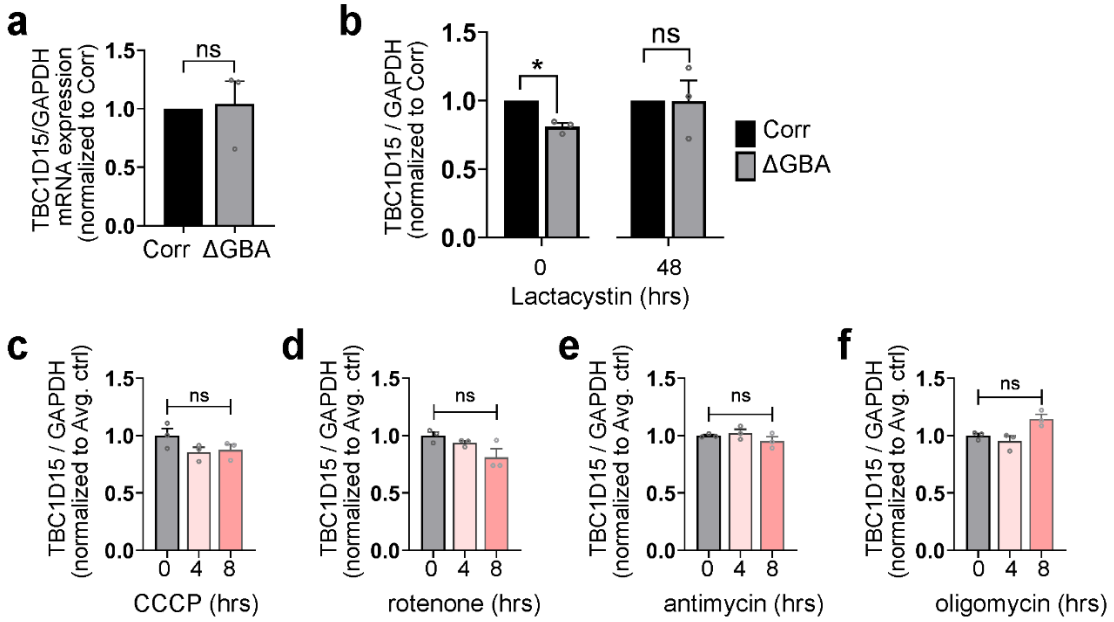


**Figure 4.9 Decreased TBC1D15 protein levels in *GBA1*-PD patient dopaminergic neurons.** (a) Quantification of TBC1D15 mRNA expression levels by RT-PCR analysis in PD patient-derived mutant *GBA1* dopaminergic neurons (ΔGBA) and its CRISPR-corrected isogenic control (Corr) neurons, showing no significant difference between Corr and ΔGBA neurons. (b) Western blot analysis of TBC1D15 level in Corr and ΔGBA neurons before and after the treatment of proteasome inhibitor lactacystin (1.5μM, 48hrs), showing that inhibition of proteasomal degradation leads to similar TBC1D15 levels in ΔGBA neurons and Corr neurons. *p=0.0192 (a-b) Paired two-sided Student's t-test. (c-f) Western blot analysis of TBC1D15 level in HeLa cells treated with mitochondrial toxins, normalized to ctrl (0h): (c) CCCP (10uM); (d) rotenone (100nM); (e) Antimycin A (1uM); (f) Oligomycin (1uM) for 0, 4, 8 hrs, showing that mitochondrial dysfunction does not alter TBC1D15 protein levels. (c-f) One-way ANOVA followed by Tukey's multiple comparisons test. For all quantifications, data are the means ± S.E.M. *p≤0.05, ns: not significant.

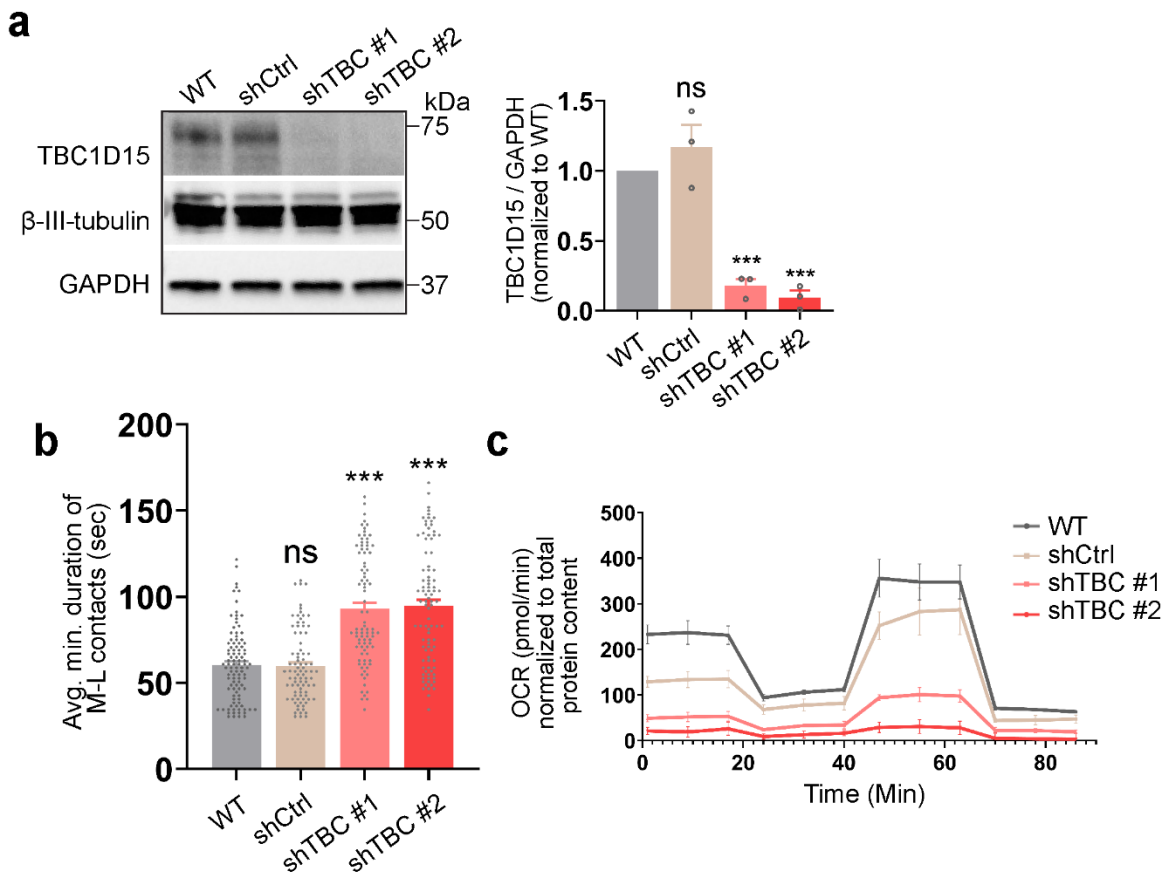


**Figure 4.10 Knockdown of TBC1D15 in human dopaminergic neurons disrupts mitochondria-lysosome contact dynamics and mitochondrial function. (a)** Neurons were infected with lentivirus expressing either non-targeting shRNA (shCtrl) or shRNAs to knock down TBC1D15 (shTBC #1 and #2) (MOI=5, 10 days). Western blot analysis shows knockdown efficiency. β-iii-tubulin and GAPDH were used as loading controls. (shTBC#1 ***p=0.0004; shTBC#2 ***p=0.0002;) **(b)** Quantification of average minimum duration of M-L contacts in wild-type neurons, non-targeting shRNA treated, and TBC-KD neurons. (shTBC#1 ***p<0.0001; shTBC#2 ***p<0.0001;) **(a-b)** One-way ANOVA followed by Tukey's multiple comparisons test. **(c)** Oxygen consumption rate (OCR) was measured by Seahorse assay and normalized to total protein content. For all quantifications, data are the means ± S.E.M. ***p≤0.001, ns: not significant.

### 4.2.4 Inhibition of GCase activity disrupts mitochondria-lysosome contact untethering

To further examine whether mitochondria-lysosome contact untethering defects were indeed dependent on loss of GCase activity, we treated wild-type human midbrain dopaminergic neurons expressing wild-type GCase with the GCase inhibitor conduritol-b-epoxide (CBE) (50μM; 7 days) which decreases neuronal GCase activity and promotes GlcCer accumulation (Burbulla et al. 2019; Cleeter et al. 2013; Mazzulli, Zunke, Tsunemi, et al. 2016). Using confocal live cell time-lapse imaging of mitochondria and lysosomes in both wild-type (Ctrl) and CBE treated (+CBE) human neurons, we found that mitochondria-lysosome contacts dynamically formed in both conditions (yellow arrows) (**Figure 4.11 a**). In addition, CBE treatment was effective in increasing lysosomal size as has been previously reported (**Figure 4.11 b, c**). Importantly, we found that inhibition of GCase activity by CBE treatment resulted in significantly prolonged mitochondria-lysosome contact tethering duration (***$P \leq 0.001$) (**Figure 4.11 a, d**), consistent with what we observed in mutant *GBA1* patient-derived neurons, and further confirming the effect of decreased GCase activity on disrupting mitochondria-lysosome contact untethering.

We additionally validated these findings in two other wild-type iPSC-derived neuronal lines which we characterized for iPSC and midbrain dopaminergic neuron specific markers (**Figure 4.12 a-c**). Inhibition of GCase activity with CBE treatment in both lines also led to significantly prolonged mitochondria-lysosome contact tethering duration (**Figure 4.12 d, e**), further supporting our results that inhibition of GCase activity disrupts mitochondria-lysosome contact dynamics in human neurons.

As loss of GCase activity results in significantly increased GlcCer levels (**Figure 4.11 e, f**), we then asked whether treatment of exogenous GlcCer in wild-type iPSC-derived neurons could be sufficient to disrupt mitochondria-lysosome contact dynamics. Using live cell microscopy of mitochondria and lysosomes in wild-type iPSC-derived neurons treated with exogenous GlcCer, we found that this also led to significantly prolonged contact site tethering duration (****P<0.001*) (**Figure 4.11 g**), highlighting a role for increased GlcCer levels in mutant *GBA1* neurons in dysregulating mitochondria-lysosome contacts.

Next, we investigated whether inhibition of GCase activity also disrupted mitochondria-lysosome contact untethering machinery. We measured the total protein levels of Rab7 together with TBC1D15 and Fis1 in wild-type (Ctrl) and CBE treated (+CBE) human neurons (**Figure 4.11 h-k**). Indeed, CBE treated neurons also showed significantly decreased TBC1C15 levels (***P* ≤ 0.01) (**Figure 4.11 h-i**), without changes in total Rab7 or Fis1 levels (**Figure 4.11 j, k**), consistent with mutant *GBA1* patient-derived neurons. To further support these findings, wild-type iPSC-derived neurons treated with exogenous GlcCer also showed reduced TBC1D15 levels (**Figure 4.12 f, g**).

We then examined whether inhibition of GCase activity by CBE treatment led to similar defects in Rab7 GTP hydrolysis, resulting in elevated GTP-bound Rab7 levels. Using the GST-RILP pull-down assay in CBE-treated neurons (**Figure 4.11 l**), we further found that GCase inhibition resulted in increased levels of RAB7-GTP / total Rab7 (**Figure 4.11 l, m**), consistent with what we observed in mutant *GBA1* neurons. In summary, our results from both mutant *GBA1* and CBE-treated neurons support the hypothesis that loss of GCase activity, which increases

GlcCer levels, leads to disruption of TBC1D15 levels and Rab7-GTP hydrolysis in neurons, resulting in the misregulation of mitochondria-lysosome contact untethering dynamics.

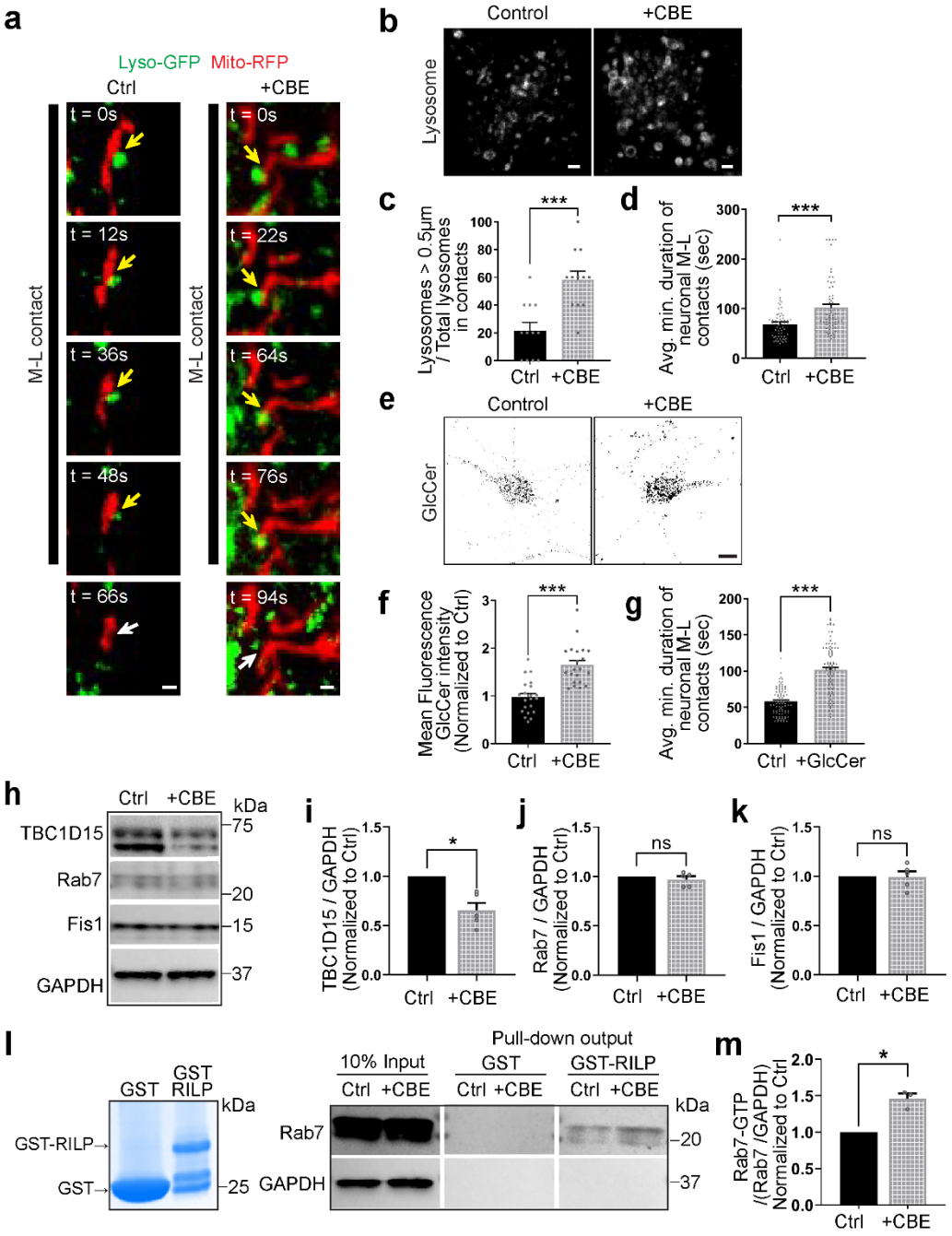


**Figure 4.11 Inhibition of GCase activity disrupts mitochondria - lysosome contact untethering in dopaminergic neurons.** (a) Healthy control WT human iPSC-derived dopaminergic neurons were treated with vehicle (Ctrl) or CBE (50µM; 7 days) to inhibit GCase activity. Representative time-lapse confocal images of contacts between mitochondria (red, Mito-RFP) and lysosomes (green, Lyso-GFP) in Ctrl (left) and CBE-treated (right) human neurons. Yellow arrows mark stable M-L contacts. White arrows mark the site of M-L contacts after contact untethering. Black line shows duration of contacts. Scale bar = 500nm. (b) Representative

confocal images of lysosomes (LAMP1–GFP) in the Ctrl (left) and CBE-treated (right) human neurons. Scale bar = 1μm. (c) The effect of CBE treatment on lysosomal morphology were confirmed by quantification of the percentage of lysosomes that were enlarged (diameter >0.5um) in M-L contacts. Unpaired two-sided Student's t-test; ***p=0.0001. (d) CBE treatment in control neurons increased the average minimum duration of stable M-L contacts. Unpaired two-sided Student's t-test; ***p=0.0001. € Representative confocal images of immunocytochemistry of GlcCer in the Ctrl (left) and CBE-treated (right) human neurons. Scale bar = 5μm. (f) Quantification of CBE treatment leading to increased GlcCer levels as measured by immunofluorescence signal of GlcCer. (g) Exogenous GlcCer treatment in control neurons increased the average minimum duration of stable M-L contacts. (f-g) Unpaired two-sided Student's t-test; ***p<0.0001. (h-k) Western blot analysis of (i) TBC1D15, (j) Rab7 and (k) Fis1 levels in Ctrl and CBE-treated neurons. Protein levels were normalized to loading control GAPDH. Values are expressed as fold-change compared to Ctrl. Paired two-sided Student's t-test; *p=0.0104. (l-m) GST-RILP pull-down to measure GTP-bound Rab7 levels in Ctrl and CBE-treated neurons. (m) Rab7-GTP levels were normalized to total Rab7 normalized to GAPDH. Values are expressed as fold-change compared to Ctrl. Paired two-sided Student's t-test; *p=0.0242. For all quantifications, data are means ± S.E.M. *p ≤0.05, ***p ≤ 0.001.

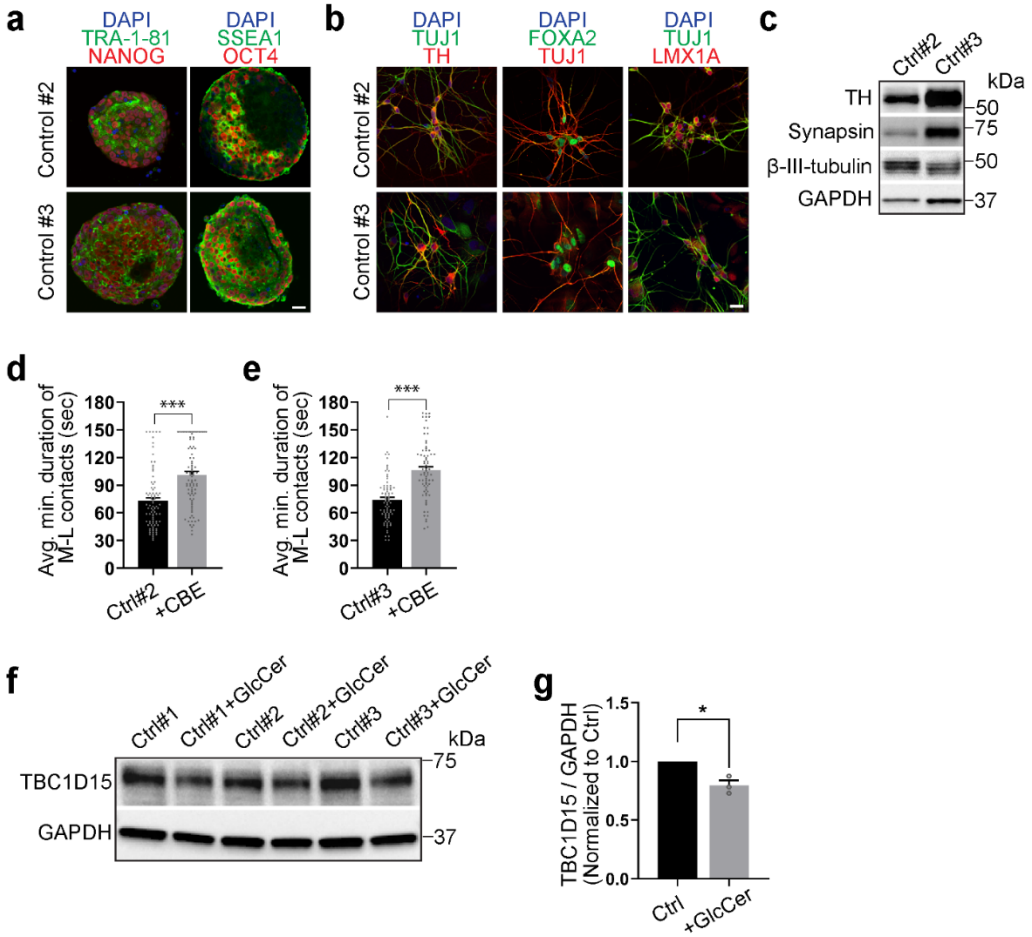


**Figure 4.12 Inhibition of GCase activity leading to increased GlcCer disrupts mitochondria-lysosome contact dynamics and machinery.** (a) Immunocytochemistry demonstrated that two additional wild-type control iPSC lines (Control #2 and Control #3) expressed pluripotency markers including Oct4, SSEA1, TRA-1-81 and Nanog. Left panel, merged images of Tra 1-81 (green), Nanog (red), and DAPI (blue) nuclear staining. Right panel, merged images of Oct4 (red), SSEA1 (green), and DAPI (blue) nuclear staining from both control lines. Scale bar, 20µm. (b-c) Characterization of wild-type control iPSC-derived dopaminergic neurons (Control #2 and Control #3). (b) Neurons were analyzed by immunofluorescence for the expression of dopamine (TH; tyrosine hydroxylase), midbrain (FOXA2, LMX1A) and neuronal cytoskeletal (Tuj1) markers at day 30. Scale bar = 20µm. (c) Western blot analysis of human dopaminergic neurons at day 50. The expression of dopaminergic neuronal markers (TH, Synapsin and β−iii Tubulin) were confirmed in two control lines. (d-e) CBE treatment in control neurons increased the average minimum duration of stable M-L contacts. Unpaired two-sided Student's t-test; ***$p<0.0001$ (f-g) Western blot analysis of TBC1D15 in Ctrl (#1, #2, and #3) and GlcCer-treated neurons. Protein levels were normalized to loading control GAPDH. Values are expressed as fold-change compared to Ctrl. Paired two-sided Student's t-test; *$p=0.0401$. For all quantifications, data are the means ± S.E.M. *$p\leq0.05$, ***$p\leq0.001$.

## 4.3 DISCUSSION

Parkinson's disease has been both genetically and functionally linked to mitochondrial and lysosomal dysfunction with the identification of familial mutations in mitochondrial-associated genes (Parkin, PINK1, and DJ-1) and endolysosomal-associated genes (VPS35, PARK9, and GBA1) (Plotegher and Duchen 2017a). Moreover, both mitochondrial and lysosomal dysfunction have been observed in human dopaminergic neurons from idiopathic PD patients (Burbulla et al. 2017), suggesting that these two organelles play a critical role in disease progression.

Utilizing WT healthy control and *GBA1*-PD patient iPSC-derived dopaminergic neurons, we showed reduced GCase activity caused by either *GBA1* mutation or CBE inhibition downregulates the level of mitochondria-lysosome contact tethering protein, TBC1D15, and therefore, leads to mitochondria-lysosome contacts dysfunction. We further observed that misregulation of mitochondria-lysosome contact dynamics was preferentially caused by loss of GCase activity but not by other lysosomal enzymes such as lysosomal acid ceramidase, cysteine protease, or aspartyl proteases. Finally, addition of GlcCer, a substrate of GCase which accumulates upon loss of GCase activity, was also sufficient to prolong mitochondria-lysosome contacts, consistent with what was observed upon loss of GCase activity in both *GBA1*-PD neurons and CBE-treated neurons.

Thus, misregulation of mitochondria-lysosome contact dynamics may simultaneously give rise to dysfunction in both organelles. As both mitochondria and lysosomes are critical for neuronal homeostasis and have been implicated in both familial and idiopathic PD, our research offers new insights into disease mechanisms by highlighting a potential role for defective mitochondria-lysosome contact regulation in PD pathogenesis.

# CHAPTER 5.

# MITOCHONDRIAL DEFECTS OCCUR DOWNSTREAM OF MITOCHONDRIA – LYSOSOME CONTACT DYSFUNCTION IN *GBA1*-LINKED PARKINSON'S DISEASE NEURONS

## 5.1 OVERVIEW

We previously showed that mitochondria-lysosome contacts are prolonged in *GBA1*-PD neurons (**Figure 4.2 a-b**). However, it was unclear how the misregulation of mitochondria-lysosome contacts further affect dopaminergic neurons in PD pathogenesis. Recent studies have revealed that mitochondria-lysosome contacts directly regulate both mitochondrial dynamics and motility (Cioni et al. 2019; Guo et al. 2018a; Wong, Peng, and Krainc 2019; Wong, Ysselstein, and Krainc 2018). Based on these finding, we investigated whether mitochondrial dynamics might be disrupted in PD patient-derived mutant *GBA1* dopaminergic neurons. In addition to mitochondrial distribution, we also examined mitochondrial function in these neurons.

Here, we observed disrupted axonal mitochondrial density in *GBA1*-PD neurons, together with decreased oxygen consumption rate (OCR) and cellular ATP levels which were further confirmed by decreased AMPK activation (**Figure 5.2 d-f**). To further examine the relationship between misregulated mitochondria-lysosome contacts and mitochondrial dysfunction in *GBA1*-PD neurons, we expressed the contact regulator TBC1D15 which rescued prolonged contact duration (**Figure 5.2 b**). Importantly, TBC1D15 expression was also sufficient to rescue defects

in mitochondrial density in axons and ATP levels in mutant *GBA1* neurons (**Figure 5.4 e**). Together, our findings suggest that reduced GCase activity results in the misregulation of mitochondria–lysosome contact dynamics, which contributes to downstream defects in both mitochondrial distribution and function to drive Parkinson's disease pathogenesis in *GBA1*-PD patient neurons.

## 5.2 RESULTS

### 5.2.1 *GBA1* mutant disrupts mitochondrial distribution and function

Mitochondria-lysosome contacts mediate the bidirectional regulation of both mitochondrial and lysosomal network dynamics, and importantly are able to directly regulate both mitochondrial dynamics and motility (Cioni et al. 2019; Guo et al. 2018a; Wong, Peng, and Krainc 2019; Wong, Ysselstein, and Krainc 2018). We thus investigated whether mitochondrial dynamics might be disrupted in PD patient-derived mutant *GBA1* dopaminergic neurons, consistent with defective mitochondria-lysosome contact untethering, by analyzing the distribution of mitochondria in the soma and axons. Healthy mitochondria with intact mitochondrial membrane potential were imaged by live cell imaging in patient-derived mutant *GBA1* (ΔGBA) and CRISPR-corrected isogenic control (Corr) neurons (**Figure 5.1 a**). Interestingly, while there was no difference in mitochondrial density in the soma (**Figure 5.2 a, b; Figure 5.1 b**), we found that axonal mitochondrial density was significantly decreased in mutant *GBA1* neurons compared to axons of isogenic control neurons (**Figure 5.2 a, c**), suggesting that mutant *GBA1* preferentially disrupts axonal mitochondrial distribution in Parkinson's patient neurons. In addition, we also

observed defective mitochondrial respiration as measured by decreased oxygen consumption rate (OCR) in mutant *GBA1* neurons (**Figure 5.2 d**), as well as decreased AMPK activation (**Figure 5.2 e**), compared to isogenic control neurons. We also measured cellular ATP level and found significantly decreased ATP levels in mutant *GBA1* neurons compared to isogenic controls (**Figure 5.2 f**), even after normalization for mitochondrial mass (***P<0.001; Corr vs GBA [ATP intensity/TOM20 levels]). Consistent with our findings that TBC1D15 levels were decreased in mutant *GBA1* neurons, we also observed mitochondrial dysfunction in TBC1D15 knockdown neurons (**Figure 4.10**).

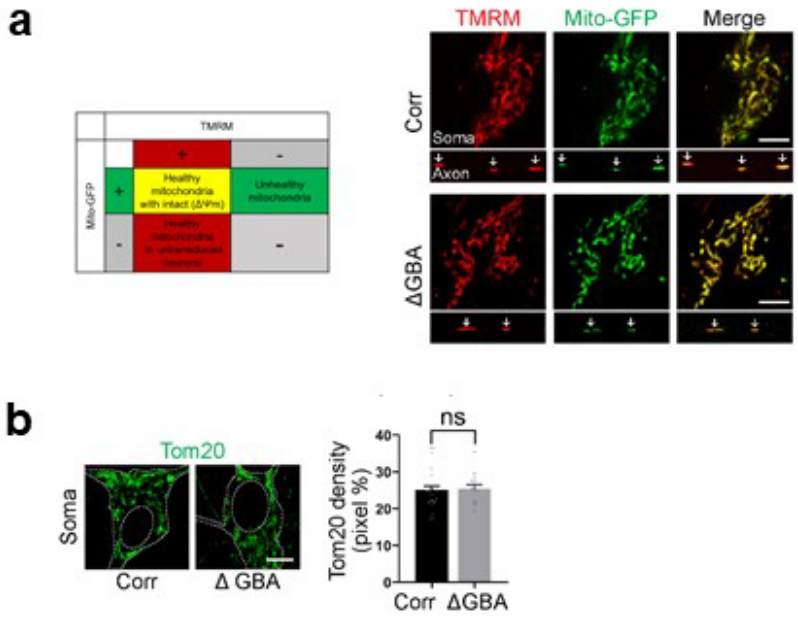


**Figure 5.1 TMRM and immunofluorescence staining of mitochondria in *GBA1*-PD patient dopaminergic neurons.** (c) Tetramethylrhodamine ethyl ester (TMRM, red) accumulates in active mitochondria with intact membrane potentials (ΔΨm), and colocalized with CellLight® Mitochondria-GFP (Mito-GFP, green) which labels all mitochondria in transduced neurons (table). Representative confocal images of mitochondria labelled with TMRM and/or Mito-GFP in PD patient-derived mutant *GBA1* dopaminergic neurons (ΔGBA) and its CRISPR-corrected isogenic control (Corr) neurons. Arrows mark mitochondria in a single axon. Scale bar, 5µm. (b) Immunocytochemistry of mitochondrial marker Tom20 (green) in soma. The density of signal was calculated as the percentage of green pixels divided by the total number of pixels in a neuron. For all quantifications, data are the means ± S.E.M. ns: not significant.

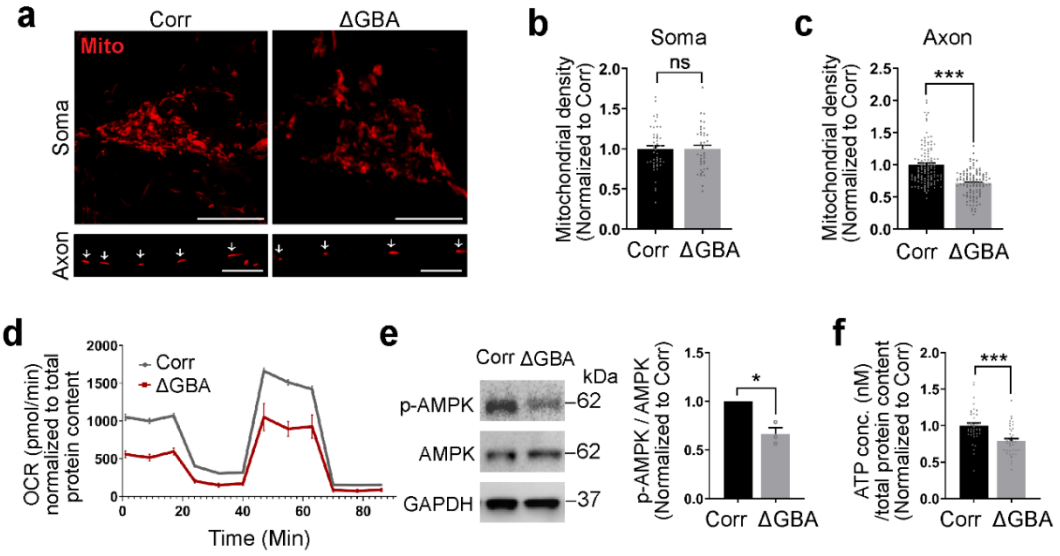


**Figure 5.2 Mitochondrial dysfunction due to prolonged mitochondria-lysosome contacts is partially rescued by expression of TBC1D15 in *GBA*1-PD patient dopaminergic neurons.** (a) Live cell distribution of mitochondria (TMRM, red) in the soma and axons from PD patient-derived mutant *GBA1* dopaminergic neurons (ΔGBA) and its CRISPR-corrected isogenic control (Corr) neurons. White arrows mark mitochondria in a single axon. Scale bar, 10μm. (b) Quantified mitochondrial density in the soma (TMRM-positive pixels / pixels of soma). (c) Quantified mitochondrial density in axons (mitochondria count / length of dendrite (μm)). (b-c) Unpaired two-sided Student's t-test; ***p<0.0001. (d) Oxygen consumption rate (OCR) was measured and normalized to total protein content. (e) Western blot analysis of phospho-AMPKα and AMPKα levels in Corr and ΔGBA neurons. Ratio of p-AMPKα/AMPKα are expressed as fold-change compared to Corr. Paired two-sided Student's t-test; *p=0.0354. (f) Total cellular ATP content was measured and normalized to total protein content (ng/μl). Unpaired two-sided Student's t-test; ***p<0.0001. For all quantifications, data are the means ± S.E.M. *p≤ 0.05, ***p≤0.001, ns: not significant.

### 5.2.2 Mitochondrial dysfunction due to prolonged mitochondria-lysosome contacts is partially rescued by TBC1D15 expression

Based on our finding of abnormal mitochondrial distribution and function in mutant *GBA1* neurons, we hypothesized that dysregulated mitochondria-lysosome contact untethering dynamics

in mutant *GBA1* neurons might contribute to these defects in mitochondrial distribution and function. Thus, to test if these defects could be rescued by promoting mitochondria-lysosome contact untethering in mutant *GBA1* neurons, we expressed human TBC1D15 in mutant *GBA1* neurons by lentiviral transduction (**Figure 5.3 a**). The expression of exogenous TBC1D15 in neurons was confirmed by western blot analysis and fluorescence imaging (**Figure 5.3 b, c**). Importantly, consistent with our previous findings that TBC1D15 promotes mitochondria-lysosome contact untethering (Wong, Ysselstein, and Krainc 2018), transduction of wild-type TBC1D15 in mutant *GBA1* neurons (ΔGBA+TBC1D15) was able to promote mitochondria-lysosome contact untethering, resulting in significantly decreased mitochondria-lysosome contact durations compared to lentiviral vehicle-treated neurons (ΔGBA+veh) (***P ≤ 0.001) (**Figure 5.4 b**).

We further investigated the effect of rescuing mitochondria-lysosome contact dynamics on axonal mitochondrial density in mutant *GBA1* neurons. Interestingly, while TBC1D15 expression did not alter mitochondrial densities in the soma of mutant *GBA1* neurons (**Figure 5.4 a, c**), it significantly rescued the decreased mitochondrial density in axons of mutant *GBA1* neurons (**Figure 5.4 a, d**). Moreover, TBC1D15 expression was also able to partially rescue ATP levels in mutant *GBA1* neurons (**Figure 5.4 e**). Together, our results suggest that upregulation of TBC1D15 in PD patient mutant *GBA1* neurons is sufficient to rescue the misregulation of mitochondria-lysosome contact untethering, as well as downstream defects in mitochondrial dynamics and function.

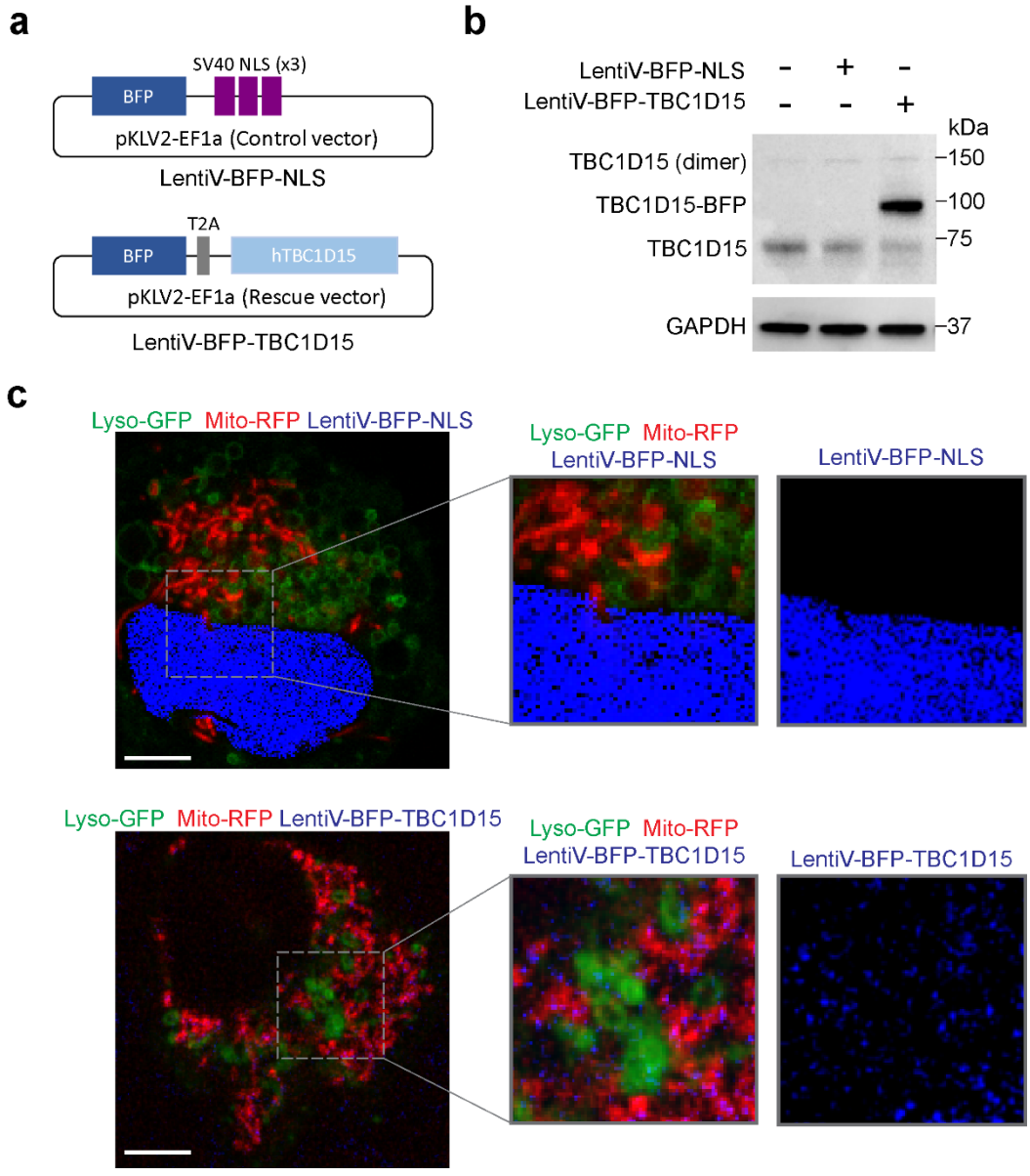


**Figure 5.3 Lentiviral expression of human TBC1D15 in iPSC-derived dopaminergic neurons.** (a) Lentiviral vector constructs expressing the BFP-NLS (vehicle control vector) or BFP-TBC1D15 (rescue vector) under control of the EF-1α promoter. (b) Western blot analysis of TBC1D15 in wild-type human iPSC-derived dopaminergic neurons transduced by lentivirus expressing nuclear-localized BFP or BFP-tagged TBC1D15. GAPDH was used as a loading control. (c) Representative confocal images of lentiviral BFP, mitochondria (Mito-RFP, red) and lysosomes (Lyso-GFP, green) in live wild-type neurons. Scale bar, 5μm.

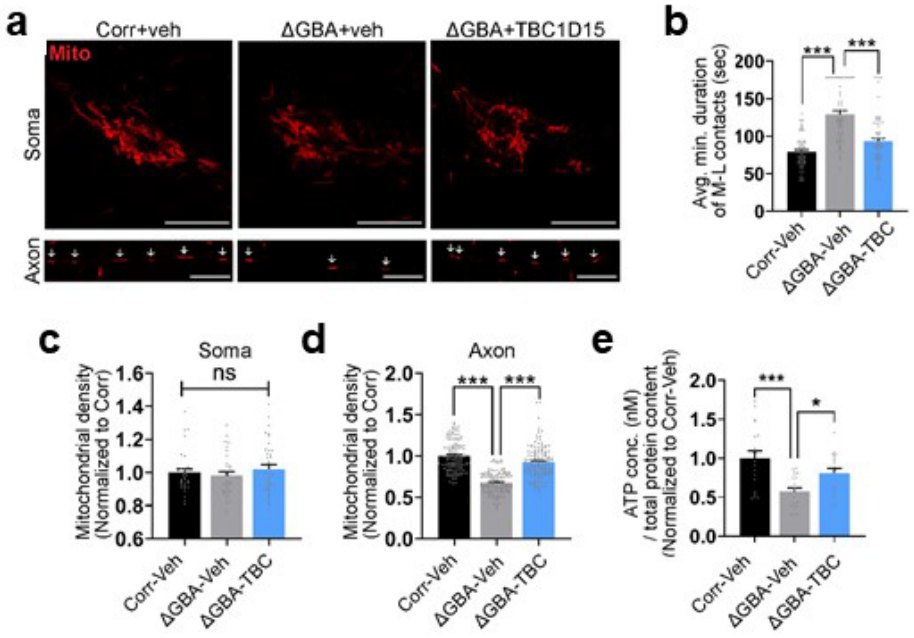


**Figure 5.4 Mitochondrial dysfunction due to prolonged mitochondria-lysosome contacts is partially rescued by expression of TBC1D15 in *GBA1*-PD patient dopaminergic neurons.** (a) Live cell distribution of mitochondria (TMRM, red) in the soma and axons from Corr and ΔGBA human neurons with or without human TBC1D15 lentiviral expression. White arrows mark mitochondria in a single axon. Scale bar, 10μm. (b) Quantification of average minimum duration of M-L contacts in Corr-vehicle, ΔGBA-vehicle, ΔGBA-TBC1D15. ***p<0.0001. (c) Quantified mitochondrial density in the soma (TMRM-positive pixels / pixels of soma). Corr-vehicle, ΔGBA-vehicle, ΔGBA-TBC1D15. (d) Quantified mitochondrial density in axons (mitochondria count / length of axon (μm)). Corr-vehicle, ΔGBA-vehicle, ΔGBA-TBC1D15. ***p<0.0001. (e) Total cellular ATP concentration was measured and normalized to total protein content (ng/μl). Corr-vehicle, ΔGBA-vehicle, ΔGBA-TBC1D15. ***p=0.0002, *p=0.0493. (b-e) One-way ANOVA followed by Tukey's multiple comparisons test. For all quantifications, data are the means ± S.E.M. *p≤ 0.05, ***p≤0.001, ns: not significant.

### 5.2.3 Prolonged mitochondria-lysosome contacts and mitochondrial phenotypes in neurons harboring mutant *GBA1* N370S

Finally, we extended our analysis to additional PD mutant *GBA1* patient neurons (Δhet N370S) and CRISPR-edited isogenic control neurons (**Figure 5.5 a-c**). Mutant *GBA1* (N370S) patient neurons also showed decreased GCase levels and enzymatic activity (**Figure 5.5 d-g**). Importantly, they also had significantly increased GTP-bound Rab7 due to lower TBC1D15 levels (**Figure 5.5 h-m**), which resulted in prolonged mitochondria-lysosome contact tethering (**Figure 5.5 n**). Moreover, S-181 modulator treatment in mutant *GBA1* (N370S) neurons was sufficient to rescue both mitochondria-lysosome contact dynamics (**Figure 5.5 n**) as well as TBC1D15 levels (**Figure 5.5 o**). In addition, mutant *GBA1* (N370S) neurons also demonstrated reduced mitochondrial function (**Figure 5.5 p**). Thus, these findings further highlight the role of defective GCase activity in PD *GBA1*-linked patient neurons on disrupting Rab7 GTP hydrolysis machinery and mitochondria-lysosome contact site dynamics.

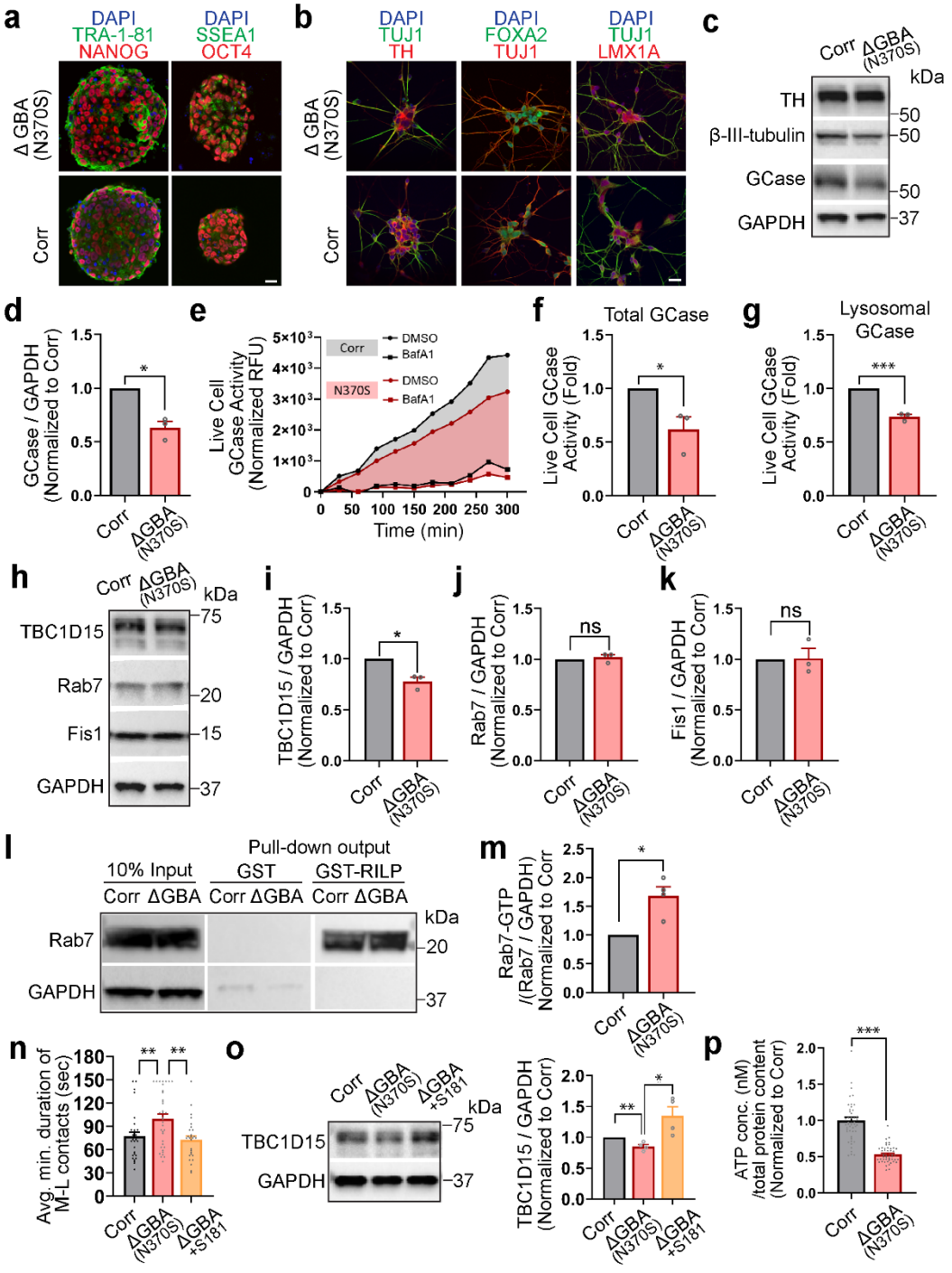


**Figure 5.5 Defective mitochondria-lysosome contact dynamics in mutant *GBA1* (N370S) Parkinson's patient-derived neurons.** (a) Immunocytochemistry demonstrated that mutant *GBA1* (ΔGBA (het N370S)) and CRISPR-corrected isogenic control (Corr) iPSCs expressed pluripotency markers including Oct4, SSEA1, TRA-1-81 and Nanog. Left panel, merged images of Tra 1-81 (green), Nanog (red), and DAPI (blue) nuclear staining. Right panel, merged images

of Oct4 (red), SSEA1 (green), and DAPI (blue) nuclear staining from each line. Scale bar, 20μm. (b-d) Characterization of ΔGBA (N370S) and Corr iPSC-derived dopaminergic neurons. (b) Neurons were analyzed by immunofluorescence for the expression of dopamine (TH; tyrosine hydroxylase), midbrain (FOXA2, LMX1A) and neuronal cytoskeletal (Tuj1) markers at day 30. Scale bar = 20μm. (c) Western blot analysis of human dopaminergic neurons at day 50. The expression of dopaminergic neuronal markers (TH and β−iii Tubulin) was confirmed in Corr and ΔGBA (N370S) lines. (d) GCase levels were significantly reduced in ΔGBA (N370S) neurons. Paired two-sided Student's t-test; *p=0.0249. (e-g) ΔGBA (N370S) and Corr neurons were treated with either DMSO or BafA1 and subjected to live cell GCase activity analysis. (f) Quantification of the area under each curve (AUC) demonstrates decreased total GCase activity in ΔGBA (N370S) neurons. (g) Lysosomal GCase activity was calculated by subtracting BafA1 values from DMSO. Values are expressed as fold-change compared to Corr. (f-g) Paired two-sided Student's t-test; *p=0.0304; ***p=0.0002. (h-k) Western blot analysis of (i) TBC1D15, (j) Rab7 and (k) Fis1 levels in Corr and ΔGBA (N370S) neurons. Protein levels were normalized to loading control GAPDH. Values are expressed as fold-change compared to Corr. Paired two-sided Student's t-test; *p=0.0344. (l-m) GST-RILP pull-down to measure GTP-bound Rab7 levels in ΔGBA (N370S) and Corr neurons. (m) Rab7-GTP levels were normalized to total Rab7 normalized to GAPDH. Values are expressed as fold-change compared to Corr. Paired two-sided Student's t-test; *p=0.0242 (n) Quantification of average minimum duration of stable M-L contacts showing increased duration of stable M-L contacts in ΔGBA (N370S) neurons, which was rescued by GCase modulator S181. One-way ANOVA followed by Tukey's multiple comparisons test; **p=0.0099(left); **p=0.0023(right). (o) Western blot analysis of TBC1D15 in Corr, ΔGBA (N370S) and S181-treated ΔGBA (N370S) neurons. GAPDH was used as a loading control. Values are expressed as fold-change compared to Ctrl. One-way ANOVA followed by Tukey's multiple comparisons test; **p=0.0040(left); *p=0.0183(right). (p) Total cellular ATP content was measured and normalized to total protein content (ng/μl). Corr, ΔGBA (N370S). Unpaired two-sided Student's t-test; ***p<0.0001. For all quantifications, data are the means ± S.E.M. *p≤ 0.05, **p≤0.01, ***p≤0.001, ns: not significant.

## 5.3 DISCUSSION

Recent studies on genetic forms of PD have provided useful insights into cellular pathways associated with disease etiology. Importantly, the dysfunction of multiple pathways related to mitochondria has been markedly implicated in PD pathogenesis (Chen, Turnbull, and Reeve 2019; Nguyen et al. 2019; Sironi et al. 2020). In addition, while *GBA1* encodes a lysosomal enzyme GCase, loss of GCase activity has previously been linked to mitochondrial dysfunction (Cleeter et al. 2013; Do et al. 2019; Moren et al. 2019).

Here, we demonstrated that misregulation of mitochondria-lysosome contacts in *GBA1*-PD may help to explain how loss of lysosomal enzyme activity can contribute to mitochondrial dysfunction and mislocalization. First, we showed that *GBA1* mutant 84GG disrupts axonal mitochondrial distribution. Given that mitochondria, by providing ATP, play an important role in neuronal survival and synaptic function, the reduced number of mitochondria in axons may further contribute to neuronal death in PD. Additionally, we observed decreased cellular ATP levels and decreased OCR in *GBA1*-PD neurons as further evidence of disrupted mitochondrial function. Next, to identify the potential mechanisms driving mitochondrial dysfunction, we modulated the levels of the mitochondria-lysosome contact regulator, TBC1D15, using lentiviral overexpression or shRNA-based knock down. As TBC1D15 promotes mitochondria-lysosome contact untethering by driving Rab7 GTP hydrolysis, we confirmed that TBC1D15 expression promoted mitochondria-lysosome contact untethering. Interestingly, up-regulation of TBC1D15 was sufficient to further rescue mitochondrial phenotypes in *GBA1*-PD neurons. In contrast, down-regulation of TBC1D15 in control neurons led to prolonged mitochondria-lysosome contact tethering, and further decreased OCR, consistent with what was observed in *GBA1*-PD neurons.

Importantly, phenotypes observed in *GBA1* het 84GG neurons (reduced GCase activity, decreased TBC1D15 level, increased Rab7-GTP level and prolonged mitochondria-lysosome contact tethering) were also recapitulated in patient neurons expressing another *GBA1* mutant het N370S. Moreover, increasing GCase activity by S-181 treatment rescued the prolonged M-L contact tethering in both 84GG and N370S mutant *GBA1* neurons. Taken together, loss of activity in the lysosomal enzyme GCase is sufficient to cause mitochondria-lysosome contact dysfunction in multiple *GBA1*-PD patient neurons.

Our work demonstrates a potential role of mitochondria-lysosome contacts as an upstream regulator of mitochondrial function and dynamics in midbrain dopaminergic neurons in *GBA1*-linked Parkinson's disease. This study is highly relevant for advancing our understanding of fundamental neuronal biology and for elucidating the interplay between mitochondria and lysosomes in neurons. Ultimately, this work provides important insight into establishing therapeutic targets and treatment for Parkinson's disease, and potentially other neurodegenerative diseases linked to both mitochondrial and/or lysosomal dysfunction.

# CHAPTER 6.

# DISCUSSION

## 6.1 Use of iPSC-derived neurons for Parkinson's disease modeling

Since the discovery of the factors capable of rendering cells into a state of pluripotency, many advancements have been made in Parkinson's disease research. One of the main benefits to using iPSCs to model Parkinson's disease is the genetic background of the patient cells, which allows for direct study of relevant disease mutations. Moreover, pluripotency can lead to the generation of disease specific cell types, allowing for the study of Parkinson's disease mechanisms in human dopaminergic neurons. In addition, the ability to generate isogenic controls from patient lines using CRISPR/Cas9 -based correction technologies has proven to be essential for identifying which phenotypes arise from specific mutations.

Importantly, human neurons have also provided a unique opportunity for screening and testing novel therapeutics that could not have been revealed by traditional cell culture or animal model experiments. Indeed, human PD iPSC-DA neurons in long-term culture show time-dependent onset of PD phenotypes such as early defects in lysosomal dysfunction followed by subsequent α-synuclein accumulation (Tsunemi et al. 2019). Patient-derived PD iPSC-DA neurons also exhibit multiple pathogenic phenotypes that are not observed in mouse models of PD, which display negligible levels of oxidized dopamine. In particular, human DJ-1 KO iPSC-derived neurons demonstrate decreased lysosomal GCase activity and reduced tyrosine hydroxylase (TH) in the SNc which are not observed in DJ-1 KO mice (Burbulla et al. 2017). Thus, patient-derived

iPSC-based PD modeling may allow for the study of distinct pathogenic phenotypes arising over time which were not previously found in animal or traditional cell models.

## 6.2 Dysregulation of mitochondria-lysosome contacts in neuronal models of Parkinson's disease

Our work demonstrates that mitochondria-lysosome contact sites dynamically form in human neurons, and further investigates their role in neurons from patients with *GBA1*-linked PD. We found that loss of lysosomal GCase enzymatic activity in PD patient-derived dopaminergic neurons led to prolonged mitochondria-lysosome contact tethering dynamics due to defective contact untethering machinery, and resulted in misregulated axonal distribution of mitochondria and decreased ATP levels. Importantly, we showed that rescuing mitochondria-lysosome contact site dynamics in PD patient neurons is sufficient to ameliorate defects in mitochondrial distribution and function, thus highlighting a potential role for mitochondria-lysosome contact site dysregulation in PD pathogenesis.

Multiple genes linked to mitochondria or lysosomes have been identified as causative or risk genes of PD (Abeliovich and Gitler 2016; Chang et al. 2017). Moreover, both mitochondrial and lysosomal dysfunction have been implicated in PD (Burbulla et al. 2017; Cuddy et al. 2019; Giaime et al. 2017; Kim et al. 2013; Mazzulli et al. 2011; Nguyen et al. 2019; Ordonez, Lee, and Feany 2018; Pickrell and Youle 2015; Valadas et al. 2018), suggesting a functional crosstalk between these two organelles.

Despite the previously studied role of mitochondria and lysosomes in PD pathogenesis, a direct homeostatic relationship between these two organelles that is independent of eventual lysosomal degradation of mitochondria has not been examined. In this context, our work provides evidence for the role of mitochondria-lysosome contacts not only in the homeostasis of dopaminergic neurons but also as a link between mitochondrial and lysosomal dysfunction in PD pathogenesis. We specifically focused on *GBA1* mutations which represent the greatest genetic risk factor for PD (Sidransky and Lopez 2012; Sidransky et al. 2009). Importantly, wild-type GCase enzyme activity is also reduced in patient neurons with genetic or idiopathic PD who do not harbor *GBA1* mutations (Burbulla et al. 2019; Burbulla et al. 2017; Mazzulli et al. 2011; Nguyen et al. 2018), suggesting that loss of GCase activity is an important contributor to PD pathogenesis. Previously, we reported that the loss of GCase function in patient neurons compromises lysosomal protein degradation (Mazzulli et al. 2011) which contributes to other key PD pathogenic phenotypes including α-synuclein accumulation (Bae et al. 2014; Mazzulli et al. 2011; Mazzulli, Zunke, Isacson, et al. 2016). In addition to its primary lysosomal dysfunction, *GBA1* mutations and abnormal GCase activity have also been linked to mitochondrial dysfunction (Burbulla et al. 2017; Cleeter et al. 2013; de la Mata et al. 2015; Gegg and Schapira 2016; Li et al. 2019; Osellame et al. 2013; Schondorf et al. 2018).

We show that *GBA1* mutant PD patient neurons have defective mitochondria-lysosome contact dynamics, resulting in prolonged contact tethering. While previous studies did not examine the GTP-bound state of Rab7 (Aflaki et al. 2017; Magalhaes et al. 2016), we found that loss of GCase activity resulted in an increased percentage of active GTP-bound lysosomal Rab7, which directly mediates mitochondria-lysosome contact tethering (Wong, Ysselstein, and Krainc 2018).

This is likely due to decreased levels of TBC1D15 (Rab7 GAP) in mutant *GBA1* patient neurons, as TBC1D15's GAP activity promotes Rab7 GTP hydrolysis and subsequent mitochondria-lysosome contact untethering (Wong, Ysselstein, and Krainc 2018). Indeed, we found that increasing TBC1D15 expression was sufficient to rescue the prolonged mitochondria-lysosome contact tethering we observed in mutant *GBA1* neurons. In addition, we further observed mitochondrial dysfunction in patient neurons, including abnormal mitochondrial distribution in axons, decreased mitochondrial respiration and lower ATP levels. Of note, TBC1D15 expression was also able to rescue mitochondrial dysfunction. Thus, dysregulation of mitochondria-lysosome contacts may play an important role in *GBA1*-linked PD pathogenesis, and targeting contact machinery may help ameliorate downstream mitochondrial dysfunction. Given that mitochondria play key roles as energy suppliers especially in the synapses of active neurons, we hypothesize that such abnormal distribution of mitochondria may further contribute to synaptic dysfunction in PD (Nguyen et al. 2019).

While inter-organelle contact sites have been found to be essential subdomains for modulating cellular function and homeostasis (Daniele and Schiaffino 2014; Eisenberg-Bord et al. 2016; Helle et al. 2013), only recently have studies reported the function and molecular architecture of inter-organelle contacts in neurons, such as those between the mitochondria and endoplasmic reticulum (Hirabayashi et al. 2017; Valadas et al. 2018; Wu et al. 2017). In addition, dysfunction of inter-organelle contacts in disease have been shown to be key contributors in the development of various diseases (Allison et al. 2017; Chu et al. 2015; Cioni et al. 2019; Hoglinger et al. 2019; Lee et al. 2018; Liao et al. 2019; Lim et al. 2019; Peng, Wong, and Krainc 2020; Valadas et al. 2018; Wong et al. 2019; Wong, Peng, and Krainc 2019). Moreover, the recent

identification of mitochondria-lysosome contact sites has shed new light on the direct relationship between mitochondria and lysosomes in a pathway independent of lysosomal degradation of mitochondria (Aston et al. 2017; Cioni et al. 2019; Fermie et al. 2018; Han et al. 2017; Valm et al. 2017; Wong, Ysselstein, and Krainc 2018), allowing for direct crosstalk and regulation of both organelles in a dynamic manner (Wong et al. 2019). In our previous study, we showed the formation of mitochondria-lysosome contacts in non-neuronal cells and identified protein mediators responsible for contact untethering (Wong et al. 2019; Wong, Ysselstein, and Krainc 2018). Here, we demonstrate that mitochondria-lysosome contacts are also key contributors in human neurons and that contacts dynamically form in multiple neuronal compartments, suggesting that they act as important sites for the neuronal regulation of mitochondrial and lysosomal dynamics. Together, our findings not only provide insights into inter-organelle contacts in maintaining the cellular homeostasis of human neurons, but also suggest the importance of mitochondria-lysosome contacts as a potential target for therapeutic development in PD.

### 6.3 Additional roles of mitochondria-lysosome contact sites

Inter-organelle contact sites are important platforms for multiple types of organelle crosstalk. In addition to regulating organelle dynamics and motiilty, inter-organelle contacts have also been shown to regulate metabolite exchange between organelles (Gatta and Levine 2017). Thus, mitochondria-lysosome contact sites may further mediate additional functions such as the transfer of metabolites including lipids, nucleotides or ions between the two organelles.

In particular, calcium is a highly regulated ion that plays a crucial role in fundamental cellular processes such as apoptosis, exocytosis, signal transduction and gene transcription

(Raffaello et al. 2016b). While the primary cellular store of calcium is located in the ER, both mitochondria and lysosomes have also been implicated as important players in calcium homeostasis. The voltage-dependent anion channel-1 (VDAC1) on the outer mitochondrial membrane and the mitochondrial calcium uniporter (MCU) on the inner mitochondrial membrane mediate calcium transport into mitochondria. This process is important to remove excessive sytosolic calcium and to serve metabolic pathways such as ATP production (Todkar, Ilamathi, and Germain 2017). On the other hands, recent studies on lysosomal calcium homeostasis identified TRPML1 as a mucolipin channel on the lysosomal membrane that releases calcium (Xu and Ren 2015). Inteerstingly, mitochondria–lysosome contact sites were recently found to mediate calcium transfer from lysosomes into mitochondria, whereby lysosomal calcium released through TRPML1 led to calcium influx into mitochondria, mediated by VDAC1 and MCU (Peng, Wong, and Krainc 2020). These findings thus highlight an important role for mitochondria–lysosome contacts in regulating inter-organelle calcium dynamics.

In addition, cholesterol may also be transferred at mitochondria–lysosome contact sites to maintain cellular homeostasis. Niemann-Pick type C protein 1 (NPC1) was identified as a regulator of cholesterole transfer between ER and lysosomes across membrance contact sites. In NPC1-KO cells, ER-lysosome contacts were reduced while mitochondria-lysosome contacts were significantly increased (Hoglinger et al. 2019). Thus, increased mitochondria-lysosome contacts in Niemann pick disease Type C may potentially contribute to the increased mitochondrial cholesterol accumulation observed, and further point to additional functions of mitochondria-lysosome contacts in metabolite exchange.

Taken together, future studies will help to shed light on additional unexplored roles for mitochondria-lysosome contact sites in maintaining cellular and neuronal homeostasis. Moreover, these findings will significantly advance our understanding of how mitochondrial and lysosomal dynamics and function are bidirectionally regulated by one another. Ultimately, insights into this key pathway will elucidate the mechanisms underlying the pathogenesis of multiple human diseases linked to both mitochondrial and lysosomal dysfunction.

# REFERENCES


Abeliovich, A., and A. D. Gitler. 2016. 'Defects in trafficking bridge Parkinson's disease pathology and genetics', *Nature*, 539: 207-16.

Abud, E. M., R. N. Ramirez, E. S. Martinez, L. M. Healy, C. H. H. Nguyen, S. A. Newman, A. V. Yeromin, V. M. Scarfone, S. E. Marsh, C. Fimbres, C. A. Caraway, G. M. Fote, A. M. Madany, A. Agrawal, R. Kayed, K. H. Gylys, M. D. Cahalan, B. J. Cummings, J. P. Antel, A. Mortazavi, M. J. Carson, W. W. Poon, and M. Blurton-Jones. 2017. 'iPSC-Derived Human Microglia-like Cells to Study Neurological Diseases', *Neuron*, 94: 278-93 e9.

Aflaki, E., D. K. Borger, R. J. Grey, M. Kirby, S. Anderson, G. Lopez, and E. Sidransky. 2017. 'Efferocytosis is impaired in Gaucher macrophages', *Haematologica*, 102: 656-65.

Aflaki, E., D. K. Borger, N. Moaven, B. K. Stubblefield, S. A. Rogers, S. Patnaik, F. J. Schoenen, W. Westbroek, W. Zheng, P. Sullivan, H. Fujiwara, R. Sidhu, Z. M. Khaliq, G. J. Lopez, D. S. Goldstein, D. S. Ory, J. Marugan, and E. Sidransky. 2016. 'A New Glucocerebrosidase Chaperone Reduces alpha-Synuclein and Glycolipid Levels in iPSC-Derived Dopaminergic Neurons from Patients with Gaucher Disease and Parkinsonism', *J Neurosci*, 36: 7441-52.

Aits, S., and M. Jaattela. 2013. 'Lysosomal cell death at a glance', *Journal of Cell Science*, 126: 1905-12.

Alcalay, R. N., O. A. Levy, C. C. Waters, S. Fahn, B. Ford, S. H. Kuo, P. Mazzoni, M. W. Pauciulo, W. C. Nichols, Z. Gan-Or, G. A. Rouleau, W. K. Chung, P. Wolf, P. Oliva, J. Keutzer, K. Marder, and X. Zhang. 2015. 'Glucocerebrosidase activity in Parkinson's disease with and without GBA mutations', *Brain*, 138: 2648-58.

Alcalay, R. N., V. Mallett, B. Vanderperre, O. Tavassoly, Y. Dauvilliers, R. Y. J. Wu, J. A. Ruskey, C. S. Leblond, A. Ambalavanan, S. B. Laurent, D. Spiegelman, A. Dionne-Laporte, C. Liong, O. A. Levy, S. Fahn, C. Waters, S. H. Kuo, W. K. Chung, B. Ford, K. S. Marder, U. J. Kang, S. Hassin-Baer, L. Greenbaum, J. F. Trempe, P. Wolf, P. Oliva, X. K. Zhang, L. N. Clark, M. Langlois, P. A. Dion, E. A. Fon, N. Dupre, G. A. Rouleau, and Z. Gan-Or. 2019. 'SMPD1 mutations, activity, and alpha-synuclein accumulation in Parkinson's disease', *Mov Disord*, 34: 526-35.

Alexander, C., M. Votruba, U. E. Pesch, D. L. Thiselton, S. Mayer, A. Moore, M. Rodriguez, U. Kellner, B. Leo-Kottler, G. Auburger, S. S. Bhattacharya, and B. Wissinger. 2000. 'OPA1, encoding a dynamin-related GTPase, is mutated in autosomal dominant optic atrophy linked to chromosome 3q28', *Nat Genet*, 26: 211-5.

Allison, R., J. R. Edgar, G. Pearson, T. Rizo, T. Newton, S. Gunther, F. Berner, J. Hague, J. W. Connell, J. Winkler, J. Lippincott-Schwartz, C. Beetz, B. Winner, and E. Reid. 2017. 'Defects in ER-endosome contacts impact lysosome function in hereditary spastic paraplegia', *J Cell Biol*, 216: 1337-55.

Arthur, K. C., A. Calvo, T. R. Price, J. T. Geiger, A. Chio, and B. J. Traynor. 2016. 'Projected increase in amyotrophic lateral sclerosis from 2015 to 2040', *Nat Commun*, 7: 12408.

Aston, D., R. A. Capel, K. L. Ford, H. C. Christian, G. R. Mirams, E. A. Rog-Zielinska, P. Kohl, A. Galione, R. A. Burton, and D. A. Terrar. 2017. 'High resolution structural evidence suggests the Sarcoplasmic Reticulum forms microdomains with Acidic Stores (lysosomes) in the heart', *Sci Rep*, 7: 40620.

Bae, E. J., N. Y. Yang, M. Song, C. S. Lee, J. S. Lee, B. C. Jung, H. J. Lee, S. Kim, E. Masliah, S. P. Sardi, and S. J. Lee. 2014. 'Glucocerebrosidase depletion enhances cell-to-cell transmission of alpha-synuclein', *Nat Commun*, 5: 4755.

Balderhaar, H. J. K., and C. Ungermann. 2013. 'CORVET and HOPS tethering complexes - coordinators of endosome and lysosome fusion', *Journal of Cell Science*, 126: 1307-16.

Bardy, C., M. van den Hurk, T. Eames, C. Marchand, R. V. Hernandez, M. Kellogg, M. Gorris, B. Galet, V. Palomares, J. Brown, A. G. Bang, J. Mertens, L. Bohnke, L. Boyer, S. Simon, and F. H. Gage. 2015. 'Neuronal medium that supports basic synaptic functions and activity of human neurons in vitro', *Proc Natl Acad Sci U S A*, 112: E2725-34.

Barker, R. A., and I. de Beaufort. 2013. 'Scientific and ethical issues related to stem cell research and interventions in neurodegenerative disorders of the brain', *Prog Neurobiol*, 110: 63-73.

Binns, D., T. Januszewski, Y. Chen, J. Hill, V. S. Markin, Y. Zhao, C. Gilpin, K. D. Chapman, R. G. Anderson, and J. M. Goodman. 2006. 'An intimate collaboration between peroxisomes and lipid bodies', *J Cell Biol*, 173: 719-31.

Bonifati, V., P. Rizzu, M. J. van Baren, O. Schaap, G. J. Breedveld, E. Krieger, M. C. Dekker, F. Squitieri, P. Ibanez, M. Joosse, J. W. van Dongen, N. Vanacore, J. C. van Swieten, A. Brice, G. Meco, C. M. van Duijn, B. A. Oostra, and P. Heutink. 2003. 'Mutations in the DJ-1 gene associated with autosomal recessive early-onset parkinsonism', *Science*, 299: 256-9.

Burbulla, L. F., S. Jeon, J. Zheng, P. Song, R. B. Silverman, and D. Krainc. 2019. 'A modulator of wild-type glucocerebrosidase improves pathogenic phenotypes in dopaminergic neuronal models of Parkinson's disease', *Sci Transl Med*, 11.

Burbulla, L. F., P. Song, J. R. Mazzulli, E. Zampese, Y. C. Wong, S. Jeon, D. P. Santos, J. Blanz, C. D. Obermaier, C. Strojny, J. N. Savas, E. Kiskinis, X. Zhuang, R. Kruger, D. J. Surmeier, and D. Krainc. 2017. 'Dopamine oxidation mediates mitochondrial and lysosomal dysfunction in Parkinson's disease', *Science*, 357: 1255-61.

Burchell, V. S., D. E. Nelson, A. Sanchez-Martinez, M. Delgado-Camprubi, R. M. Ivatt, J. H. Pogson, S. J. Randle, S. Wray, P. A. Lewis, H. Houlden, A. Y. Abramov, J. Hardy, N. W. Wood, A. J. Whitworth, H. Laman, and H. Plun-Favreau. 2013. 'The Parkinson's disease-linked proteins Fbxo7 and Parkin interact to mediate mitophagy', *Nat Neurosci*, 16: 1257-65.

Burte, F., V. Carelli, P. F. Chinnery, and P. Yu-Wai-Man. 2015. 'Disturbed mitochondrial dynamics and neurodegenerative disorders', *Nat Rev Neurol*, 11: 11-24.

Cantalupo, G., P. Alifano, V. Roberti, C. B. Bruni, and C. Bucci. 2001. 'Rab-interacting lysosomal protein (RILP): the Rab7 effector required for transport to lysosomes', *EMBO J*, 20: 683-93.

Chambers, S. M., C. A. Fasano, E. P. Papapetrou, M. Tomishima, M. Sadelain, and L. Studer. 2009. 'Highly efficient neural conversion of human ES and iPS cells by dual inhibition of SMAD signaling', *Nat Biotechnol*, 27: 275-80.

Chang, D., M. A. Nalls, I. B. Hallgrimsdottir, J. Hunkapiller, M. van der Brug, F. Cai, Consortium International Parkinson's Disease Genomics, Team andMe Research, G. A. Kerchner, G. Ayalon, B. Bingol, M. Sheng, D. Hinds, T. W. Behrens, A. B. Singleton, T. R. Bhangale, and R. R. Graham. 2017. 'A meta-analysis of genome-wide association studies identifies 17 new Parkinson's disease risk loci', *Nat Genet*, 49: 1511-16.

Chen, C., D. M. Turnbull, and A. K. Reeve. 2019. 'Mitochondrial Dysfunction in Parkinson's Disease-Cause or Consequence?', *Biology (Basel)*, 8.

Chen, Q., C. Jin, X. Shao, R. Guan, Z. Tian, C. Wang, F. Liu, P. Ling, J. L. Guan, L. Ji, F. Wang, H. Chao, and J. Diao. 2018. 'Super-Resolution Tracking of Mitochondrial Dynamics with An Iridium(III) Luminophore', *Small*, 14: e1802166.

Chu, B. B., Y. C. Liao, W. Qi, C. Xie, X. Du, J. Wang, H. Yang, H. H. Miao, B. L. Li, and B. L. Song. 2015. 'Cholesterol transport through lysosome-peroxisome membrane contacts', *Cell*, 161: 291-306.

Cilia, R., S. Tunesi, G. Marotta, E. Cereda, C. Siri, S. Tesei, A. L. Zecchinelli, M. Canesi, C. B. Mariani, N. Meucci, G. Sacilotto, M. Zini, M. Barichella, C. Magnani, S. Duga, R. Asselta, G. Solda, A. Seresini,

M. Seia, G. Pezzoli, and S. Goldwurm. 2016. 'Survival and dementia in GBA-associated Parkinson's disease: The mutation matters', *Ann Neurol*, 80: 662-73.

Cioni, J. M., J. Q. Lin, A. V. Holtermann, M. Koppers, M. A. H. Jakobs, A. Azizi, B. Turner-Bridger, T. Shigeoka, K. Franze, W. A. Harris, and C. E. Holt. 2019. 'Late Endosomes Act as mRNA Translation Platforms and Sustain Mitochondria in Axons', *Cell*, 176: 56-+.

Cleeter, M. W., K. Y. Chau, C. Gluck, A. Mehta, D. A. Hughes, M. Duchen, N. W. Wood, J. Hardy, J. Mark Cooper, and A. H. Schapira. 2013. 'Glucocerebrosidase inhibition causes mitochondrial dysfunction and free radical damage', *Neurochem Int*, 62: 1-7.

Copeland, D. E., and A. J. Dalton. 1959. 'An association between mitochondria and the endoplasmic reticulum in cells of the pseudobranch gland of a teleost', *J Biophys Biochem Cytol*, 5: 393-6.

Csordas, G., C. Renken, P. Varnai, L. Walter, D. Weaver, K. F. Buttle, T. Balla, C. A. Mannella, and G. Hajnoczky. 2006. 'Structural and functional features and significance of the physical linkage between ER and mitochondria', *J Cell Biol*, 174: 915-21.

Cuddy, L. K., W. Y. Wani, M. L. Morella, C. Pitcairn, K. Tsutsumi, K. Fredriksen, C. J. Justman, T. N. Grammatopoulos, N. R. Belur, F. Zunke, A. Subramanian, A. Affaneh, P. T. Lansbury, Jr., and J. R. Mazzulli. 2019. 'Stress-Induced Cellular Clearance Is Mediated by the SNARE Protein ykt6 and Disrupted by alpha-Synuclein', *Neuron*, 104: 869-84 e11.

Daniele, T., I. Hurbain, R. Vago, G. Casari, G. Raposo, C. Tacchetti, and M. V. Schiaffino. 2014. 'Mitochondria and melanosomes establish physical contacts modulated by Mfn2 and involved in organelle biogenesis', *Curr Biol*, 24: 393-403.

Daniele, T., and M. V. Schiaffino. 2014. 'Organelle biogenesis and interorganellar connections: Better in contact than in isolation', *Commun Integr Biol*, 7: e29587.

de la Mata, M., D. Cotan, M. Oropesa-Avila, J. Garrido-Maraver, M. D. Cordero, M. Villanueva Paz, A. Delgado Pavon, E. Alcocer-Gomez, I. de Lavera, P. Ybot-Gonzalez, A. Paula Zaderenko, C. Ortiz Mellet, J. M. Garcia Fernandez, and J. A. Sanchez-Alcazar. 2015. 'Pharmacological Chaperones and Coenzyme Q10 Treatment Improves Mutant beta-Glucocerebrosidase Activity and Mitochondrial Function in Neuronopathic Forms of Gaucher Disease', *Sci Rep*, 5: 10903.

Delettre, C., G. Lenaers, J. M. Griffoin, N. Gigarel, C. Lorenzo, P. Belenguer, L. Pelloquin, J. Grosgeorge, C. Turc-Carel, E. Perret, C. Astarie-Dequeker, L. Lasquellec, B. Arnaud, B. Ducommun, J. Kaplan, and C. P. Hamel. 2000. 'Nuclear gene OPA1, encoding a mitochondrial dynamin-related protein, is mutated in dominant optic atrophy', *Nat Genet*, 26: 207-10.

Do, J., C. McKinney, P. Sharma, and E. Sidransky. 2019. 'Glucocerebrosidase and its relevance to Parkinson disease', *Mol Neurodegener*, 14: 36.

Dolman, N. J., J. V. Gerasimenko, O. V. Gerasimenko, S. G. Voronina, O. H. Petersen, and A. V. Tepikin. 2005. 'Stable Golgi-mitochondria complexes and formation of Golgi Ca(2+) gradients in pancreatic acinar cells', *J Biol Chem*, 280: 15794-9.

Eisenberg-Bord, M., N. Shai, M. Schuldiner, and M. Bohnert. 2016. 'A Tether Is a Tether Is a Tether: Tethering at Membrane Contact Sites', *Dev Cell*, 39: 395-409.

Elbaz-Alon, Y., E. Rosenfeld-Gur, V. Shinder, A. H. Futerman, T. Geiger, and M. Schuldiner. 2014. 'A dynamic interface between vacuoles and mitochondria in yeast', *Dev Cell*, 30: 95-102.

Elbaz, Y., and M. Schuldiner. 2011. 'Staying in touch: the molecular era of organelle contact sites', *Trends Biochem Sci*, 36: 616-23.

Emdad, L., S. L. D'Souza, H. P. Kothari, Z. A. Qadeer, and I. M. Germano. 2012. 'Efficient differentiation of human embryonic and induced pluripotent stem cells into functional astrocytes', *Stem Cells Dev*, 21: 404-10.

Fermie, J., N. Liv, C. Ten Brink, E. G. van Donselaar, W. H. Muller, N. L. Schieber, Y. Schwab, H. C. Gerritsen, and J. Klumperman. 2018. 'Single organelle dynamics linked to 3D structure by correlative live-cell imaging and 3D electron microscopy', *Traffic*, 19: 354-69.

Fernandes, H. J., E. M. Hartfield, H. C. Christian, E. Emmanoulidou, Y. Zheng, H. Booth, H. Bogetofte, C. Lang, B. J. Ryan, S. P. Sardi, J. Badger, J. Vowles, S. Evetts, G. K. Tofaris, K. Vekrellis, K. Talbot, M. T. Hu, W. James, S. A. Cowley, and R. Wade-Martins. 2016. 'ER Stress and Autophagic Perturbations Lead to Elevated Extracellular alpha-Synuclein in GBA-N370S Parkinson's iPSC-Derived Dopamine Neurons', *Stem Cell Reports*, 6: 342-56.

Friedman, J. R., L. L. Lackner, M. West, J. R. DiBenedetto, J. Nunnari, and G. K. Voeltz. 2011. 'ER tubules mark sites of mitochondrial division', *Science*, 334: 358-62.

Friedman, J. R., and J. Nunnari. 2014. 'Mitochondrial form and function', *Nature*, 505: 335-43.

Gan-Or, Z., A. Bar-Shira, A. Mirelman, T. Gurevich, M. Kedmi, N. Giladi, and A. Orr-Urtreger. 2010. 'LRRK2 and GBA mutations differentially affect the initial presentation of Parkinson disease', *Neurogenetics*, 11: 121-5.

Garcia-Leon, J. A., J. Vitorica, and A. Gutierrez. 2019. 'Use of human pluripotent stem cell-derived cells for neurodegenerative disease modeling and drug screening platform', *Future Med Chem*, 11: 1305-22.

Gatta, A. T., and T. P. Levine. 2017. 'Piecing Together the Patchwork of Contact Sites', *Trends Cell Biol*, 27: 214-29.

Gegg, M. E., D. Burke, S. J. Heales, J. M. Cooper, J. Hardy, N. W. Wood, and A. H. Schapira. 2012. 'Glucocerebrosidase deficiency in substantia nigra of parkinson disease brains', *Ann Neurol*, 72: 455-63.

Gegg, M. E., and A. H. Schapira. 2016. 'Mitochondrial dysfunction associated with glucocerebrosidase deficiency', *Neurobiol Dis*, 90: 43-50.

Giaime, E., Y. Tong, L. K. Wagner, Y. Yuan, G. Huang, and J. Shen. 2017. 'Age-Dependent Dopaminergic Neurodegeneration and Impairment of the Autophagy-Lysosomal Pathway in LRRK-Deficient Mice', *Neuron*, 96: 796-807 e6.

Gitler, A. D., P. Dhillon, and J. Shorter. 2017. 'Neurodegenerative disease: models, mechanisms, and a new hope', *Dis Model Mech*, 10: 499-502.

Gu, H., X. Huang, J. Xu, L. Song, S. Liu, X. B. Zhang, W. Yuan, and Y. Li. 2018. 'Optimizing the method for generation of integration-free induced pluripotent stem cells from human peripheral blood', *Stem Cell Res Ther*, 9: 163.

Gunhanlar, N., G. Shpak, M. van der Kroeg, L. A. Gouty-Colomer, S. T. Munshi, B. Lendemeijer, M. Ghazvini, C. Dupont, W. J. G. Hoogendijk, J. Gribnau, F. M. S. de Vrij, and S. A. Kushner. 2018. 'A simplified protocol for differentiation of electrophysiologically mature neuronal networks from human induced pluripotent stem cells', *Mol Psychiatry*, 23: 1336-44.

Guo, Y., D. Li, S. Zhang, Y. Yang, J. J. Liu, X. Wang, C. Liu, D. E. Milkie, R. P. Moore, U. S. Tulu, D. P. Kiehart, J. Hu, J. Lippincott-Schwartz, E. Betzig, and D. Li. 2018a. 'Visualizing Intracellular Organelle and Cytoskeletal Interactions at Nanoscale Resolution on Millisecond Timescales', *Cell*, 175: 1430-42 e17.

Guo, Y. T., D. Li, S. W. Zhang, Y. R. Yang, J. J. Liu, X. Y. Wang, C. Liu, D. E. Milkie, R. P. Moore, U. S. Tulu, D. P. Kiehart, J. J. Hu, J. Lippincott-Schwartz, E. Betzig, and D. Li. 2018b. 'Visualizing Intracellular Organelle and Cytoskeletal Interactions at Nanoscale Resolution on Millisecond Timescales', *Cell*, 175: 1430-+.

Han, Y., M. Li, F. Qiu, M. Zhang, and Y. H. Zhang. 2017. 'Cell-permeable organic fluorescent probes for live-cell long-term super-resolution imaging reveal lysosome-mitochondrion interactions', *Nat Commun*, 8: 1307.

Hausser, M., G. Stuart, C. Racca, and B. Sakmann. 1995. 'Axonal initiation and active dendritic propagation of action potentials in substantia nigra neurons', *Neuron*, 15: 637-47.

Helle, S. C., G. Kanfer, K. Kolar, A. Lang, A. H. Michel, and B. Kornmann. 2013. 'Organization and function of membrane contact sites', *Biochim Biophys Acta*, 1833: 2526-41.

Hirabayashi, Y., S. K. Kwon, H. Paek, W. M. Pernice, M. A. Paul, J. Lee, P. Erfani, A. Raczkowski, D. S. Petrey, L. A. Pon, and F. Polleux. 2017. 'ER-mitochondria tethering by PDZD8 regulates Ca(2+) dynamics in mammalian neurons', *Science*, 358: 623-30.

Hoglinger, D., T. Burgoyne, E. Sanchez-Heras, P. Hartwig, A. Colaco, J. Newton, C. E. Futter, S. Spiegel, F. M. Platt, and E. R. Eden. 2019. 'NPC1 regulates ER contacts with endocytic organelles to mediate cholesterol egress', *Nat Commun*, 10: 4276.

Honscher, C., M. Mari, K. Auffarth, M. Bohnert, J. Griffith, W. Geerts, M. van der Laan, M. Cabrera, F. Reggiori, and C. Ungermann. 2014. 'Cellular metabolism regulates contact sites between vacuoles and mitochondria', *Dev Cell*, 30: 86-94.

Houlden, H., R. H. King, J. R. Muddle, T. T. Warner, M. M. Reilly, R. W. Orrell, and L. Ginsberg. 2004. 'A novel RAB7 mutation associated with ulcero-mutilating neuropathy', *Ann Neurol*, 56: 586-90.

Hu, Y., Z. Y. Qu, S. Y. Cao, Q. Li, L. Ma, R. Krencik, M. Xu, and Y. Liu. 2016. 'Directed differentiation of basal forebrain cholinergic neurons from human pluripotent stem cells', *J Neurosci Methods*, 266: 42-9.

Hutagalung, A. H., and P. J. Novick. 2011. 'Role of Rab GTPases in membrane traffic and cell physiology', *Physiol Rev*, 91: 119-49.

Itoh, K., Y. Adachi, T. Yamada, T. L. Suzuki, T. Otomo, H. M. McBride, T. Yoshimori, M. Iijima, and H. Sesaki. 2018. 'A brain-enriched Drp1 isoform associates with lysosomes, late endosomes, and the plasma membrane', *J Biol Chem*, 293: 11809-22.

Ji, W. K., A. L. Hatch, R. A. Merrill, S. Strack, and H. N. Higgs. 2015. 'Actin filaments target the oligomeric maturation of the dynamin GTPase Drp1 to mitochondrial fission sites', *Elife*, 4: e11553.

Jordens, I., M. Fernandez-Borja, M. Marsman, S. Dusseljee, L. Janssen, J. Calafat, H. Janssen, R. Wubbolts, and J. Neefjes. 2001. 'The Rab7 effector protein RILP controls lysosomal transport by inducing the recruitment of dynein-dynactin motors', *Curr Biol*, 11: 1680-5.

Kalia, L. V., and A. E. Lang. 2015. 'Parkinson's disease', *Lancet*, 386: 896-912.

Khalil, S., M. Holy, S. Grado, R. Fleming, R. Kurita, Y. Nakamura, and A. Goldfarb. 2017. 'A specialized pathway for erythroid iron delivery through lysosomal trafficking of transferrin receptor 2', *Blood Advances*, 1: 1181-94.

Kikuchi, T., A. Morizane, D. Doi, H. Magotani, H. Onoe, T. Hayashi, H. Mizuma, S. Takara, R. Takahashi, H. Inoue, S. Morita, M. Yamamoto, K. Okita, M. Nakagawa, M. Parmar, and J. Takahashi. 2017. 'Human iPS cell-derived dopaminergic neurons function in a primate Parkinson's disease model', *Nature*, 548: 592-96.

Kim, M. J., S. Jeon, L. F. Burbulla, and D. Krainc. 2018. 'Acid ceramidase inhibition ameliorates alpha-synuclein accumulation upon loss of GBA1 function', *Hum Mol Genet*, 27: 1972-88.

Kim, N. C., E. Tresse, R. M. Kolaitis, A. Molliex, R. E. Thomas, N. H. Alami, B. Wang, A. Joshi, R. B. Smith, G. P. Ritson, B. J. Winborn, J. Moore, J. Y. Lee, T. P. Yao, L. Pallanck, M. Kundu, and J. P. Taylor. 2013. 'VCP is essential for mitochondrial quality control by PINK1/Parkin and this function is impaired by VCP mutations', *Neuron*, 78: 65-80.

Kim, S., S. P. Yun, S. Lee, G. E. Umanah, V. V. R. Bandaru, X. Yin, P. Rhee, S. S. Karuppagounder, S. H. Kwon, H. Lee, X. Mao, D. Kim, A. Pandey, G. Lee, V. L. Dawson, T. M. Dawson, and H. S. Ko. 2018. 'GBA1

deficiency negatively affects physiological alpha-synuclein tetramers and related multimers', *Proc Natl Acad Sci U S A*, 115: 798-803.

Kirkeby, A., S. Grealish, D. A. Wolf, J. Nelander, J. Wood, M. Lundblad, O. Lindvall, and M. Parmar. 2012. 'Generation of regionally specified neural progenitors and functional neurons from human embryonic stem cells under defined conditions', *Cell Rep*, 1: 703-14.

Kirkeby, A., S. Nolbrant, K. Tiklova, A. Heuer, N. Kee, T. Cardoso, D. R. Ottosson, M. J. Lelos, P. Rifes, S. B. Dunnett, S. Grealish, T. Perlmann, and M. Parmar. 2017. 'Predictive Markers Guide Differentiation to Improve Graft Outcome in Clinical Translation of hESC-Based Therapy for Parkinson's Disease', *Cell Stem Cell*, 20: 135-48.

Klein, C., and A. Westenberger. 2012. 'Genetics of Parkinson's disease', *Cold Spring Harb Perspect Med*, 2: a008888.

Korobova, F., V. Ramabhadran, and H. N. Higgs. 2013. 'An actin-dependent step in mitochondrial fission mediated by the ER-associated formin INF2', *Science*, 339: 464-7.

Kriks, S., J. W. Shim, J. Piao, Y. M. Ganat, D. R. Wakeman, Z. Xie, L. Carrillo-Reid, G. Auyeung, C. Antonacci, A. Buch, L. Yang, M. F. Beal, D. J. Surmeier, J. H. Kordower, V. Tabar, and L. Studer. 2011. 'Dopamine neurons derived from human ES cells efficiently engraft in animal models of Parkinson's disease', *Nature*, 480: 547-51.

Lang, C., K. R. Campbell, B. J. Ryan, P. Carling, M. Attar, J. Vowles, O. V. Perestenko, R. Bowden, F. Baig, M. Kasten, M. T. Hu, S. A. Cowley, C. Webber, and R. Wade-Martins. 2019. 'Single-Cell Sequencing of iPSC-Dopamine Neurons Reconstructs Disease Progression and Identifies HDAC4 as a Regulator of Parkinson Cell Phenotypes', *Cell Stem Cell*, 24: 93-+.

Langemeyer, L., F. Frohlich, and C. Ungermann. 2018. 'Rab GTPase Function in Endosome and Lysosome Biogenesis', *Trends Cell Biol*, 28: 957-70.

Langston, J. W., P. Ballard, J. W. Tetrud, and I. Irwin. 1983. 'Chronic Parkinsonism in humans due to a product of meperidine-analog synthesis', *Science*, 219: 979-80.

Lee, J. E., L. M. Westrate, H. Wu, C. Page, and G. K. Voeltz. 2016. 'Multiple dynamin family members collaborate to drive mitochondrial division', *Nature*, 540: 139-43.

Lee, K. S., S. Huh, S. Lee, Z. Wu, A. K. Kim, H. Y. Kang, and B. Lu. 2018. 'Altered ER-mitochondria contact impacts mitochondria calcium homeostasis and contributes to neurodegeneration in vivo in disease models', *Proc Natl Acad Sci U S A*, 115: E8844-E53.

Lesage, S., M. Anheim, C. Condroyer, P. Pollak, F. Durif, C. Dupuits, F. Viallet, E. Lohmann, J. C. Corvol, A. Honore, S. Rivaud, M. Vidailhet, A. Durr, A. Brice, and Group French Parkinson's Disease Genetics Study. 2011. 'Large-scale screening of the Gaucher's disease-related glucocerebrosidase gene in Europeans with Parkinson's disease', *Hum Mol Genet*, 20: 202-10.

Lewis, S. C., L. F. Uchiyama, and J. Nunnari. 2016. 'ER-mitochondria contacts couple mtDNA synthesis with mitochondrial division in human cells', *Science*, 353: aaf5549.

Lewis, S. J., T. Foltynie, A. D. Blackwell, T. W. Robbins, A. M. Owen, and R. A. Barker. 2005. 'Heterogeneity of Parkinson's disease in the early clinical stages using a data driven approach', *J Neurol Neurosurg Psychiatry*, 76: 343-8.

Li, H., A. Ham, T. C. Ma, S. H. Kuo, E. Kanter, D. Kim, H. S. Ko, Y. Quan, S. P. Sardi, A. Li, O. Arancio, U. J. Kang, D. Sulzer, and G. Tang. 2019. 'Mitochondrial dysfunction and mitophagy defect triggered by heterozygous GBA mutations', *Autophagy*, 15: 113-30.

Li, S., S. Xu, B. A. Roelofs, L. Boyman, W. J. Lederer, H. Sesaki, and M. Karbowski. 2015. 'Transient assembly of F-actin on the outer mitochondrial membrane contributes to mitochondrial fission', *J Cell Biol*, 208: 109-23.

Liao, Y. C., M. S. Fernandopulle, G. Wang, H. Choi, L. Hao, C. M. Drerup, R. Patel, S. Qamar, J. Nixon-Abell, Y. Shen, W. Meadows, M. Vendruscolo, T. P. J. Knowles, M. Nelson, M. A. Czekalska, G. Musteikyte, M. A. Gachechiladze, C. A. Stephens, H. A. Pasolli, L. R. Forrest, P. St George-Hyslop, J. Lippincott-Schwartz, and M. E. Ward. 2019. 'RNA Granules Hitchhike on Lysosomes for Long-Distance Transport, Using Annexin A11 as a Molecular Tether', *Cell*, 179: 147-64 e20.

Lim, C. Y., O. B. Davis, H. R. Shin, J. Zhang, C. A. Berdan, X. Jiang, J. L. Counihan, D. S. Ory, D. K. Nomura, and R. Zoncu. 2019. 'ER-lysosome contacts enable cholesterol sensing by mTORC1 and drive aberrant growth signalling in Niemann-Pick type C', *Nat Cell Biol*, 21: 1206-18.

Little, Daniel, Robin Ketteler, Paul Gissen, and Michael J. Devine. 2019. 'Using stem cell–derived neurons in drug screening for neurological diseases', *Neurobiology of Aging*, 78: 130-41.

Lopez-Crisosto, C., C. Pennanen, C. Vasquez-Trincado, P. E. Morales, R. Bravo-Sagua, A. F. G. Quest, M. Chiong, and S. Lavandero. 2017. 'Sarcoplasmic reticulum-mitochondria communication in cardiovascular pathophysiology', *Nat Rev Cardiol*, 14: 342-60.

Lu, J., X. Zhong, H. Liu, L. Hao, C. T. Huang, M. A. Sherafat, J. Jones, M. Ayala, L. Li, and S. C. Zhang. 2016. 'Generation of serotonin neurons from human pluripotent stem cells', *Nat Biotechnol*, 34: 89-94.

Lucking, C. B., A. Durr, V. Bonifati, J. Vaughan, G. De Michele, T. Gasser, B. S. Harhangi, G. Meco, P. Denefle, N. W. Wood, Y. Agid, A. Brice, Group French Parkinson's Disease Genetics Study, and Disease European Consortium on Genetic Susceptibility in Parkinson's. 2000. 'Association between early-onset Parkinson's disease and mutations in the parkin gene', *N Engl J Med*, 342: 1560-7.

Magalhaes, J., M. E. Gegg, A. Migdalska-Richards, M. K. Doherty, P. D. Whitfield, and A. H. Schapira. 2016. 'Autophagic lysosome reformation dysfunction in glucocerebrosidase deficient cells: relevance to Parkinson disease', *Hum Mol Genet*, 25: 3432-45.

Manor, U., S. Bartholomew, G. Golani, E. Christenson, M. Kozlov, H. Higgs, J. Spudich, and J. Lippincott-Schwartz. 2015. 'A mitochondria-anchored isoform of the actin-nucleating spire protein regulates mitochondrial division', *Elife*, 4.

Maraganore, D. M., T. G. Lesnick, A. Elbaz, M. C. Chartier-Harlin, T. Gasser, R. Kruger, N. Hattori, G. D. Mellick, A. Quattrone, J. Satoh, T. Toda, J. Wang, J. P. Ioannidis, M. de Andrade, W. A. Rocca, and Uchl Global Genetics Consortium. 2004. 'UCHL1 is a Parkinson's disease susceptibility gene', *Ann Neurol*, 55: 512-21.

Maroof, A. M., S. Keros, J. A. Tyson, S. W. Ying, Y. M. Ganat, F. T. Merkle, B. Liu, A. Goulburn, E. G. Stanley, A. G. Elefanty, H. R. Widmer, K. Eggan, P. A. Goldstein, S. A. Anderson, and L. Studer. 2013. 'Directed differentiation and functional maturation of cortical interneurons from human embryonic stem cells', *Cell Stem Cell*, 12: 559-72.

Marotta, N., S. Kim, and D. Krainc. 2020. 'Organoid and pluripotent stem cells in Parkinson's disease modeling: an expert view on their value to drug discovery', *Expert Opin Drug Discov*, 15: 427-41.

Marras, C., J. C. Beck, J. H. Bower, E. Roberts, B. Ritz, G. W. Ross, R. D. Abbott, R. Savica, S. K. Van Den Eeden, A. W. Willis, C. M. Tanner, and P. Group Parkinson's Foundation. 2018. 'Prevalence of Parkinson's disease across North America', *NPJ Parkinsons Dis*, 4: 21.

Mazzulli, J. R., Y. H. Xu, Y. Sun, A. L. Knight, P. J. McLean, G. A. Caldwell, E. Sidransky, G. A. Grabowski, and D. Krainc. 2011. 'Gaucher disease glucocerebrosidase and alpha-synuclein form a bidirectional pathogenic loop in synucleinopathies', *Cell*, 146: 37-52.

Mazzulli, J. R., F. Zunke, O. Isacson, L. Studer, and D. Krainc. 2016. 'alpha-Synuclein-induced lysosomal dysfunction occurs through disruptions in protein trafficking in human midbrain synucleinopathy models', *Proc Natl Acad Sci U S A*, 113: 1931-6.

Mazzulli, J. R., F. Zunke, T. Tsunemi, N. J. Toker, S. Jeon, L. F. Burbulla, S. Patnaik, E. Sidransky, J. J. Marugan, C. M. Sue, and D. Krainc. 2016. 'Activation of beta-Glucocerebrosidase Reduces Pathological

alpha-Synuclein and Restores Lysosomal Function in Parkinson's Patient Midbrain Neurons', *J Neurosci*, 36: 7693-706.

Mc Donald, J. M., and D. Krainc. 2017. 'Lysosomal Proteins as a Therapeutic Target in Neurodegeneration', *Annu Rev Med*, 68: 445-58.

McLelland, G. L., V. Soubannier, C. X. Chen, H. M. McBride, and E. A. Fon. 2014. 'Parkin and PINK1 function in a vesicular trafficking pathway regulating mitochondrial quality control', *Embo Journal*, 33: 282-95.

Meggouh, F., H. M. Bienfait, M. A. Weterman, M. de Visser, and F. Baas. 2006. 'Charcot-Marie-Tooth disease due to a de novo mutation of the RAB7 gene', *Neurology*, 67: 1476-8.

Merkle, F. T., A. Maroof, T. Wataya, Y. Sasai, L. Studer, K. Eggan, and A. F. Schier. 2015. 'Generation of neuropeptidergic hypothalamic neurons from human pluripotent stem cells', *Development*, 142: 633-43.

Mishra, P., and D. C. Chan. 2016. 'Metabolic regulation of mitochondrial dynamics', *J Cell Biol*, 212: 379-87.

Moore, A. S., Y. C. Wong, C. L. Simpson, and E. L. Holzbaur. 2016. 'Dynamic actin cycling through mitochondrial subpopulations locally regulates the fission-fusion balance within mitochondrial networks', *Nat Commun*, 7: 12886.

Moren, C., D. L. Juarez-Flores, K. Y. Chau, M. Gegg, G. Garrabou, I. Gonzalez-Casacuberta, M. Guitart-Mampel, E. Tolosa, M. J. Marti, F. Cardellach, and A. H. V. Schapira. 2019. 'GBA mutation promotes early mitochondrial dysfunction in 3D neurosphere models', *Aging (Albany NY)*, 11: 10338-55.

Muallem, S., W. Y. Chung, A. Jha, and M. Ahuja. 2017. 'Lipids at membrane contact sites: cell signaling and ion transport', *EMBO Rep*, 18: 1893-904.

Murphy, K. E., A. M. Gysbers, S. K. Abbott, N. Tayebi, W. S. Kim, E. Sidransky, A. Cooper, B. Garner, and G. M. Halliday. 2014. 'Reduced glucocerebrosidase is associated with increased alpha-synuclein in sporadic Parkinson's disease', *Brain*, 137: 834-48.

Nakagawa, M., M. Koyanagi, K. Tanabe, K. Takahashi, T. Ichisaka, T. Aoi, K. Okita, Y. Mochiduki, N. Takizawa, and S. Yamanaka. 2008. 'Generation of induced pluripotent stem cells without Myc from mouse and human fibroblasts', *Nat Biotechnol*, 26: 101-6.

Nalls, M. A., N. Pankratz, C. M. Lill, C. B. Do, D. G. Hernandez, M. Saad, A. L. DeStefano, E. Kara, J. Bras, M. Sharma, C. Schulte, M. F. Keller, S. Arepalli, C. Letson, C. Edsall, H. Stefansson, X. Liu, H. Pliner, J. H. Lee, R. Cheng, Consortium International Parkinson's Disease Genomics, GENetics Initiative Parkinson's Study Group Parkinson's Research: The Organized, andMe, GenePd, Consortium NeuroGenetics Research, Genomics Hussman Institute of Human, Investigator Ashkenazi Jewish Dataset, Health Cohorts for, Epidemiology Aging Research in Genetic, Consortium North American Brain Expression, Consortium United Kingdom Brain Expression, Consortium Greek Parkinson's Disease, Group Alzheimer Genetic Analysis, M. A. Ikram, J. P. Ioannidis, G. M. Hadjigeorgiou, J. C. Bis, M. Martinez, J. S. Perlmutter, A. Goate, K. Marder, B. Fiske, M. Sutherland, G. Xiromerisiou, R. H. Myers, L. N. Clark, K. Stefansson, J. A. Hardy, P. Heutink, H. Chen, N. W. Wood, H. Houlden, H. Payami, A. Brice, W. K. Scott, T. Gasser, L. Bertram, N. Eriksson, T. Foroud, and A. B. Singleton. 2014. 'Large-scale meta-analysis of genome-wide association data identifies six new risk loci for Parkinson's disease', *Nat Genet*, 46: 989-93.

Neumann, J., J. Bras, E. Deas, S. S. O'Sullivan, L. Parkkinen, R. H. Lachmann, A. Li, J. Holton, R. Guerreiro, R. Paudel, B. Segarane, A. Singleton, A. Lees, J. Hardy, H. Houlden, T. Revesz, and N. W. Wood. 2009. 'Glucocerebrosidase mutations in clinical and pathologically proven Parkinson's disease', *Brain*, 132: 1783-94.

Nguyen, M., Y. C. Wong, D. Ysselstein, A. Severino, and D. Krainc. 2018. 'Synaptic, Mitochondrial, and Lysosomal Dysfunction in Parkinson's Disease', *Trends Neurosci*.

———. 2019. 'Synaptic, Mitochondrial, and Lysosomal Dysfunction in Parkinson's Disease', *Trends Neurosci*, 42: 140-49.

Nicholas, C. R., J. Chen, Y. Tang, D. G. Southwell, N. Chalmers, D. Vogt, C. M. Arnold, Y. J. Chen, E. G. Stanley, A. G. Elefanty, Y. Sasai, A. Alvarez-Buylla, J. L. Rubenstein, and A. R. Kriegstein. 2013. 'Functional maturation of hPSC-derived forebrain interneurons requires an extended timeline and mimics human neural development', *Cell Stem Cell*, 12: 573-86.

Nistor, G. I., M. O. Totoiu, N. Haque, M. K. Carpenter, and H. S. Keirstead. 2005. 'Human embryonic stem cells differentiate into oligodendrocytes in high purity and myelinate after spinal cord transplantation', *Glia*, 49: 385-96.

Nizzardo, M., C. Simone, M. Falcone, F. Locatelli, G. Riboldi, G. P. Comi, and S. Corti. 2010. 'Human motor neuron generation from embryonic stem cells and induced pluripotent stem cells', *Cell Mol Life Sci*, 67: 3837-47.

Oeda, T., A. Umemura, Y. Mori, S. Tomita, M. Kohsaka, K. Park, K. Inoue, H. Fujimura, H. Hasegawa, H. Sugiyama, and H. Sawada. 2015. 'Impact of glucocerebrosidase mutations on motor and nonmotor complications in Parkinson's disease', *Neurobiol Aging*, 36: 3306-13.

Onoue, K., A. Jofuku, R. Ban-Ishihara, T. Ishihara, M. Maeda, T. Koshiba, T. Itoh, M. Fukuda, H. Otera, T. Oka, H. Takano, N. Mizushima, K. Mihara, and N. Ishihara. 2013. 'Fis1 acts as a mitochondrial recruitment factor for TBC1D15 that is involved in regulation of mitochondrial morphology', *J Cell Sci*, 126: 176-85.

Ordonez, D. G., M. K. Lee, and M. B. Feany. 2018. 'alpha-synuclein Induces Mitochondrial Dysfunction through Spectrin and the Actin Cytoskeleton', *Neuron*, 97: 108-24 e6.

Osellame, L. D., A. A. Rahim, I. P. Hargreaves, M. E. Gegg, A. Richard-Londt, S. Brandner, S. N. Waddington, A. H. Schapira, and M. R. Duchen. 2013. 'Mitochondria and quality control defects in a mouse model of Gaucher disease--links to Parkinson's disease', *Cell Metab*, 17: 941-53.

Pankiv, S., E. A. Alemu, A. Brech, J. A. Bruun, T. Lamark, A. Overvatn, G. Bjorkoy, and T. Johansen. 2010. 'FYCO1 is a Rab7 effector that binds to LC3 and PI3P to mediate microtubule plus end-directed vesicle transport', *J Cell Biol*, 188: 253-69.

Park, J. S., N. F. Blair, and C. M. Sue. 2015. 'The role of ATP13A2 in Parkinson's disease: Clinical phenotypes and molecular mechanisms', *Mov Disord*, 30: 770-9.

Peng, W., Y. C. Wong, and D. Krainc. 2020. 'Mitochondria-lysosome contacts regulate mitochondrial Ca(2+) dynamics via lysosomal TRPML1', *Proc Natl Acad Sci U S A*, 117: 19266-75.

Peralta, E. R., B. C. Martin, and A. L. Edinger. 2010. 'Differential effects of TBC1D15 and mammalian Vps39 on Rab7 activation state, lysosomal morphology, and growth factor dependence', *J Biol Chem*, 285: 16814-21.

Phillips, M. J., and G. K. Voeltz. 2016. 'Structure and function of ER membrane contact sites with other organelles', *Nat Rev Mol Cell Biol*, 17: 69-82.

Pickrell, A. M., and R. J. Youle. 2015. 'The roles of PINK1, parkin, and mitochondrial fidelity in Parkinson's disease', *Neuron*, 85: 257-73.

Plotegher, N., and M. R. Duchen. 2017a. 'Crosstalk between Lysosomes and Mitochondria in Parkinson's Disease', *Front Cell Dev Biol*, 5: 110.

———. 2017b. 'Mitochondrial Dysfunction and Neurodegeneration in Lysosomal Storage Disorders', *Trends Mol Med*, 23: 116-34.

Polymeropoulos, M. H., J. J. Higgins, L. I. Golbe, W. G. Johnson, S. E. Ide, G. Di Iorio, G. Sanges, E. S. Stenroos, L. T. Pho, A. A. Schaffer, A. M. Lazzarini, R. L. Nussbaum, and R. C. Duvoisin. 1996. 'Mapping of a gene for Parkinson's disease to chromosome 4q21-q23', *Science*, 274: 1197-9.

Polymeropoulos, M. H., C. Lavedan, E. Leroy, S. E. Ide, A. Dehejia, A. Dutra, B. Pike, H. Root, J. Rubenstein, R. Boyer, E. S. Stenroos, S. Chandrasekharappa, A. Athanassiadou, T. Papapetropoulos, W. G. Johnson, A. M. Lazzarini, R. C. Duvoisin, G. Di Iorio, L. I. Golbe, and R. L. Nussbaum. 1997. 'Mutation in the alpha-synuclein gene identified in families with Parkinson's disease', *Science*, 276: 2045-7.

Qu, X., T. Liu, K. Song, X. Li, and D. Ge. 2012. 'Induced pluripotent stem cells generated from human adipose-derived stem cells using a non-viral polycistronic plasmid in feeder-free conditions', *PLoS One*, 7: e48161.

Raffaello, A., C. Mammucari, G. Gherardi, and R. Rizzuto. 2016a. 'Calcium at the Center of Cell Signaling: Interplay between Endoplasmic Reticulum, Mitochondria, and Lysosomes', *Trends Biochem Sci*, 41: 1035-49.

———. 2016b. 'Calcium at the Center of Cell Signaling: Interplay between Endoplasmic Reticulum, Mitochondria, and Lysosomes', *Trends in Biochemical Sciences*, 41: 1035-49.

Ran, F. A., P. D. Hsu, J. Wright, V. Agarwala, D. A. Scott, and F. Zhang. 2013. 'Genome engineering using the CRISPR-Cas9 system', *Nat Protoc*, 8: 2281-308.

Robak, L. A., I. E. Jansen, J. van Rooij, A. G. Uitterlinden, R. Kraaij, J. Jankovic, Consortium International Parkinson's Disease Genomics, P. Heutink, and J. M. Shulman. 2017. 'Excessive burden of lysosomal storage disorder gene variants in Parkinson's disease', *Brain*, 140: 3191-203.

Robertson, John A. 2001. 'Human embryonic stem cell research: ethical and legal issues', *Nature Reviews Genetics*, 2: 74-78.

Romero Rosales, K., E. R. Peralta, G. G. Guenther, S. Y. Wong, and A. L. Edinger. 2009. 'Rab7 activation by growth factor withdrawal contributes to the induction of apoptosis', *Mol Biol Cell*, 20: 2831-40.

Rowland, A. A., P. J. Chitwood, M. J. Phillips, and G. K. Voeltz. 2014. 'ER contact sites define the position and timing of endosome fission', *Cell*, 159: 1027-41.

Schondorf, D. C., M. Aureli, F. E. McAllister, C. J. Hindley, F. Mayer, B. Schmid, S. P. Sardi, M. Valsecchi, S. Hoffmann, L. K. Schwarz, U. Hedrich, D. Berg, L. S. Shihabuddin, J. Hu, J. Pruszak, S. P. Gygi, S. Sonnino, T. Gasser, and M. Deleidi. 2014. 'iPSC-derived neurons from GBA1-associated Parkinson's disease patients show autophagic defects and impaired calcium homeostasis', *Nat Commun*, 5: 4028.

Schondorf, D. C., D. Ivanyuk, P. Baden, A. Sanchez-Martinez, S. De Cicco, C. Yu, I. Giunta, L. K. Schwarz, G. Di Napoli, V. Panagiotakopoulou, S. Nestel, M. Keatinge, J. Pruszak, O. Bandmann, B. Heimrich, T. Gasser, A. J. Whitworth, and M. Deleidi. 2018. 'The NAD+ Precursor Nicotinamide Riboside Rescues Mitochondrial Defects and Neuronal Loss in iPSC and Fly Models of Parkinson's Disease', *Cell Rep*, 23: 2976-88.

Shai, N., E. Yifrach, C. W. T. van Roermund, N. Cohen, C. Bibi, I. Jlst L, L. Cavellini, J. Meurisse, R. Schuster, L. Zada, M. C. Mari, F. M. Reggiori, A. L. Hughes, M. Escobar-Henriques, M. M. Cohen, H. R. Waterham, R. J. A. Wanders, M. Schuldiner, and E. Zalckvar. 2018. 'Systematic mapping of contact sites reveals tethers and a function for the peroxisome-mitochondria contact', *Nat Commun*, 9: 1761.

Sheng, Z. H. 2014. 'Mitochondrial trafficking and anchoring in neurons: New insight and implications', *J Cell Biol*, 204: 1087-98.

Shi, Y., P. Kirwan, and F. J. Livesey. 2012. 'Directed differentiation of human pluripotent stem cells to cerebral cortex neurons and neural networks', *Nat Protoc*, 7: 1836-46.

Shin, J. J. H., A. K. Gillingham, F. Begum, J. Chadwick, and S. Munro. 2017. 'TBC1D23 is a bridging factor for endosomal vesicle capture by golgins at the trans-Golgi', *Nat Cell Biol*, 19: 1424-32.

Sidransky, E., and G. Lopez. 2012. 'The link between the GBA gene and parkinsonism', *Lancet Neurol*, 11: 986-98.

Sidransky, E., M. A. Nalls, J. O. Aasly, J. Aharon-Peretz, G. Annesi, E. R. Barbosa, A. Bar-Shira, D. Berg, J. Bras, A. Brice, C. M. Chen, L. N. Clark, C. Condroyer, E. V. De Marco, A. Durr, M. J. Eblan, S. Fahn, M. J. Farrer, H. C. Fung, Z. Gan-Or, T. Gasser, R. Gershoni-Baruch, N. Giladi, A. Griffith, T. Gurevich, C. Januario, P. Kropp, A. E. Lang, G. J. Lee-Chen, S. Lesage, K. Marder, I. F. Mata, A. Mirelman, J. Mitsui, I. Mizuta, G. Nicoletti, C. Oliveira, R. Ottman, A. Orr-Urtreger, L. V. Pereira, A. Quattrone, E. Rogaeva, A. Rolfs, H. Rosenbaum, R. Rozenberg, A. Samii, T. Samaddar, C. Schulte, M. Sharma, A. Singleton, M. Spitz, E. K. Tan, N. Tayebi, T. Toda, A. R. Troiano, S. Tsuji, M. Wittstock, T. G. Wolfsberg, Y. R. Wu, C. P. Zabetian, Y. Zhao, and S. G. Ziegler. 2009. 'Multicenter analysis of glucocerebrosidase mutations in Parkinson's disease', *N Engl J Med*, 361: 1651-61.

Simmen, T., and M. S. Herrera-Cruz. 2018. 'Plastic mitochondria-endoplasmic reticulum (ER) contacts use chaperones and tethers to mould their structure and signaling', *Current Opinion in Cell Biology*, 53: 61-69.

Sironi, L., L. M. Restelli, M. Tolnay, A. Neutzner, and S. Frank. 2020. 'Dysregulated Interorganellar Crosstalk of Mitochondria in the Pathogenesis of Parkinson's Disease', *Cells*, 9.

Smirnova, E., L. Griparic, D. L. Shurland, and A. M. van der Bliek. 2001. 'Dynamin-related protein Drp1 is required for mitochondrial division in mammalian cells', *Mol Biol Cell*, 12: 2245-56.

Spillantini, M. G., M. L. Schmidt, V. M. Lee, J. Q. Trojanowski, R. Jakes, and M. Goedert. 1997. 'Alpha-synuclein in Lewy bodies', *Nature*, 388: 839-40.

Stauffer, W., H. Sheng, and H. N. Lim. 2018. 'EzColocalization: An ImageJ plugin for visualizing and measuring colocalization in cells and organisms', *Sci Rep*, 8: 15764.

Sugiura, A., G. L. McLelland, E. A. Fon, and H. M. McBride. 2014. 'A new pathway for mitochondrial quality control: mitochondrial-derived vesicles', *EMBO J*, 33: 2142-56.

Sun, N., R. J. Youle, and T. Finkel. 2016. 'The Mitochondrial Basis of Aging', *Molecular Cell*, 61: 654-66.

Takahashi, K., and S. Yamanaka. 2006. 'Induction of pluripotent stem cells from mouse embryonic and adult fibroblast cultures by defined factors', *Cell*, 126: 663-76.

Takenaka, C., N. Nishishita, N. Takada, L. M. Jakt, and S. Kawamata. 2010. 'Effective generation of iPS cells from CD34+ cord blood cells by inhibition of p53', *Exp Hematol*, 38: 154-62.

Thaler, A., T. Gurevich, A. Bar Shira, M. Gana Weisz, E. Ash, T. Shiner, A. Orr-Urtreger, N. Giladi, and A. Mirelman. 2017. 'A "dose" effect of mutations in the GBA gene on Parkinson's disease phenotype', *Parkinsonism Relat Disord*, 36: 47-51.

Todkar, K., H. S. Ilamathi, and M. Germain. 2017. 'Mitochondria and Lysosomes: Discovering Bonds', *Front Cell Dev Biol*, 5: 106.

Tsunemi, T., K. Hamada, and D. Krainc. 2014. 'ATP13A2/PARK9 regulates secretion of exosomes and alpha-synuclein', *J Neurosci*, 34: 15281-7.

Tsunemi, T., T. Perez-Rosello, Y. Ishiguro, A. Yoroisaka, S. Jeon, K. Hamada, M. Rammonhan, Y. C. Wong, Z. Xie, W. Akamatsu, J. R. Mazzulli, D. J. Surmeier, N. Hattori, and D. Krainc. 2019. 'Increased Lysosomal Exocytosis Induced by Lysosomal Ca(2+) Channel Agonists Protects Human Dopaminergic Neurons from alpha-Synuclein Toxicity', *J Neurosci*, 39: 5760-72.

Tysnes, O. B., and A. Storstein. 2017. 'Epidemiology of Parkinson's disease', *J Neural Transm (Vienna)*, 124: 901-05.

Urbach, A., M. Schuldiner, and N. Benvenisty. 2004. 'Modeling for Lesch-Nyhan disease by gene targeting in human embryonic stem cells', *Stem Cells*, 22: 635-41.

Valadas, J. S., G. Esposito, D. Vandekerkhove, K. Miskiewicz, L. Deaulmerie, S. Raitano, P. Seibler, C. Klein, and P. Verstreken. 2018. 'ER Lipid Defects in Neuropeptidergic Neurons Impair Sleep Patterns in Parkinson's Disease', *Neuron*, 98: 1155-+.

Valente, E. M., P. M. Abou-Sleiman, V. Caputo, M. M. Muqit, K. Harvey, S. Gispert, Z. Ali, D. Del Turco, A. R. Bentivoglio, D. G. Healy, A. Albanese, R. Nussbaum, R. Gonzalez-Maldonado, T. Deller, S. Salvi, P. Cortelli, W. P. Gilks, D. S. Latchman, R. J. Harvey, B. Dallapiccola, G. Auburger, and N. W. Wood. 2004. 'Hereditary early-onset Parkinson's disease caused by mutations in PINK1', *Science*, 304: 1158-60.

Valm, A. M., S. Cohen, W. R. Legant, J. Melunis, U. Hershberg, E. Wait, A. R. Cohen, M. W. Davidson, E. Betzig, and J. Lippincott-Schwartz. 2017. 'Applying systems-level spectral imaging and analysis to reveal the organelle interactome', *Nature*, 546: 162-67.

Verhoeven, K., P. De Jonghe, K. Coen, N. Verpoorten, M. Auer-Grumbach, J. M. Kwon, D. FitzPatrick, E. Schmedding, E. De Vriendt, A. Jacobs, V. Van Gerwen, K. Wagner, H. P. Hartung, and V. Timmerman. 2003. 'Mutations in the small GTP-ase late endosomal protein RAB7 cause Charcot-Marie-Tooth type 2B neuropathy', *Am J Hum Genet*, 72: 722-7.

Vidailhet, M. 2003. '[Heterogeneity of Parkinson's disease]', *Bull Acad Natl Med*, 187: 259-75; discussion 75-6.

Wang, S., B. Wang, N. Pan, L. Fu, C. Wang, G. Song, J. An, Z. Liu, W. Zhu, Y. Guan, Z. Q. Xu, P. Chan, Z. Chen, and Y. A. Zhang. 2015. 'Differentiation of human induced pluripotent stem cells to mature functional Purkinje neurons', *Sci Rep*, 5: 9232.

Wang, X., C. Han, W. Liu, P. Wang, and X. Zhang. 2014. 'A novel RAB7 mutation in a Chinese family with Charcot-Marie-Tooth type 2B disease', *Gene*, 534: 431-4.

Wiedemann, A., K. Hemmer, I. Bernemann, G. Gohring, O. Pogozhykh, C. Figueiredo, S. Glage, A. Schambach, J. C. Schwamborn, R. Blasczyk, and T. Muller. 2012. 'Induced pluripotent stem cells generated from adult bone marrow-derived cells of the nonhuman primate (Callithrix jacchus) using a novel quad-cistronic and excisable lentiviral vector', *Cell Reprogram*, 14: 485-96.

Wong, Y. C., S. Kim, W. Peng, and D. Krainc. 2019. 'Regulation and Function of Mitochondria-Lysosome Membrane Contact Sites in Cellular Homeostasis', *Trends Cell Biol*, 29: 500-13.

Wong, Y. C., and D. Krainc. 2016. 'Lysosomal trafficking defects link Parkinson's disease with Gaucher's disease', *Mov Disord*, 31: 1610-18.

Wong, Y. C., W. Peng, and D. Krainc. 2019. 'Lysosomal Regulation of Inter-mitochondrial Contact Fate and Motility in Charcot-Marie-Tooth Type 2', *Dev Cell*, 50: 339-54 e4.

Wong, Y. C., D. Ysselstein, and D. Krainc. 2018. 'Mitochondria-lysosome contacts regulate mitochondrial fission via RAB7 GTP hydrolysis', *Nature*, 554: 382-86.

Woodard, C. M., B. A. Campos, S. H. Kuo, M. J. Nirenberg, M. W. Nestor, M. Zimmer, E. V. Mosharov, D. Sulzer, H. Zhou, D. Paull, L. Clark, E. E. Schadt, S. P. Sardi, L. Rubin, K. Eggan, M. Brock, S. Lipnick, M. Rao, S. Chang, A. Li, and S. A. Noggle. 2014. 'iPSC-derived dopamine neurons reveal differences between monozygotic twins discordant for Parkinson's disease', *Cell Rep*, 9: 1173-82.

Wu, H. X., P. Carvalho, and G. K. Voeltz. 2018. 'Here, there, and everywhere: The importance of ER membrane contact sites', *Science*, 361: 466-+.

Wu, Y., C. Whiteus, C. S. Xu, K. J. Hayworth, R. J. Weinberg, H. F. Hess, and P. De Camilli. 2017. 'Contacts between the endoplasmic reticulum and other membranes in neurons', *Proc Natl Acad Sci U S A*, 114: E4859-E67.

Xu, H., and D. Ren. 2015. 'Lysosomal physiology', *Annu Rev Physiol*, 77: 57-80.

Yamano, K., A. I. Fogel, C. Wang, A. M. van der Bliek, and R. J. Youle. 2014. 'Mitochondrial Rab GAPs govern autophagosome biogenesis during mitophagy', *Elife*, 3: e01612.

Yang, N., S. Chanda, S. Marro, Y. H. Ng, J. A. Janas, D. Haag, C. E. Ang, Y. Tang, Q. Flores, M. Mall, O. Wapinski, M. Li, H. Ahlenius, J. L. Rubenstein, H. Y. Chang, A. A. Buylla, T. C. Sudhof, and M. Wernig. 2017. 'Generation of pure GABAergic neurons by transcription factor programming', *Nat Methods*, 14: 621-28.

Ysselstein, D., M. Nguyen, T. J. Young, A. Severino, M. Schwake, K. Merchant, and D. Krainc. 2019. 'LRRK2 kinase activity regulates lysosomal glucocerebrosidase in neurons derived from Parkinson's disease patients', *Nat Commun*, 10: 5570.

Yu, Diana Xuan, Francesco Paolo Di Giorgio, Jun Yao, Maria Carolina Marchetto, Kristen Brennand, Rebecca Wright, Arianna Mei, Lauren McHenry, David Lisuk, Jaeson Michael Grasmick, Pedro Silberman, Giovanna Silberman, Roberto Jappelli, and Fred H Gage. 2014. 'Modeling Hippocampal Neurogenesis Using Human Pluripotent Stem Cells', *Stem Cell Reports*, 2: 295-310.

Yu, Junying, Maxim A. Vodyanik, Kim Smuga-Otto, Jessica Antosiewicz-Bourget, Jennifer L. Frane, Shulan Tian, Jeff Nie, Gudrun A. Jonsdottir, Victor Ruotti, Ron Stewart, Igor I. Slukvin, and James A. Thomson. 2007. 'Induced Pluripotent Stem Cell Lines Derived from Human Somatic Cells', *Science*, 318: 1917-20.

Zhang, X. K., C. S. Elbin, W. L. Chuang, S. K. Cooper, C. A. Marashio, C. Beauregard, and J. M. Keutzer. 2008. 'Multiplex enzyme assay screening of dried blood spots for lysosomal storage disorders by using tandem mass spectrometry', *Clin Chem*, 54: 1725-8.

Zhang, X. M., B. Walsh, C. A. Mitchell, and T. Rowe. 2005. 'TBC domain family, member 15 is a novel mammalian Rab GTPase-activating protein with substrate preference for Rab7', *Biochem Biophys Res Commun*, 335: 154-61.

Zhen, Y., and H. Stenmark. 2015. 'Cellular functions of Rab GTPases at a glance', *J Cell Sci*, 128: 3171-6.

Zheng, J., S. Jeon, W. Jiang, L. F. Burbulla, D. Ysselstein, K. Oevel, D. Krainc, and R. B. Silverman. 2019. 'Conversion of Quinazoline Modulators from Inhibitors to Activators of beta-Glucocerebrosidase', *J Med Chem*, 62: 1218-30.

Zuchner, S., I. V. Mersiyanova, M. Muglia, N. Bissar-Tadmouri, J. Rochelle, E. L. Dadali, M. Zappia, E. Nelis, A. Patitucci, J. Senderek, Y. Parman, O. Evgrafov, P. D. Jonghe, Y. Takahashi, S. Tsuji, M. A. Pericak-Vance, A. Quattrone, E. Battaloglu, A. V. Polyakov, V. Timmerman, J. M. Schroder, and J. M. Vance. 2004. 'Mutations in the mitochondrial GTPase mitofusin 2 cause Charcot-Marie-Tooth neuropathy type 2A', *Nat Genet*, 36: 449-51.

Zunke, F., A. C. Moise, N. R. Belur, E. Gelyana, I. Stojkovska, H. Dzaferbegovic, N. J. Toker, S. Jeon, K. Fredriksen, and J. R. Mazzulli. 2018. 'Reversible Conformational Conversion of alpha-Synuclein into Toxic Assemblies by Glucosylceramide', *Neuron*, 97: 92-+.